

SDAC-TR-78-1

LEVEL

ANALYSIS OF SELECTED SEISMIC EVENTS FROM ASIA IN A SEISMIC DISCRIMINATION CONTEXT

P.A. Sebel & D.H. von Seggern

Seismic Data Analysis Center

Teledyne Geotech, 314 Montgomery Street, Alexandria Virginia 22314

21 September 1978

APPROVED FOR PUBLIC RELEASE; DISTRIBUTION UNLIMITED.

Sponsored by

The Defense Advanced Research Projects Agency (DARPA)

DARPA Order No. 2551

Monitored By

AFTAC/VSC

312 Montgomery Street, Alexandria, Virginia 22314

DTIC
ELECT
JUN 24 1979

ADA 085879

DC FILE COPY

80 6 23 033

Disclaimer: Neither the Defense Advanced Research Projects Agency nor the Air Force Technical Applications Center will be responsible for information contained herein which has been supplied by other organizations or contractors, and this document is subject to later revision as may be necessary. The views and conclusions presented are those of the authors and should not be interpreted as necessarily representing the official policies, either expressed or implied, of the Defense Advanced Research Projects Agency, the Air Force Technical Applications Center, or the US Government.

Unclassified
SECURITY CLASSIFICATION OF THIS PAGE (When Data Entered)

REPORT DOCUMENTATION PAGE		READ INSTRUCTIONS BEFORE COMPLETING FORM
1. REPORT NUMBER SDAC-TR-78-5	2. GOVT ACCESSION NO. AD-A085879	3. RECIPIENT'S CATALOG NUMBER
4. TITLE (and Subtitle) ANALYSIS OF SELECTED SEISMIC EVENTS FROM ASIA IN A SEISMIC DISCRIMINATION CONTEXT.		5. TYPE OF REPORT & PERIOD COVERED Technical rept.
6. PERFORMING ORG. REPORT NUMBER		7. CONTRACT OR GRANT NUMBER(s) F08606-78-C-0007
8. AUTHOR P. A. Sobel D. H. von Seggern		9. PROGRAM ELEMENT PROJECT TASK AREA & WORK UNIT NUMBERS VT/8709
10. PERFORMING ORGANIZATION NAME AND ADDRESS Teledyne Geotech 314 Montgomery Street Alexandria, Virginia 22314		11. REPORT DATE 21 Sept 1978
12. CONTROLLING OFFICE NAME AND ADDRESS Defense Advanced Research Projects Agency Nuclear Monitoring Research Office 1400 Wilson Blvd. Arlington, Virginia 22209		13. NUMBER OF PAGES 101
14. MONITORING AGENCY NAME & ADDRESS (if different from Controlling Office) VELA Seismological Center 312 Montgomery Street Alexandria, Virginia 22314		15. SECURITY CLASS (of this report) Unclassified
16. DISTRIBUTION STATEMENT (of this Report) APPROVED FOR PUBLIC RELEASE; DISTRIBUTION UNLIMITED.		15a. DECLASSIFICATION DOWNGRADING SCHEDULE
17. DISTRIBUTION STATEMENT (of the abstract entered in Block 20, if different from Report)		
18. SUPPLEMENTARY NOTES Author's Report Date 02/17/78		
19. KEY WORDS (Continue on reverse side if necessary and identify by block number) Seismic Discrimination M _s -m _b Seismic Source Spectrum Seismic Attenuation		
20. ABSTRACT (Continue on reverse side if necessary and identify by block number) This study examines earthquakes in Kamchatka, the Tien Shan, the Pamirs, the Baikal rift zone, and the Caucasus and explosions in the Aleutians, East Kazakh, West Kazakh, Southwest Russia, Lop Nor, and Baikal in a seismic discrimination context. Because of their low magnitudes (m _b from 4.2 to 6.0 and M _s from 3.2 to 5.8) and their varying propagation effects, it was impossible on the basis of first motions or LR amplitudes to determine source mechanisms for most of the earthquakes. Seismograms from the arrays ALPA, LASA, and NORSAR, the HGLP and the WWSSN stations were analyzed for m _b , M _s .		

DD FORM 1 JAN 73 1473 EDITION OF 1 NOV 65 IS OBSOLETE

Unclassified
SECURITY CLASSIFICATION OF THIS PAGE (When Data Entered)

408258 JLM

Unclassified

SECURITY CLASSIFICATION OF THIS PAGE(When Data Entered)

corner frequency, long-period spectral level, long-period and short-period body-wave excitation, complexities, spectral ratios, radiation patterns, depth of focus, and higher-mode surface waves. The major successful discriminants for our data set were found to be M_s , m_b , and identification of pP. In a stepwise linear discrimination analysis using the discrimination parameters m_b , M_s , corner frequency, complexity, spectral ratio, and long-period spectral level, the earthquakes were separated from the explosions with high confidence. In addition, some separation by region was evident for the earthquakes alone.

However, it is clear that in many regions a shot array could be used to successfully evade discrimination which would then have to be made using other means such as depth, relative P and pP amplitude, and ratio of compressional to shear phases at similar frequencies.

M. J. ... *M. J. ...*

Accession For	
NTIS GRA&I	<input checked="checked" type="checkbox"/>
DDC TAB	<input type="checkbox"/>
Unannounced	<input type="checkbox"/>
Justification	<input type="checkbox"/>
By _____	
Distribution/ _____	
Availability _____	
Dist.	Available or special
A	

Unclassified

SECURITY CLASSIFICATION OF THIS PAGE(When Data Entered)

ANALYSIS OF SELECTED SEISMIC EVENTS FROM
ASIA IN A SEISMIC DISCRIMINATION CONTEXT

SEISMIC DATA ANALYSIS CENTER REPORT NO.: SDAC-TR-78-5

AFTAC Project Authorization No.:	VELA VT/8709
Project Title:	Seismic Data Analysis Center
ARPA Order No.:	2551
Name of Contractor:	TELEDYNE GEOTECH
Contract No.:	F08606-78-C-0007
Date of Contract:	01 October 1977
Amount of Contract:	\$2,674,245
Contract Expiration Date:	30 September 1978
Project Manager:	Robert R. Blandford (703) 836-3882

P. O. Box 334, Alexandria, Virginia 22313

APPROVED FOR PUBLIC RELEASE; DISTRIBUTION UNLIMITED.

ABSTRACT

This study examines earthquakes in Kamchatka, the Tien Shan, the Pamirs, the Baikal rift zone, and the Caucasus and explosions in the Aleutians, East Kazakh, West Kazakh, Southwest Russia, Lop Nor, and Baikal in a seismic discrimination context. Because of their low magnitudes (m_b from 4.2 to 6.0 and M_s from 3.2 to 5.8) and their varying propagation effects, it was impossible on the basis of first motions or LR amplitudes to determine source mechanisms for most of the earthquakes. Seismograms from the arrays ALPA, LASA, and NORSAR, the HGLP and the WWSSN stations were analyzed for m_b , M_s , corner frequency, long-period spectral level, long-period and short-period body-wave excitation, complexities, spectral ratios, radiation patterns, depth of focus, and higher-mode surface waves. The major successful discriminants for our data set were found to be M_s-m_b and identification of pP. In a stepwise linear discrimination analysis using the discrimination parameters m_b , M_s , corner frequency, complexity, spectral ratio, and long-period spectral level, the earthquakes were separated from the explosions with high confidence. In addition, some separation by region was evident for the earthquakes alone.

However, it is clear that in many regions a shot array could be used to successfully evade discrimination which would then have to be made using other means such as depth, relative P and pP amplitudes, and ratio of compressional to shear phases at similar frequencies.

TABLE OF CONTENTS

	Page
ABSTRACT	2
LIST OF FIGURES	5
LIST OF TABLES	8
INTRODUCTION	9
TECTONIC SETTING	11
DATA	14
Earthquake Selection	14
Explosion Selection	14
Seismic Stations	14
Short-period Waveforms at LASA and NORSAR	17
Long-period Waveforms at NORSAR	26
SIGNAL ANALYSIS	35
Source Mechanisms	35
Corner Frequencies, Long-period Spectral Levels, and Seismic Moments	38
Attenuation (t^*)	49
DISCRIMINATION ASPECTS	57
$M_s - m_b$	57
Corner Frequencies and Long-period Spectral Levels	60
Long-period Body-wave Excitation	64
Short-period Body-wave Excitation	65
Complexities	65
Spectral Ratios	70
Radiation Patterns	76
Depth of Focus	77
Higher-Mode Observations	77
Correlation with Active Faults	85
STEPWISE CLASSIFICATION OF ASIAN SEISMIC EVENTS	86
Classification of Events According to Regions	87

TABLE OF CONTENTS (Continued)

	Page
Discrimination of Earthquakes and Explosions on a Regional Basis	88
Discrimination of Earthquakes and Explosions without Regionalization	90
Value of Different Discrimination Parameters for Asian Events	91
SUMMARY	96
REFERENCES	99

LIST OF FIGURES

Figure No.	Title	Page
1	Map of Eurasia showing the earthquakes and explosions used in this study.	12
2	LASA and NORSAR short-period P waveforms for the Kamchatka earthquakes.	18
3	LASA and NORSAR short-period P waveforms for the Tien Shan earthquakes.	19
4	LASA and NORSAR short-period P waveforms for the Pamir earthquakes.	20
5	LASA and NORSAR short-period P waveforms for the Baikal earthquakes.	21
6	LASA and NORSAR short-period P waveforms for the Caucasus earthquakes.	22
7	LASA and NORSAR short-period P waveforms for the explosions used in this study	23
8	NORSAR long-period waveforms for the Kamchatka earthquakes.	27
9	NORSAR long-period waveforms for the Tien Shan earthquakes.	28
10	NORSAR long-period waveforms for the Pamir earthquakes.	29
11	NORSAR long-period waveforms for the Baikal earthquakes.	30
12	NORSAR long-period waveforms for the Caucasus earthquakes.	31
13	NORSAR long-period waveforms for representative explosions used in this study.	32
14	First motions for a Tien Shan earthquake (730517) in the lower half of the focal sphere (Wulff net).	36
15	Observed LR amplitudes normalized back to the source (T=20 sec) for a Tien Shan event on 730517.	37
16	Predicted LR raypaths (T=20 sec) for a Tien Shan event on 730124.	39

LIST OF FIGURES (Continued)

Figure No.	Title	Page
17	LASA A0 and NORSAR C3 subarray spectra of P waves from the 740226 Kamchatka earthquake, the 720102 Tien Shann earthquake, and the 730815 W. Kazakh explosion.	40
18	Seismic moment versus corner frequency for earthquakes from all regions from LASA P recordings.	47
19	Seismic moment versus corner frequency for earthquakes from all regions from NORSAR P recordings.	48
20	Normalized and summed spectra for the paths from East Kazakh to LASA and to NORSAR.	50
21	$\ln A(f) + 2 \ln(f)$ frequency for the paths E. Kazakh to LASA and to NORSAR.	52
22	M_s versus m_b for earthquakes and explosions from all regions.	59
23	Long-period body-wave spectral level versus corner frequency.	61
24	Long-period spectral level versus corner frequency for earthquakes and explosions from all regions from LASA P recordings.	62
25	Long-period spectral level versus corner frequency for earthquakes and explosions from all regions from NORSAR P recordings.	63
26	Complexity versus m_b for all events from LASA and NORSAR P recordings.	67
27	Complexity versus m_b for earthquakes and explosions from all regions from LASA P recordings.	68
28	Complexity versus m_b for earthquakes and explosions from all regions from NORSAR P recordings.	69
29	Short-period P spectral ratio versus m_b for all events recorded at LASA and NORSAR using spectra uncorrected for attenuation.	71
30	Short-period P spectral ratio versus m_b for earthquakes and explosions from all regions using LASA spectra uncorrected for attenuation.	72

LIST OF FIGURES (Continued)

Figure No.	Title	Page
31	Short-period P spectral ratio versus m_b for earthquakes and explosions from all regions using NORSAR spectra uncorrected for attenuation.	73
32	Short-period P spectral ratio versus m_b for earthquakes and explosions from all regions using LASA spectra corrected for attenuation. The t^* values are for f^{-2} source models for earthquakes and explosions and f^{-3} source models for earthquakes.	74
33	Short-period P spectral ratio versus m_b for earthquakes and explosions from all regions using NORSAR spectra corrected for attenuation. The t^* values are for f^{-2} source models for earthquakes and explosions and f^{-3} source models for earthquakes.	75
34	Rayleigh-wave arrivals at NORSAR for five earthquakes and two explosions and velocity-versus-period plots for determining group-velocity curves.	78

LIST OF TABLES

Table No.	Title	Page
I	NEIS Data for Earthquakes	15
II	NEIS Data for Explosions	16
III	t* values for all Source Paths to LASA and NORSAR	55
IV	Results for Classification of Earthquakes into Five Regions	89
V	Results for Classification of Events from Kamchatka/Amchitka	92
VI	Results for Classification of Events from Tien Shan/Lop Nor, E. Kazakh	92
VII	Results for Classification of Events from Pamirs/E. Kazakh, W. Kazakh.	93
VIII	Results for Classification of Events from Baikal/Siberia	93
IX	Results for Classification of Events from Caucasus/W Kazakh, S. W. Russia.	94
X	Results for Classification of Events from all Asian Regions	94
XI	Results for Classification of Events from all Asian Regions Using all Short-period data.	95

INTRODUCTION

Variation of source characteristics and path effects from events in various regions is likely to compound the problem of seismic discrimination of explosions and earthquakes, unless reasonably accurate descriptions of the cause and degree of such variations are obtained. To accomplish this the authors have recently attempted, for five different source regions in and around the Union of Soviet Socialist Republic (USSR) (von Seggern and Sobel, 1976; Sobel and von Seggern, 1976; Sobel et al., 1977a, 1977b, and 1977c), to identify the major source and path effects which impact upon discrimination of Asian events and to assess likelihood of correct event identification in these regions. However, the problem of regional effects can be circumvented by limiting the computation of a discriminant function for earthquakes and explosions to events within a geophysically distinct region. This type of analysis was conducted on a suite of events in the Southwestern United States (von Seggern and Rivers, 1977) with encouraging results for discrimination on a regional basis.

von Seggern, D. H., and P. A. Sobel, 1976. Study of selected Kamchatka earthquakes in a seismic discrimination context, SDAC Report No. TR-76-10, Teledyne Geotech, Alexandria, Va. 22314.

Sobel, P. A., and D. H. von Seggern, 1976. Study of selected events in the Tien Shan Region in a seismic discrimination context, SDAC Report No. TR-76-9, Teledyne Geotech Alexandria, Va. 22314.

Sobel, P. A., D. H. von Seggern, E. I. Sweetser, and D. W. Rivers, 1977a. Study of selected events in the Pamirs in a seismic discrimination context, SDAC Report No. TR-77-3, Teledyne Geotech, Alexandria, Va. 22314.

Sobel, P. A., D. H. von Seggern, E. I. Sweetser, and D. W. Rivers, 1977b. Study of selected events in the Baikal rift zone in a seismic discrimination context, SDAC Report No. TR-77-5, Teledyne Geotech, Alexandria, Va. 22314.

Sobel, P. A., D. H. von Seggern, E. I. Sweetser, and D. W. Rivers, 1977c. Study of selected events in the Caucasus in a seismic discrimination context, SDAC Report No. TR-77-6, Teledyne Geotech, Alexandria, Va. 22314.

von Seggern D. H., and W. D. Rivers, 1977. Seismic discrimination of earthquakes and explosions with applications to the Southwestern United States, SDAC Report No. TR-77-10, Teledyne Geotech, Alexandria, Va. 22314.

The purpose of this report is to synthesize and analyze the work contained in the five regional Asian studies. Through this presentation, the diversities and similarities of the recorded data can be appreciated because a nearly uniform approach to the study of each of the five regions was made. In this report, the five previous efforts are collectively labeled the "Asian regional studies" or "Asian regional reports."

The scheme of this report is as follows: First, because the basic illustrations of the signal waveforms are one of the more important parts of this document, the data used in the Asian regional studies will be reviewed and depicted. For short-period data, primarily LASA and NORSAR recordings were used, with some supplementary work on WWSSN recordings for first motions and magnitude. For long-period data, the large arrays ALPA, LASA, and NORSAR were used, with additional readings from the HGLP network and the WWSSN network for magnitude. The dates of events in the five Asian regional studies were from 1971 to 1975, before the advent of the SRO network of high-quality stations.

Second, the signal analysis sections of the Asian regional reports are summarized, leading to discussions of various discrimination parameters and the effects of source mechanisms and travel path on them. Discrimination parameters for all five regions will be plotted together without "regional" corrections. The discriminants treated are: M_s , m_b , corner frequency, long-period spectral level, complexity, spectral ratio, radiation pattern, depth of focus, higher-mode generation, and shear-waves.

Finally, new work is added on stepwise classification experiments not contained in the original Asian regional reports. This section will treat classification of events on a regional basis and classification of all the Asian events together. In this manner, the relative value of various discriminant parameters for these events will be established.

TECTONIC SETTING

The earthquakes studied here occurred in five different tectonic settings: the Kamchatka Peninsula, the Tien Shan uplift, the Pamirs uplift, the Baikal rift zone, and the Caucasus fold belt. The locations of these earthquakes are depicted on Figure 1. Each of the regions is seismic; and they have therefore been extensively studied by Soviet seismologists (Medvedev, 1968). The Tien Shan, Pamir, and Caucasus earthquakes lie in distinct seismic regions, but all are undergoing uplift as a result of the collision of the Indian and Eurasian plates (Molnar and Tapponier, 1975). The Baikal rift zone is a region of crustal extension which Molnar and Tapponier thought to be a distant manifestation of the stress system created by the Indian-Eurasian collision. The Kamchatka seismic region is unique in this study because it is connected with the underthrusting of the Pacific plate.

The Kamchatka earthquakes occurred along the coastline within the upper margin of the dipping Pacific plate (25-50 km deep). A typical source mechanism for these events would be a fault plane striking NNE parallel to the tectonic trend and dipping approximately 25 degrees WNW. The events are characteristically thrust faults with a slip angle of roughly 90 degrees. The maxima of the P radiation pattern is downward, giving positive first motions to all teleseismic signals. Most of the earthquakes in the Tien Shan area are associated with large, sub-parallel, strike-slip faults inferred from analysis of a satellite photomosaic of the area. Review of earthquake focal mechanisms in the Tien Shan show both strike-slip and thrust movements mainly along planes with steep dip angles (Sobel et al., 1977a). The seismicity in the Caucasus Mountains generally follows the northwest-southeast trend of the principal geological features: thrust faulting, with the fault planes perpendicular to the trend of the geological structures, is dominant, but considerable variance to the fault-plane orientations exists and strike-slip motion is not uncommon (Sobel et al., 1977c). In the Baikal rift zone, normal faulting is prevalent;

Molnar, P., and P. Tapponnier, 1975. Cenozoic tectonics of Asia: effects of a continental collision, Science, **189**, 419.

Medvedev, S. V. (ed.), 1968. Seismic Zoning in the USSR, Keter Publ. House, Jerusalem, Israel (English translation).

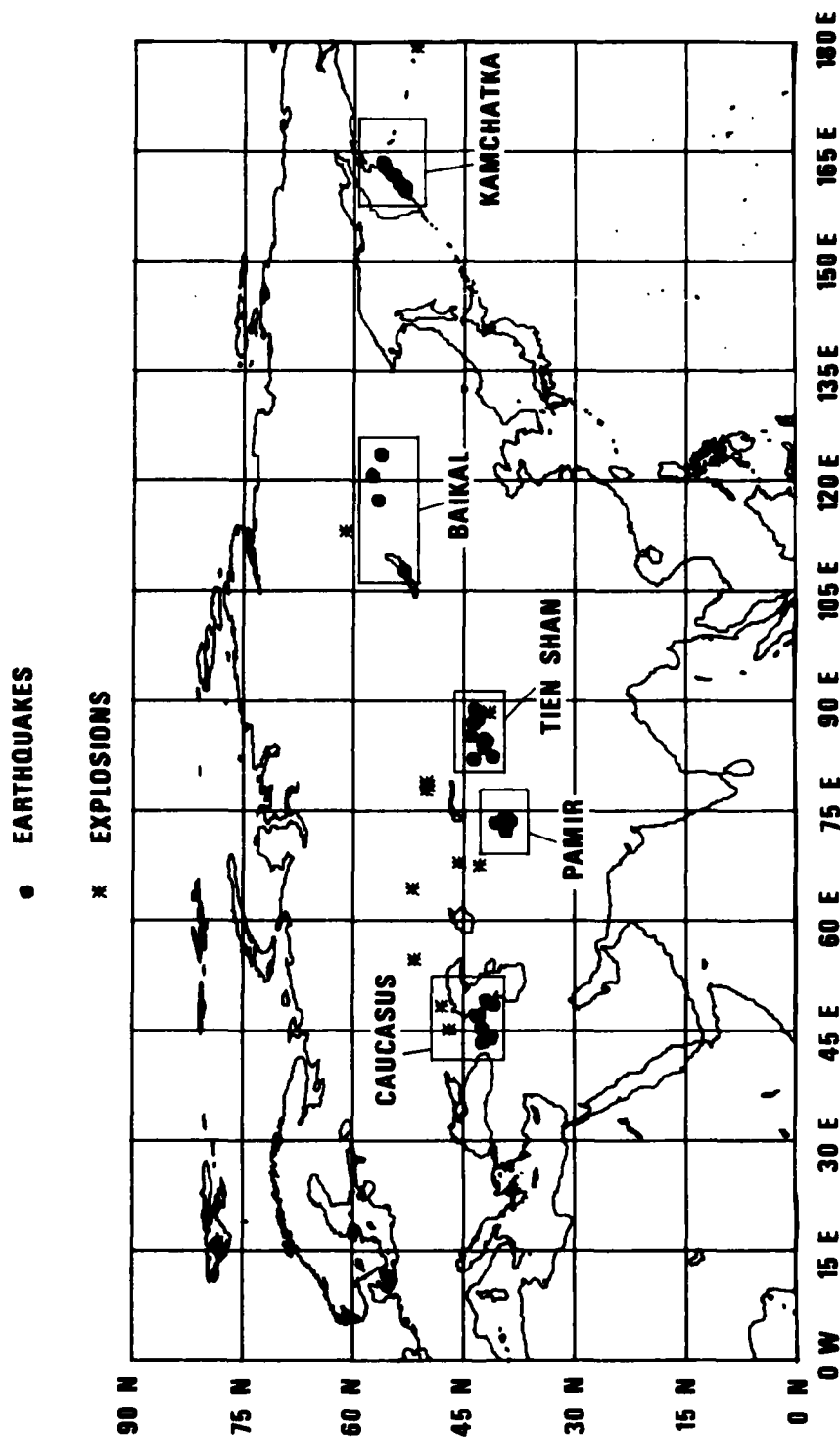


Figure 1 Map of Eurasia showing the earthquakes and explosions used in this study.

and faults bordering a system of grabens are clearly observed on satellite photographs of the area (Sobel et al., 1977b). With normal faulting the nodal plane of the P radiation pattern is downward, giving positive and negative first motions to teleseismic signals.

DATA

Earthquake Selection

Since the emphasis is on discrimination, only crustal depth earthquakes, except one subcrustal event in the Caspian Sea, were chosen for this study. Earthquakes were selected in the years 1971-1975 so digital data could be utilized from the ALPA, LASA, and NORSAR arrays and the HGLP network. In the Kamchatka, Tien Shan, and Pamir regions, earthquakes were chosen that had low reported M_s for their m_b so that these events fall close to the explosion population on an M_s - m_b diagram. In the Baikal and Caucasus regions such low M_s events were not found, and all crustal events were selected in the years 1971-1975 for which array data could be recovered with at least fair signal-to-noise ratios. These few earthquakes cannot be claimed to represent adequately the true variability within the five source regions, but they are representative of the type of earthquakes most troublesome in a discrimination context. The epicentral data for the earthquakes is listed in Table I, and the locations are shown in Figure 1.

Explosion Selection

In the five Eurasian reports, earthquakes in the regions of study were compared to explosions detonated as closely as possible to these seismic regions. Explosions were selected from the Aleutians (MILROW), East Kazakh, West Kazakh, Southwest Russia, Lop Nor, and Baikal. The explosion epicenter data and the earthquake regions to which they are compared are listed in Table II, and their locations are shown in Figure 1.

Seismic Stations

Digital data from the arrays ALPA, LASA, and NORSAR and from the available HGLP stations were gathered for these events. A significant percentage of the HGLP data either could not be recovered or it was not usable. Also examined were short-period and long-period data on film chips from reliable sites in the WWSSN to supplement the magnitude calculations and focal-mechanism investigations. WWSSN stations were selected on the basis of magnification, proximity to the regions of study, and azimuthal relation to the source regions. The Baikal explosion was added late to the data set; and since WWSSN data of the Baikal explosion was not available at the time, SRO data for this event was used instead.

NEIS Data for Earthquakes

-15-

Table II

NEIS Data for Earthquakes

REGION	DATE	ORIGIN TIME			LAT (ON)	LONG (OE)	NEIS m_b	M_s (THIS STUDY)
		HR	MIN	SEC				
MILROW	691002	22	06	00.0	51.4	179.2	5.5	5.2
E. KAZAKH	710322	14	32	57.8	49.7	78.2	5.3	5.3
E. KAZAKH	711129	06	02	57.1	49.8	78.1	5.3	5.3
E. KAZAKH	711230	06	02	57.7	49.8	78.1	5.3	5.3
E. KAZAKH	720210	05	22	57.3	50.0	78.0	5.3	5.3
E. KAZAKH	740627	03	56	56.0	49.9	77.2	5.3	5.3
E. KAZAKH	741124	05	59	56.8	49.8	77.2	5.3	5.3
W. KAZAKH	721124	04	59	57.8	49.7	67.3	5.3	5.3
W. KAZAKH	730813	04	59	57.2	49.6	67.3	5.3	5.3
W. KAZAKH	730920	04	59	57.3	49.6	67.3	5.3	5.3
SW RUSSIA	731222	08	59	56.3	49.8	45.0	5.3	5.3
SW RUSSIA	721003	08	59	57.8	49.8	45.0	5.3	5.3
LOP NOR	711027	04	00	03.4	41.4	88.3	5.3	5.3
BAIKAL	761105	04	00	03.4	51.0	113.0	5.3	5.3

(N) - M_s value based solely on noise measurements. Maximum noise
 M_s value used in these cases.

* - Bungum and Tjostheim, 1976

Short-period Waveforms at LASA and NORSAR

Short-period P phases recorded at LASA and NORSAR for the five earthquake regions are shown in Figures 2 through 6; those for the explosions are shown in Figure 7. Phased A0 subarray beams from LASA and phased C3 subarray beams from NORSAR were used to avoid signal loss at high frequencies due to full-array beaming. Where there are no records shown, the data for that time period was unrecoverable or there was no detected signal.

The short-period P waveforms for the Kamchatka earthquakes are shown in Figure 2. Although a source mechanism solution exists for only one of these events, the 730304 (year-month-day) earthquake, the association of these events with the underthrusting of the oceanic plate and the dominance of teleseismic compressional first motion indicate that these are thrust faults. In addition, synthetic seismograms computed for the 730304 earthquake match the directions of first motion, arrival times of pP, P-wave amplitudes, and the shape of the first few cycles of observed long-period P at LASA, NORSAR, and eight worldwide stations (von Seggern and Sobel, 1976). The pP phase is observed on all LASA records but only on two of nine NORSAR records. Observations of pP at NORSAR are lacking because the pP raypath to the surface for NORSAR lies near the auxiliary focal plane, where the amplitudes are low. This difference in the P to pP ratios serves as a powerful counter evasion technique to shot arrays. For LASA, the predicted amplitude of pP is close to that of P, and this is observed in most cases. There were similarities among many of the initial P waveforms at LASA, but the waveforms recorded at NORSAR show little uniformity and are always of higher frequency content than corresponding LASA signals.

Short-period P waveforms for the Tien Shan earthquakes are shown in Figure 3. Definite source mechanisms could not be determined for any of these events using teleseismic data due to their small size ($m_b \leq 5.0$); satellite photographs suggest that the mechanisms could be either thrust faulting or strike-slip faulting (Sobel and von Seggern, 1976). There are many differences in signal shape and frequency content of these P waveforms at both LASA and NORSAR, and again the NORSAR signals have higher frequency content than the LASA ones. Clearly, no one waveform could be used to approximate the P signals at either LASA or NORSAR. The pP phases were not well recorded at either LASA or NORSAR for the Tien Shan events.

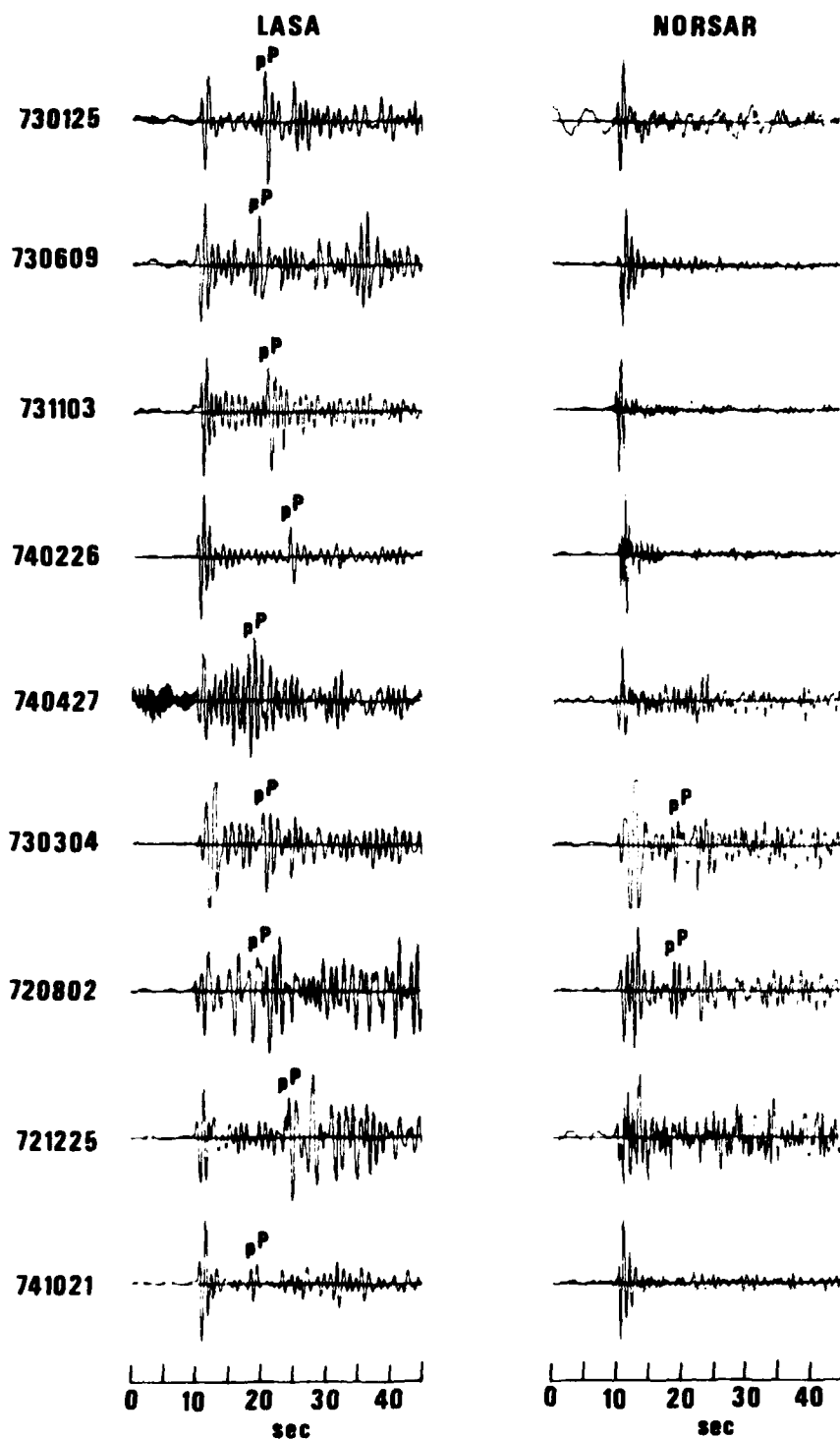


Figure 2 LASA and NORSAR short-period P waveforms for the Kamchatka earthquakes.

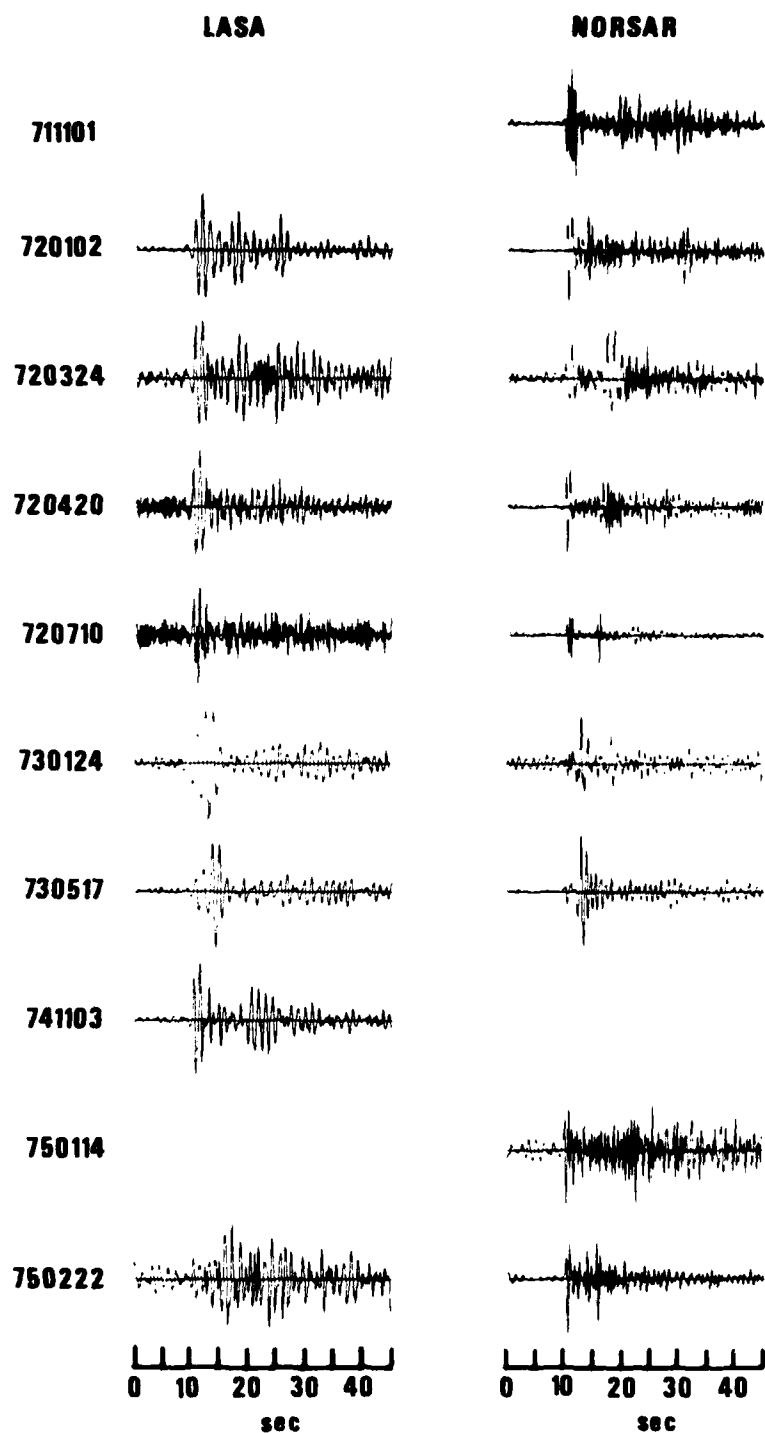


Figure 3 LASA and NORSAR short-period P waveforms for the Tien Shan earthquakes.

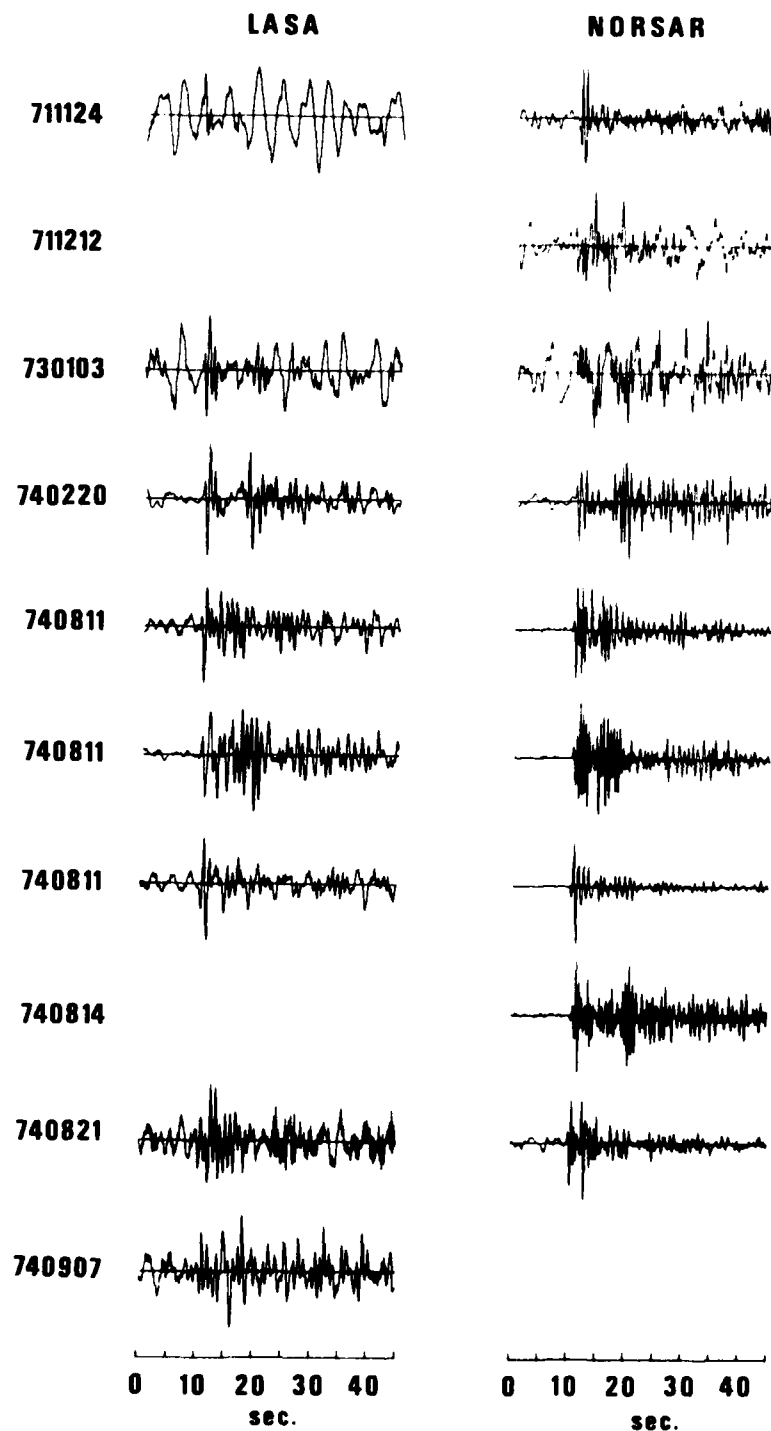


Figure 4 LASA and NORSAR short-period waveforms for the Pamir earthquakes.

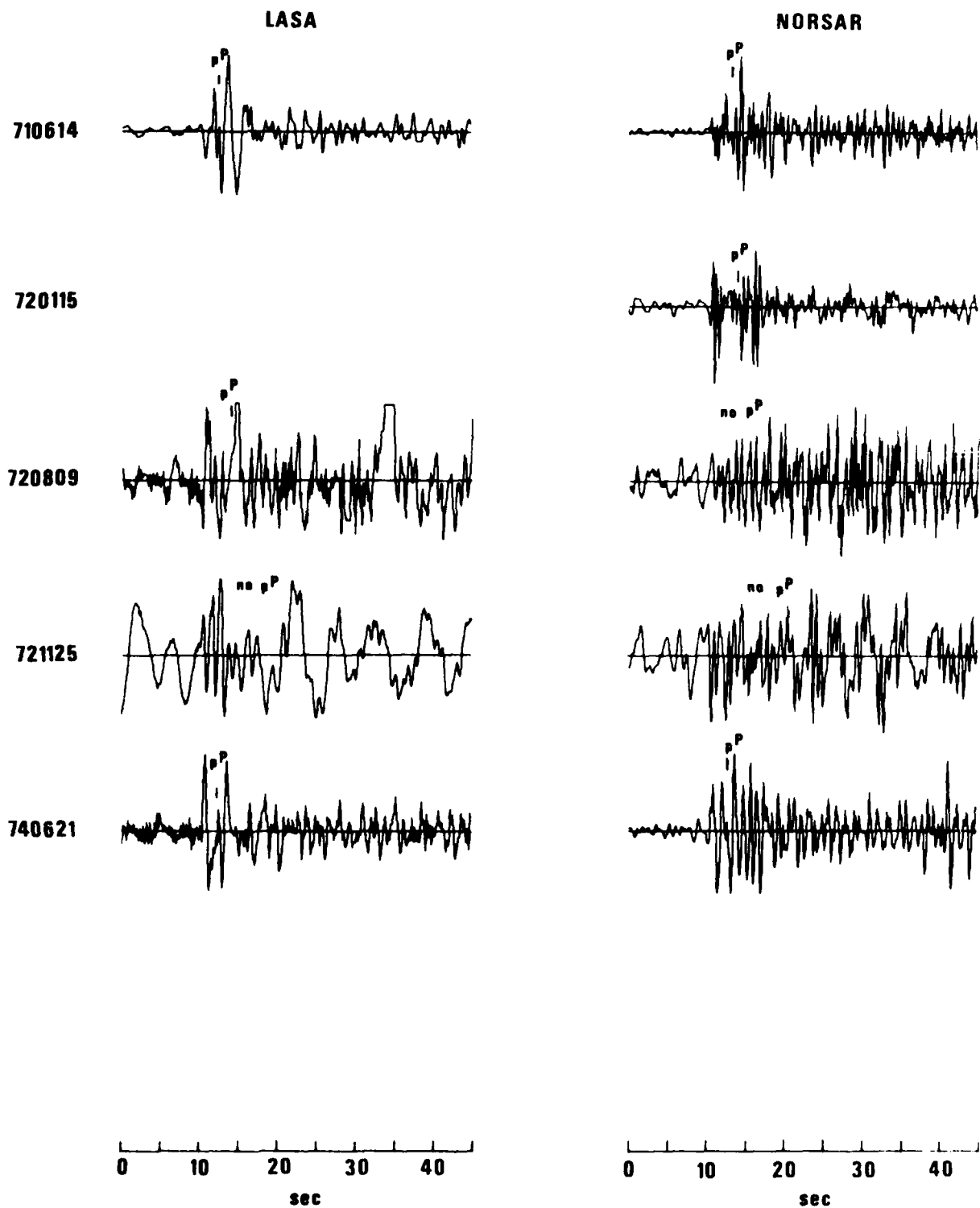


Figure 5 LASA and NORSAR short-period P waveforms for the Baikal earthquakes.

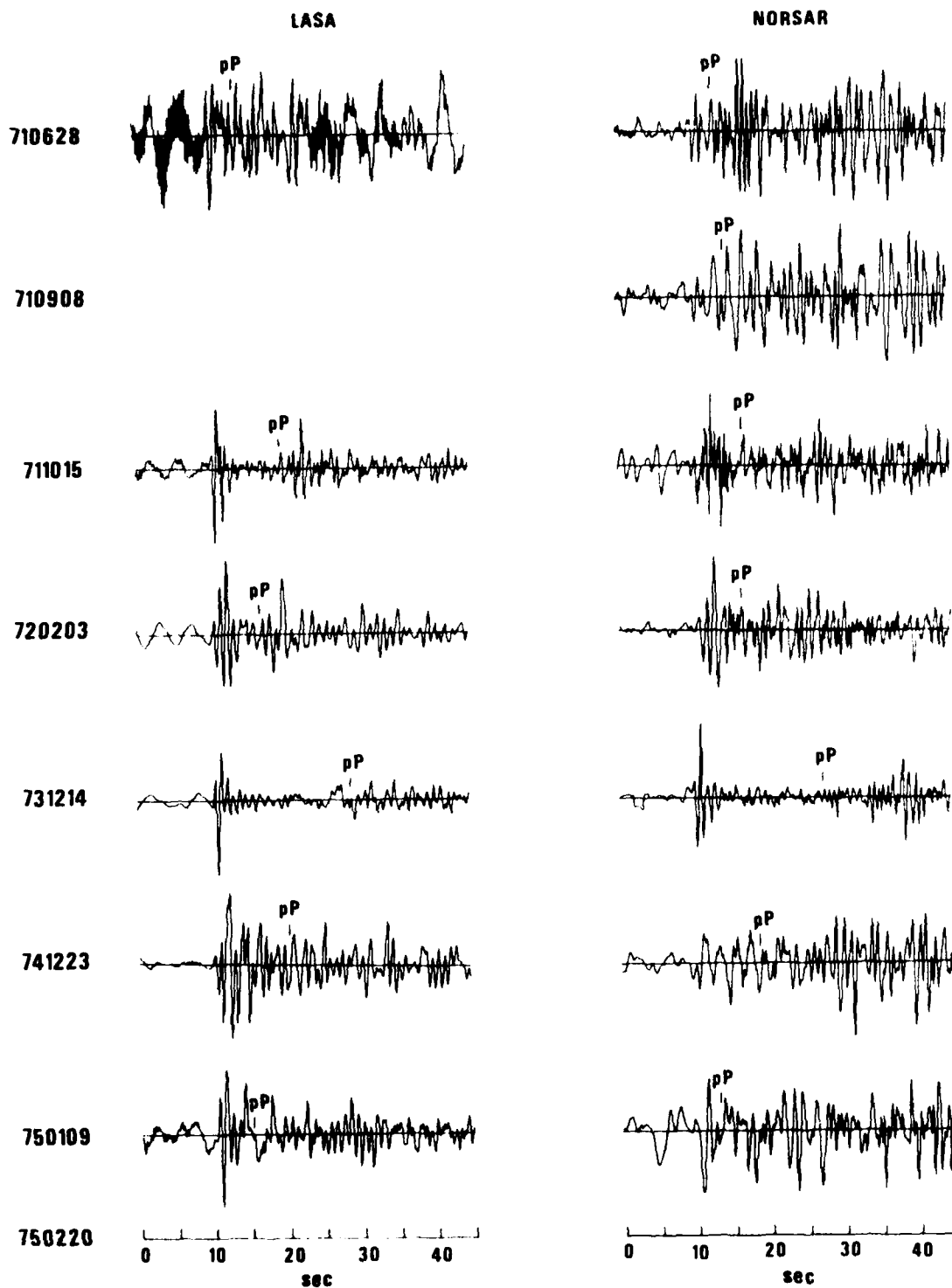


Figure 6 LASA and NORSAR short-period P waveforms for the Caucasus earthquakes.

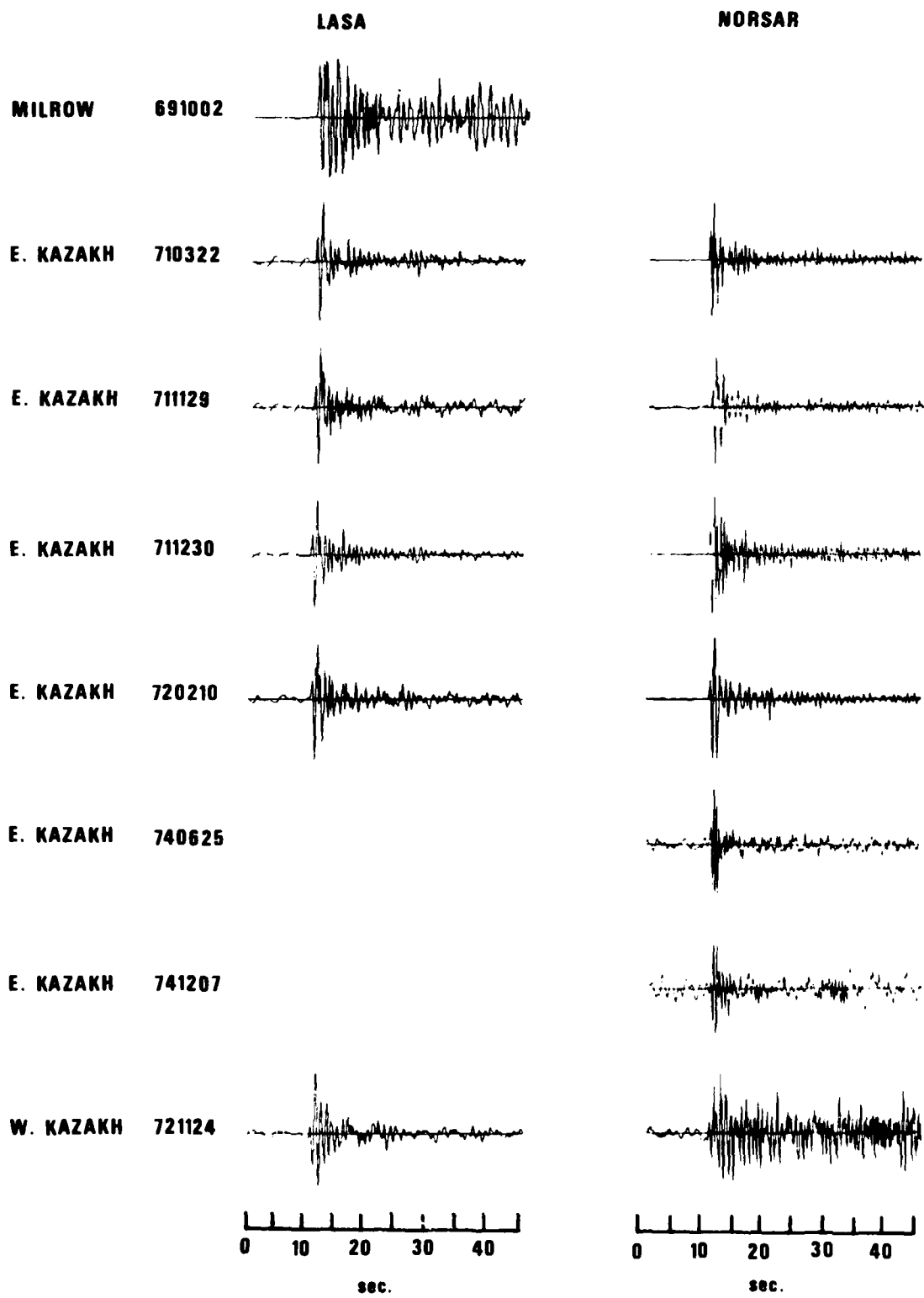


Figure 7 LASA and NORSAR short-period P waveforms for the explosions used in this study.

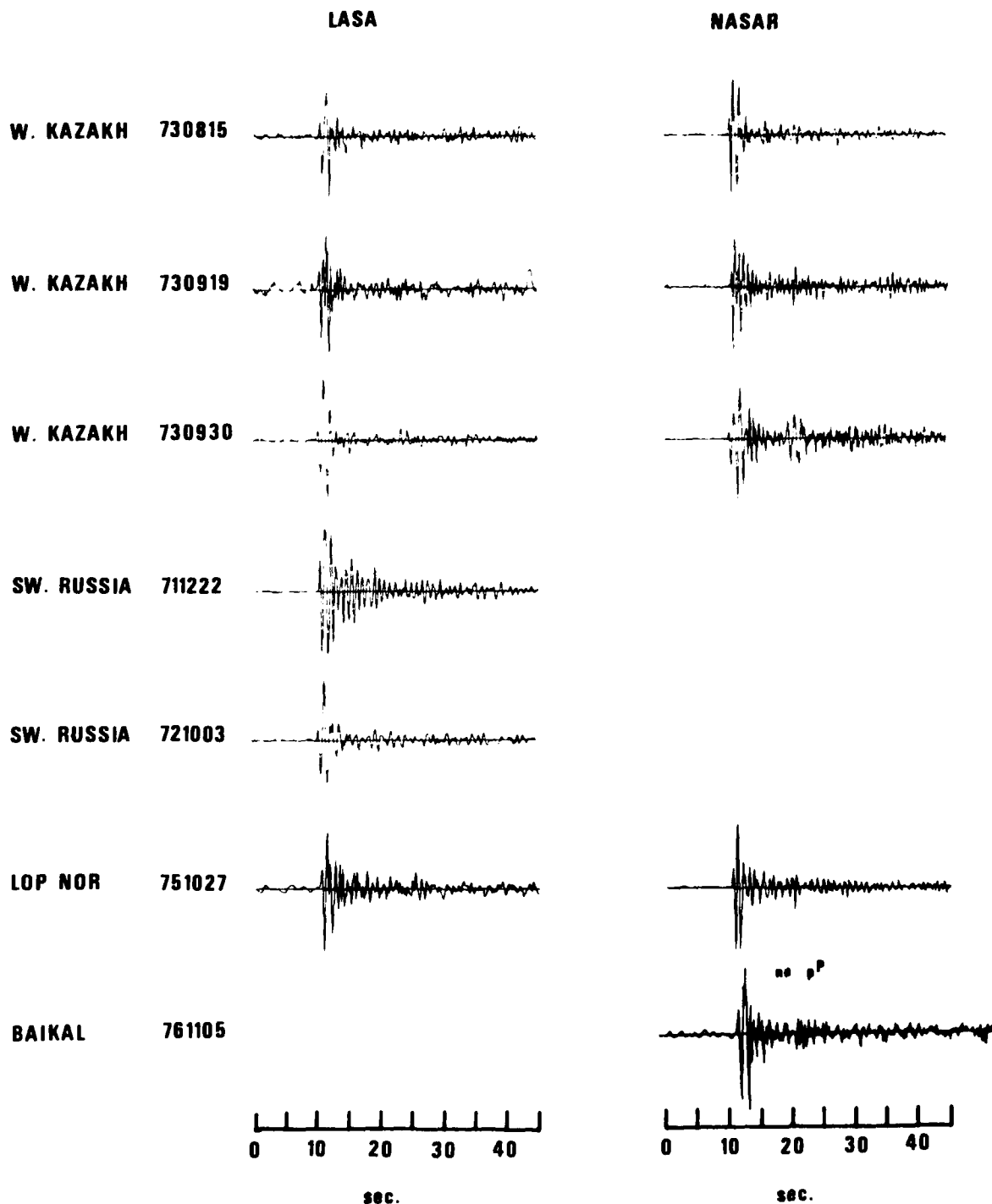


Figure 7 (Cont.) LASA and NORSAR short-period P waveforms for the explosions used in this study.

Short-period P waveforms for the Pamir earthquakes are shown in Figure 4. Again, focal mechanism solutions for these events could not be determined due to their small size ($m_b \leq 4.8$). For these events the presence of negative and positive first motions at teleseismic distances, without any definite overall pattern, indicates that they are not thrust faults and that there is probably no common source mechanism for them (Sobel et al., 1977a). The phase pP was present on some of the LASA and NORSAR records. There are many differences in the sign of first motion, frequency content, and waveform among these events; such dissimilarity is perhaps unexpected because of the epicenters of all but the 730103 and the 740220 events were located within a one-degree square on the earth's surface. Note, however, that this degree of variability was also found among recordings of Kamchatka events within such a small area by Blandford and Clark (1975). Clearly, no one signal represents the waveforms at LASA or NORSAR for these Pamir events. The frequency content of the NORSAR signals is strikingly higher than that of the LASA ones.

Short-period P waveforms for the Baikal earthquakes are shown in Figure 5. Again, small magnitudes ($m_b \leq 5.3$) preclude determination of source mechanisms for these events. However, the predominance of negative first motions at teleseismic distances suggests that these events are normal faults on steeply dipping planes, which agrees with known focal mechanisms for this region (Sobel et al., 1977b). Note that some LASA and NORSAR first motions are positive, indicating the vagaries of presumed first-motion directions for small-magnitude events. None of the waveforms are similar, and the contrast between NORSAR and LASA recordings is pronounced for at least two of the events, 710614 and 740621. The pP was observed at LASA or NORSAR for only three of the events, but in each case identification is not certain and resulted only from corroborating WWSSN recordings.

Short-period LASA and NORSAR P waveforms for the Caucasus earthquakes are shown in Figure 6. Again, we were not able to determine the focal mechanisms due to the small size ($m_b \leq 5.1$) of the events. The variable patterns of

Blandford, R., and D. Clark, 1975. Variability of seismic waveforms recorded at LASA from small subregions of Kamchatka, SDAC TR-75-12, Teledyne Geotech, Alexandria, Va. 22314.

negative and positive first motions at teleseismic distances suggest that these are not thrust faults and that probably no common source mechanism for all these events exists (Sobel et al., 1977c). Waveforms for the events were not similar at either LASA or NORSAR. The phase pP was apparently recorded, although poorly in most cases, at either LASA or NORSAR for all the earthquakes. In contrast to the previous four regions, the NORSAR signals for these Caucasus events do not appear to have higher frequency content than LASA recordings.

Short-period P waveforms for the explosions used in this study are shown in Figure 7. For three of the explosions, no signals were recorded at LASA due to the small size of the events ($m_b \leq 4.8$). Although several waveforms from nearby events were present at LASA and NORSAR from the two Kazakh test sites, only the East Kazakh signals recorded at LASA showed enough similarity that one waveform represented the entire group. This is true in spite of the fact that the explosion locations within either East or West Kazakh (Table II) were in close proxim.

Long-period waveforms at NORSAR

Of the three long-period arrays used, only NORSAR had enough good surface waves recorded to warrant discussion here. All observed Rayleigh waves at NORSAR for the earthquake regions are shown in Figures 8 through 12; those for the explosions are shown in Figure 13. Missing records for an event indicate that no data or no detected signal for the time period existed. The beams are all formed with delays corresponding to a velocity of 3.6 km/sec. Recordings displayed here begin at approximately the group arrival time of 4.5 km/sec energy and end at the group arrival time of 2.7 km/sec energy, and they are roughly aligned according to time after origin time.

Figure 8 shows the long-period NORSAR waveforms for the Kamchatka earthquakes. Epicentral distance is roughly 65° . All the traces show effects of lateral refractions predicted by ray tracing for 20-second Rayleigh waves from Kamchatka to NORSAR in von Seggern and Sobel (1976). The maxima in the period range 17-23 sec, normally used for M_s estimation, arrives with a group velocity of roughly 3.0 km/sec in all cases. While there was some similarity among the waveforms, there was also considerable variability relative to the small

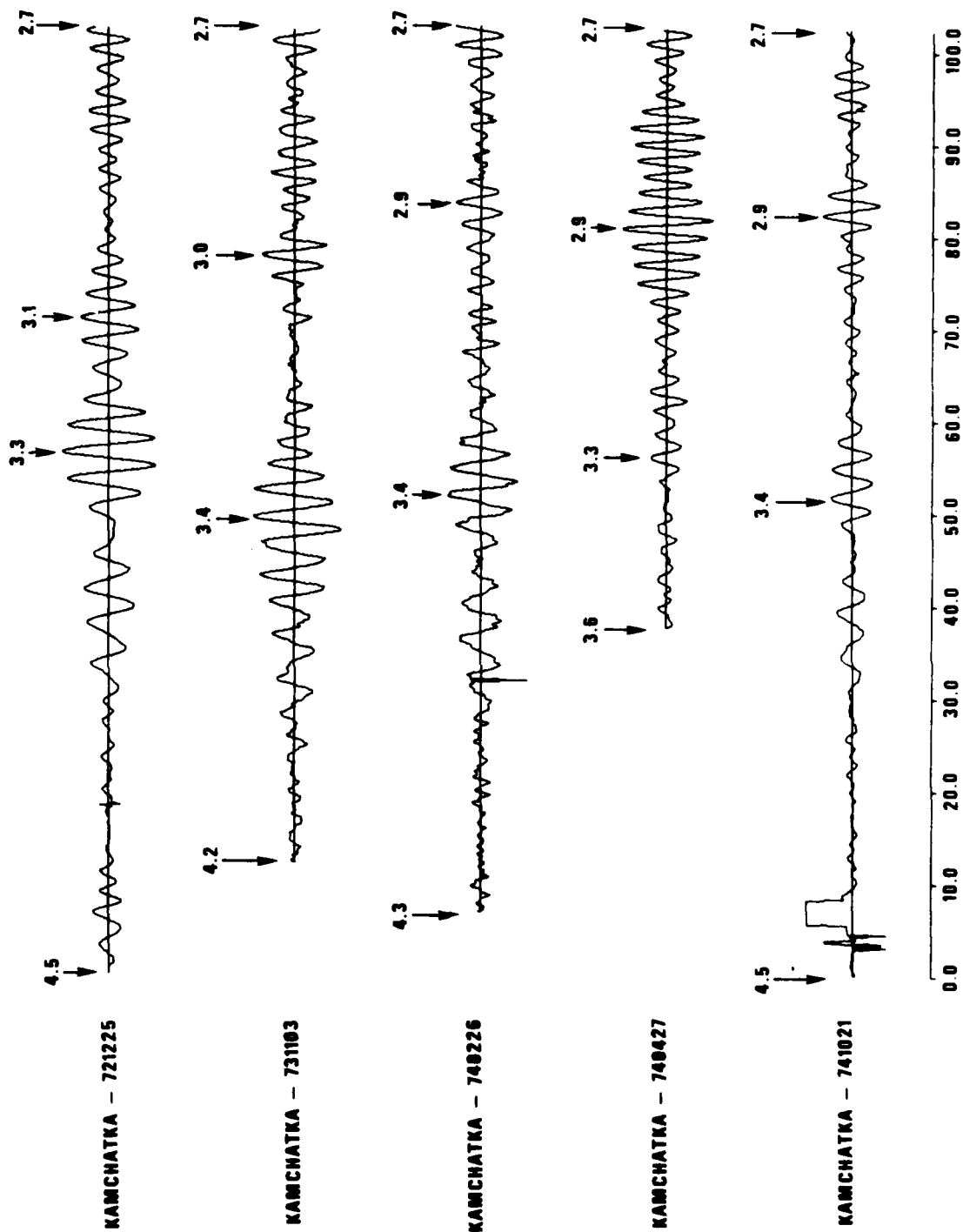


Figure 8 NORSAR long-period waveforms for the Kamchatka earthquakes.

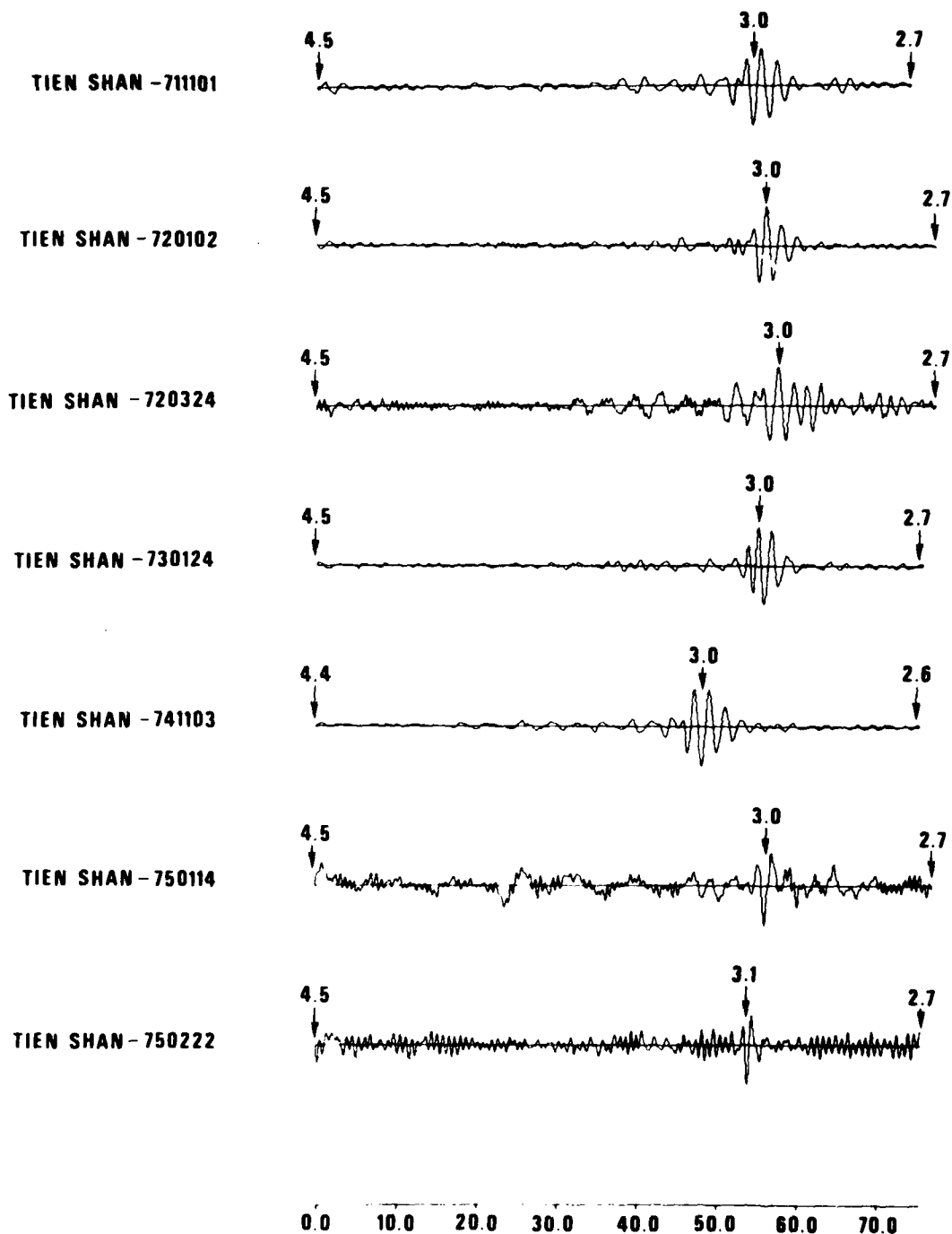


Figure 9 NORSAR long-period waveforms for the Tien Shan earthquakes.

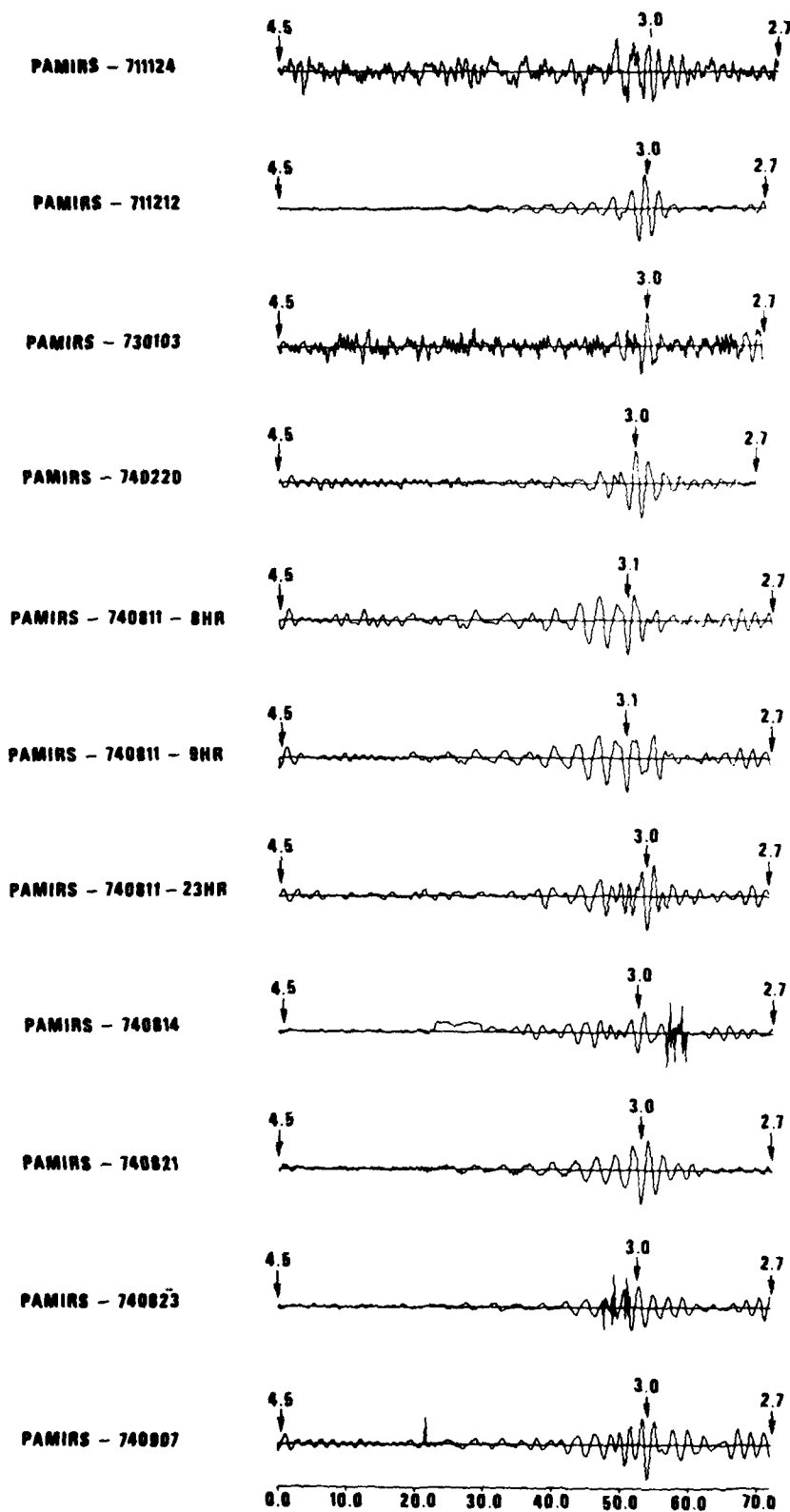


Figure 10 NOR SAR long-period waveforms for the Pamir earthquakes.

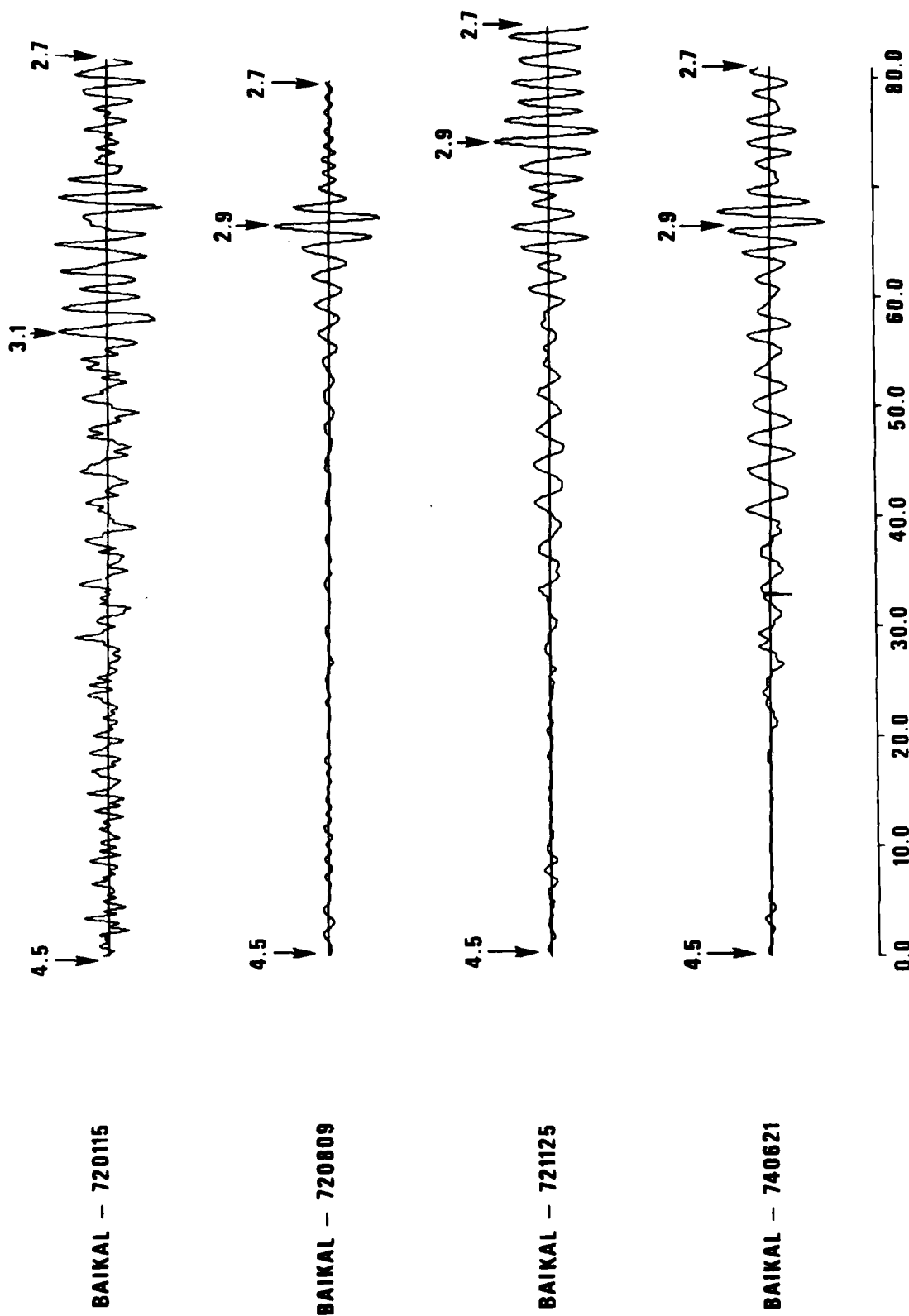
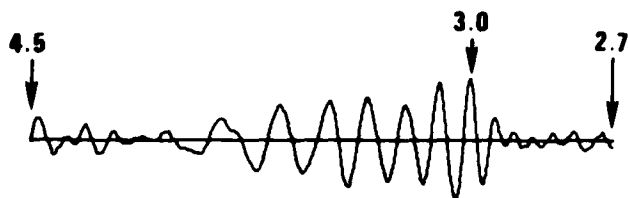


Figure 11 NOR SAR long-period waveforms for the Baikal earthquakes.

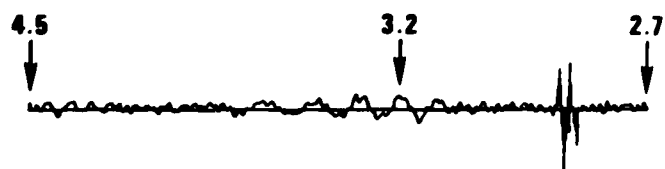
CAUCASUS - 710908



CAUCASUS - 711015



CAUCASUS - 731214



CAUCASUS - 750109

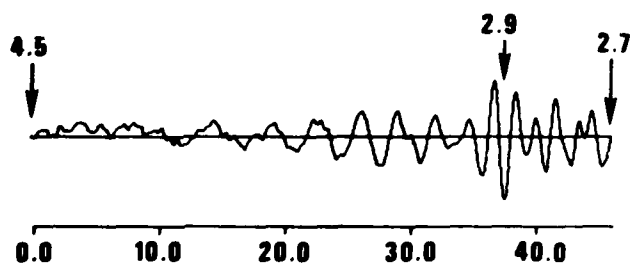
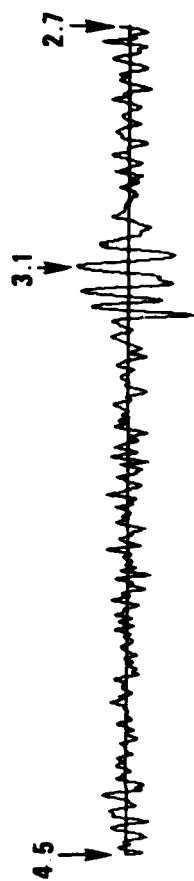
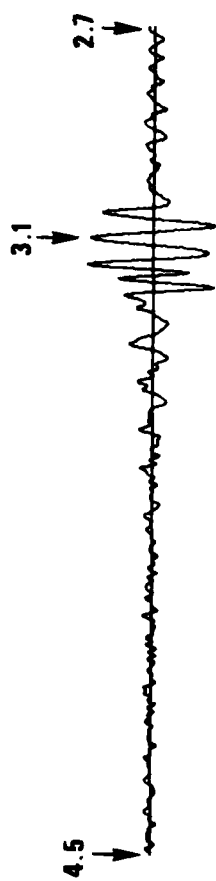


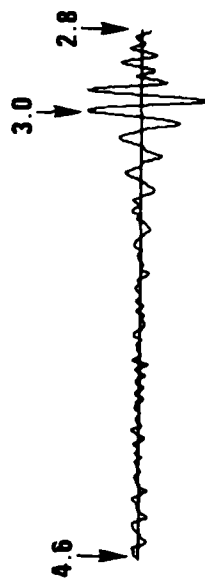
Figure 12 NORSAR long-period waveforms for the Caucasus earthquakes.



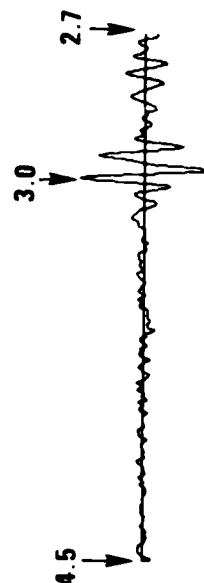
E. KAZAKH - 711129



E. KAZAKH - 711230



SW. RUSSIA - 711222



SW. RUSSIA - 721003

0.0 10.0 20.0 30.0

Figure 13 NORSAR long-period waveforms for representative explosions used in this study.

dimension of the source area. The least similar record of the group is for the 740427 event, which is also the farthest north of the five events. The ray paths from Kamchatka to NORSAR traverse the continental margins of Northeast Asia and Northern Scandinavia, both sites of possible lateral refractions which could create the multipathing observed at NORSAR. The waveforms may also be affected by the spatial relation of the exact hypocenters to the structure of the dipping lithospheric plate under Kamchatka and by the frequency-dependent source excitation.

Figure 9 shows the NORSAR long-period waveforms for the Tien Shan earthquakes. The epicentral distance is roughly 45° . All records have approximately the same arrival time of 20-second energy, contained within a distinct Airy phase. Ray paths to NORSAR are entirely continental, which explains the arrival time and shape of this Airy phase. No evidence exists of multipathing predicted by the 20-second Rayleigh-wave ray tracing of Sobel and von Seggern (1976), but the predicted phase arrival times were not greatly different. While the first five events have several cycles in the Airy phase, and the waveforms show some similarity, events 750114 and 750222 apparently have a more concentrated Airy phase. These latter two events occurred geographically in the middle of the other five events.

The NORSAR long-period records for the Pamir events are shown in Figure 10. The epicentral distance is roughly 40° . Little, if any, multipathing is present, and the low Rayleigh-wave group velocity for 20-sec energy reflects the continental path of the rays from the Pamirs to NORSAR. An Airy phase is distinct only on some recordings, and it is not as strong as for the Tien Shan events. All except the first four events occur within a small geographic area, and yet the waveforms recorded at NORSAR show only some similarity. Although differences between the second and third 740811 events, for instance, could be attributed to focal depth, our depth determinations (Table I) indicated that they had similar depths. Tectonically active structures in the Northern Pamirs may in part be responsible for differences in waveforms from event located in this region.

Figure 11 shows the NORSAR long-period signals for events in the Baikal rift zone. The epicentral distances are roughly 50° . There is evidence of

multipathing on the 720115 and 721125 records. All the waveforms are different because of refraction effects within the Baikal rift zone or because the rays pass through the Ural Mountains. The 720809 waveform is especially different, and the location of this event (Table I) is apart from others of the group. The late arrivals of 20-second energy (2.9 to 3.1 km/sec) reflect the totally continental ray paths.

NORSAR long-period records for the Caucasus events are shown in Figure 12. The epicentral distance is roughly 30° . The great dissimilarity among these waveforms may partially result from refraction effects as they pass through the northern border of the Black Sea and Caspian Sea sedimentary depression. Note that while events 711015 and 731214 are located close geographically, they have totally dissimilar waveforms. This lack of shorter-period energy for the 731214 event is supporting evidence for the reported NEIS subcrustal depth of 79 km. The Caucasus waveforms do not show distinct Airy phases such as those seen on the Tien Shan or Pamir waveforms.

Figure 13 shows the Rayleigh-wave signals recorded at NORSAR for two East Kazakh explosions ($\Delta \sim 38^\circ$), located in close geographical proximity and two Southwest Russia explosions ($\Delta \sim 25^\circ$), separated by approximately three degrees of epicentral distance. For each pair the waveforms are similar. The low Rayleigh-wave velocities reflect the continental ray paths to NORSAR. No multipathing is observed in these records. Note that NORSAR did not detect Rayleigh waves from either the Baikal or the Lop Nor explosion in Table II.

SIGNAL ANALYSIS

In this section are discussed effects of source radiation pattern, source spectral shape, and inelastic attenuation on observed body-wave and surface-wave signals for events in this study.

Source Mechanisms

Efforts were made to identify the effects of source mechanism on observed body-wave and surface-wave phases from the earthquakes studied here. From a knowledge of the tectonic settings of these earthquake, the Kamchatka events are assumed to be thrust faults, the Tien Shan, Pamir, and Caucasus events are assumed to be strike-slip or thrust faults, and the Baikal events are assumed to be normal faults. The only well-defined source mechanism for any of the earthquakes studied here was for the 730304 event in Kamchatka (Stauder and Maulchin, 1976), a thrust fault and the largest event in our earthquake data set ($m_b = 6.0$). Determination of the fault plane for an earthquake whose magnitude is below 6.0 is generally not reliable with teleseismic data because P waves are not recorded on the long-period seismograms and, except for the 730304 Kamchatka event, all earthquakes have $m_b < 6$. Short-period first motions have been read from array, HGLP, and WWSSN recordings for all the earthquakes in the study. An example typical of the ambiguous data sets for our events is shown in Figure 14. On the basis of such plots alone, fault planes could not be determined because dilatational and compressional first motions did not separate. A composite plot of all Kamchatka data showed a predominance of positive first motions, suggesting that these events are indeed thrust faults. A similar composite plot of all the Baikal data showed a predominance of negative first motions, suggesting that the Baikal events are normal faults. No common source mechanism was clearly indicated for the Tien Shan, Pamir, or Caucasus earthquakes.

Attempts were made to find the LR amplitude radiation pattern for several of the events by plotting the antilogs of the M_s values. Typical results for an event are shown in Figure 15. (The maximum antilog is plotted on the

Stauder, W., and L. Mualchin, 1976. Fault motion in the large earthquakes of the Kurile-Kamchatka Arc and of the Kurile-Hokkaido corner, J. Geophys. Res., 81, 297.

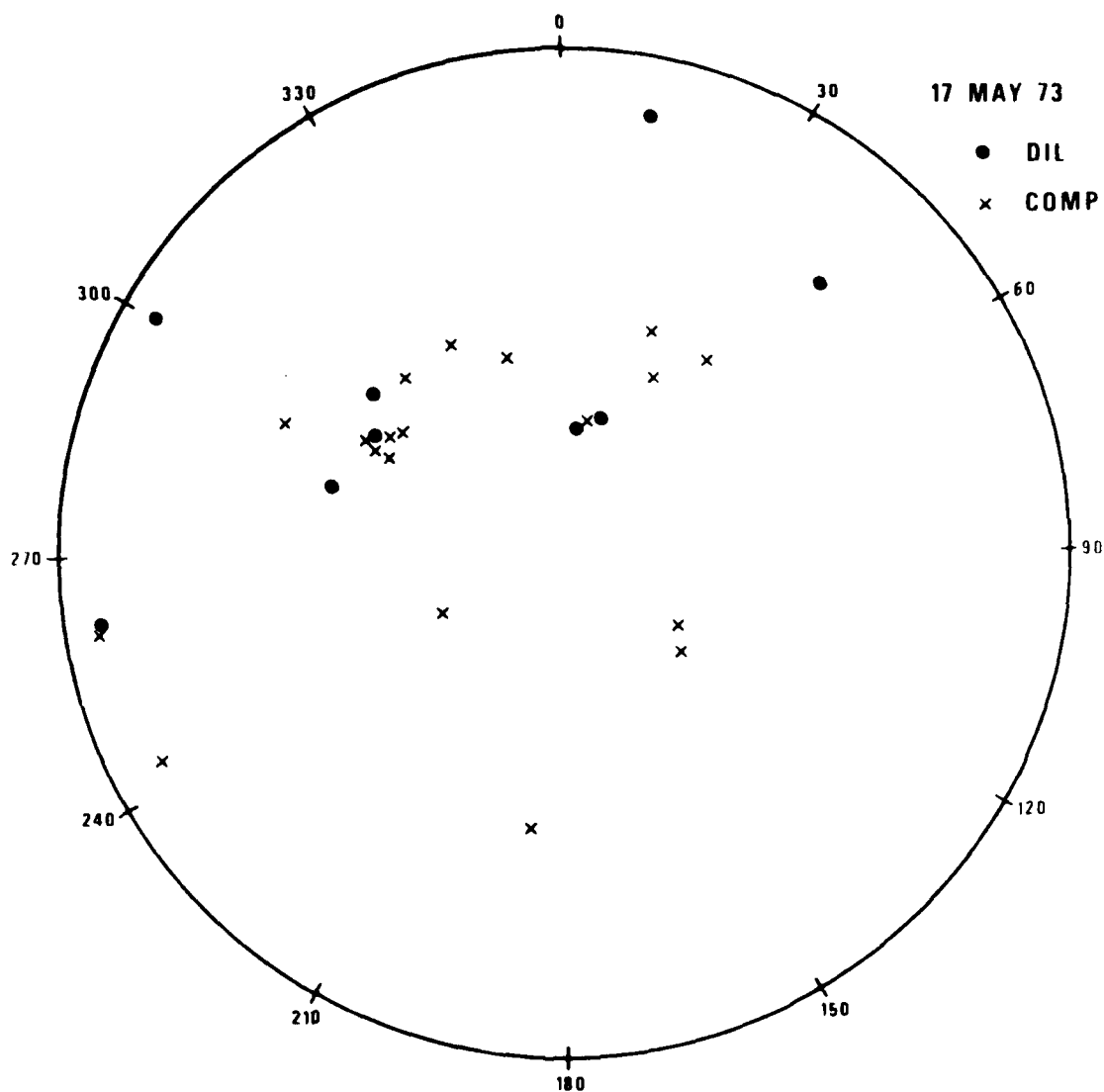


Figure 14 First motions for a Tien Shan earthquake (730517) in the lower half of the focal sphere (Wulff net).

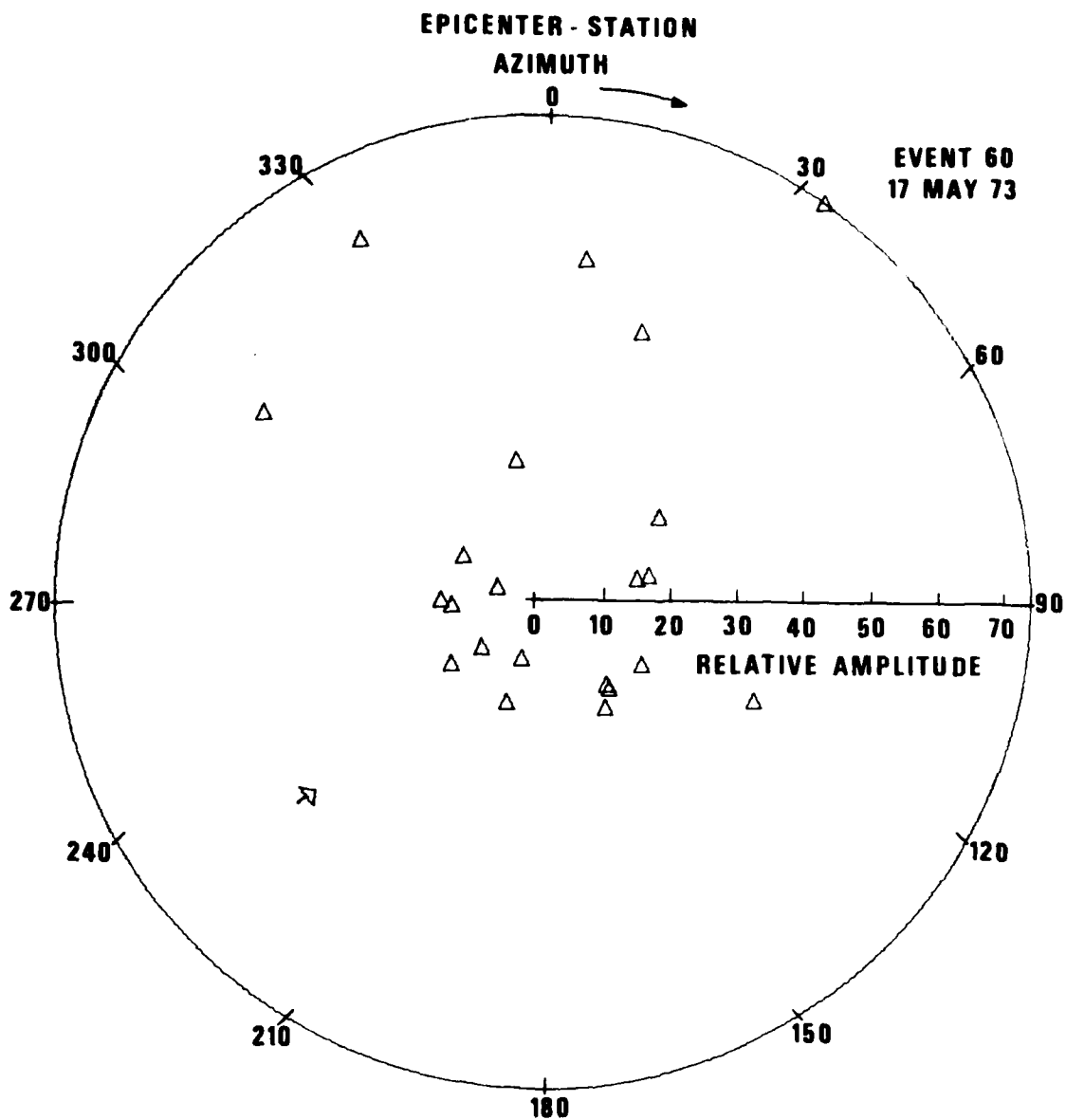


Figure 15 Observed LR amplitudes normalized back to the source ($T=20$ sec) for a Tien Shan event on 730517.

outer circle, and all other antilog values are scaled linearly between the center of the plot and the radius of the circle. (The data point with an arrow is a noise measurement). Few observed distributions of amplitudes conformed to any quadrupole radiation pattern. The scatter of data points was a result of the large epicentral distances involved, because deviations due to propagation path differences accumulated to the point where they overwhelmed the initial radiation pattern effect (Aki, 1970). For Rayleigh waves of 20-second period, a method of predicting amplitudes by geometrical ray tracing has been presented by von Seggern and Sobel (1975). Figure 16 illustrates the path of 20-second Rayleigh waves that emanated from an event in the Tien Shan Mountains. The refraction effect of the earth's non-uniformity in 20-second LR phase velocity causes focusing, defocusing, and multipathing and, therefore, large teleseismic amplitude variations. M_s residuals can be predicted in some cases from the ray-pattern density near each of the stations. No attempt was made to relate ray-tracing predictions to observed LR amplitudes since we could not correct for source mechanism and did not have enough information to correct for lateral differences in attenuation. Source locations only 100 km apart on the earth's surface will produce large amplitude differences at certain stations due to changing patterns of focusing and defocusing (von Seggern and Sobel, 1976). This phenomenon precludes determining source radiation patterns using a master-event technique, unless there is a small separation between epicenters.

Corner Frequencies, Long-Period Spectral Levels, and Seismic Moments

In the five Eurasian reports, amplitude spectra were displayed for the LASA and NORSAR short-period P recordings for all the earthquakes and explosions. Some examples of these spectra are shown in Figure 17 to illustrate how spectral parameters were determined. The mean of the noise sample was removed from the signal and noise samples shown on the left side of each figure. Then the signal and noise samples were tapered by one half a cosine bell over 6 pts at each end of the 6.4 second windows (10 s/sec). Instrument

von Seggern, D. H., and P. Sobel, 1975. Experiments in refining M_s estimates for seismic events, SDAC Report No. TR-75-17, Teledyne Geotech, Alexandria, Virginia 22314.

TIENT SHAN
WESTERN EVENT
IN BASIN
(EV 59 41.15N 82.16E)

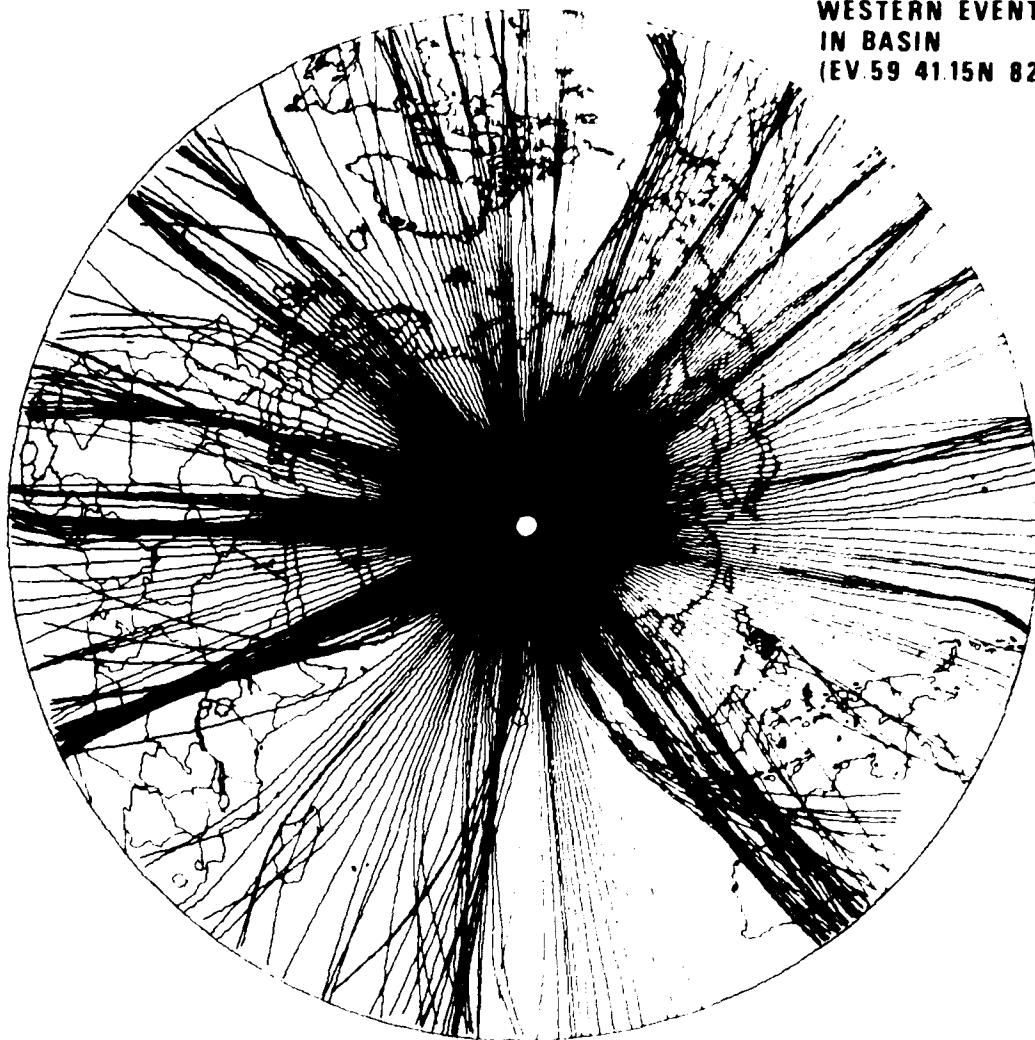


Figure 16 Predicted LR raypaths ($T=20$ sec) for a Tien Shan event on 730124.

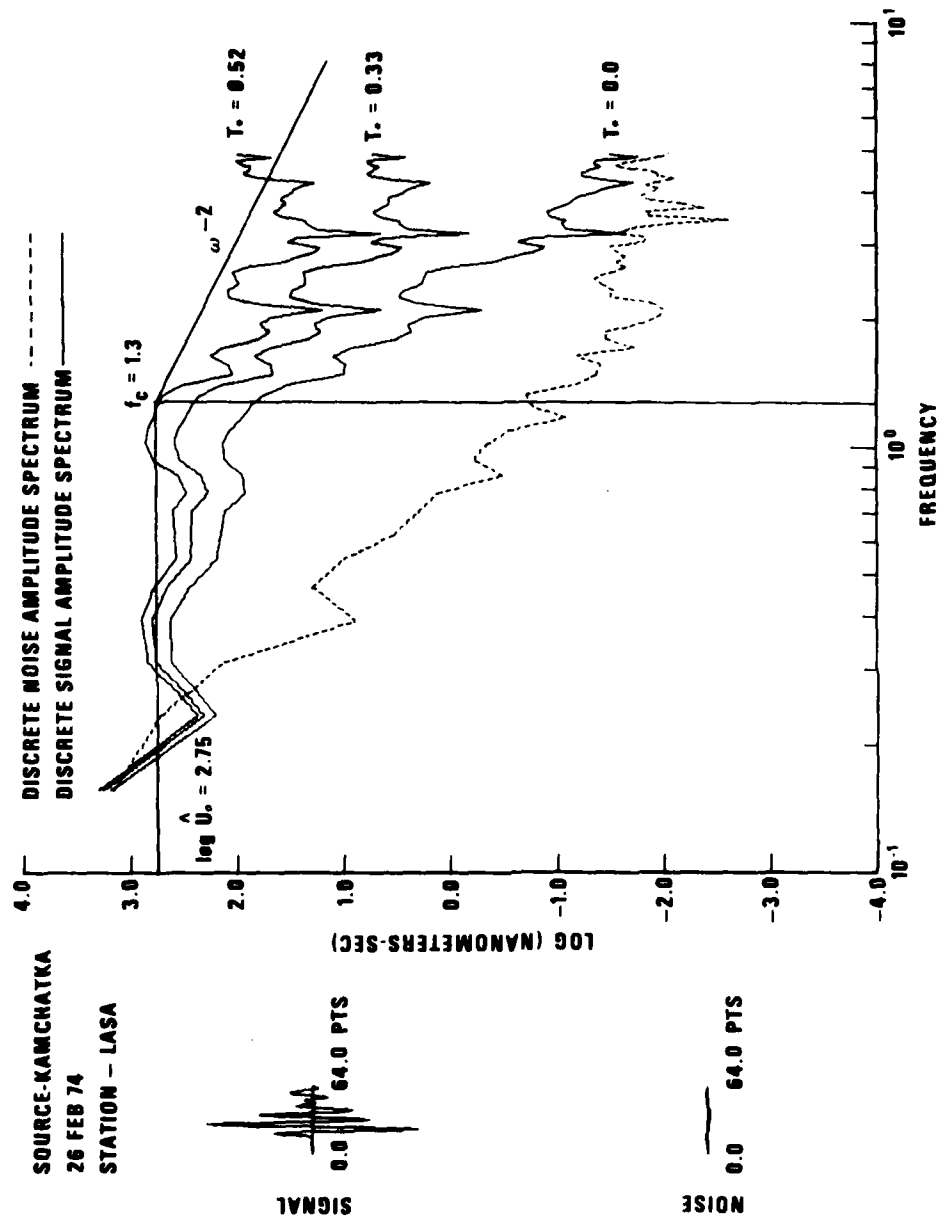


Figure 17 LASA A0 and NORSAR C3 subarray spectra of P waves from the 740226 Kamchatka earthquake, the 720102 Tien Shan earthquake, and the 730815 W. Kazakh explosion.

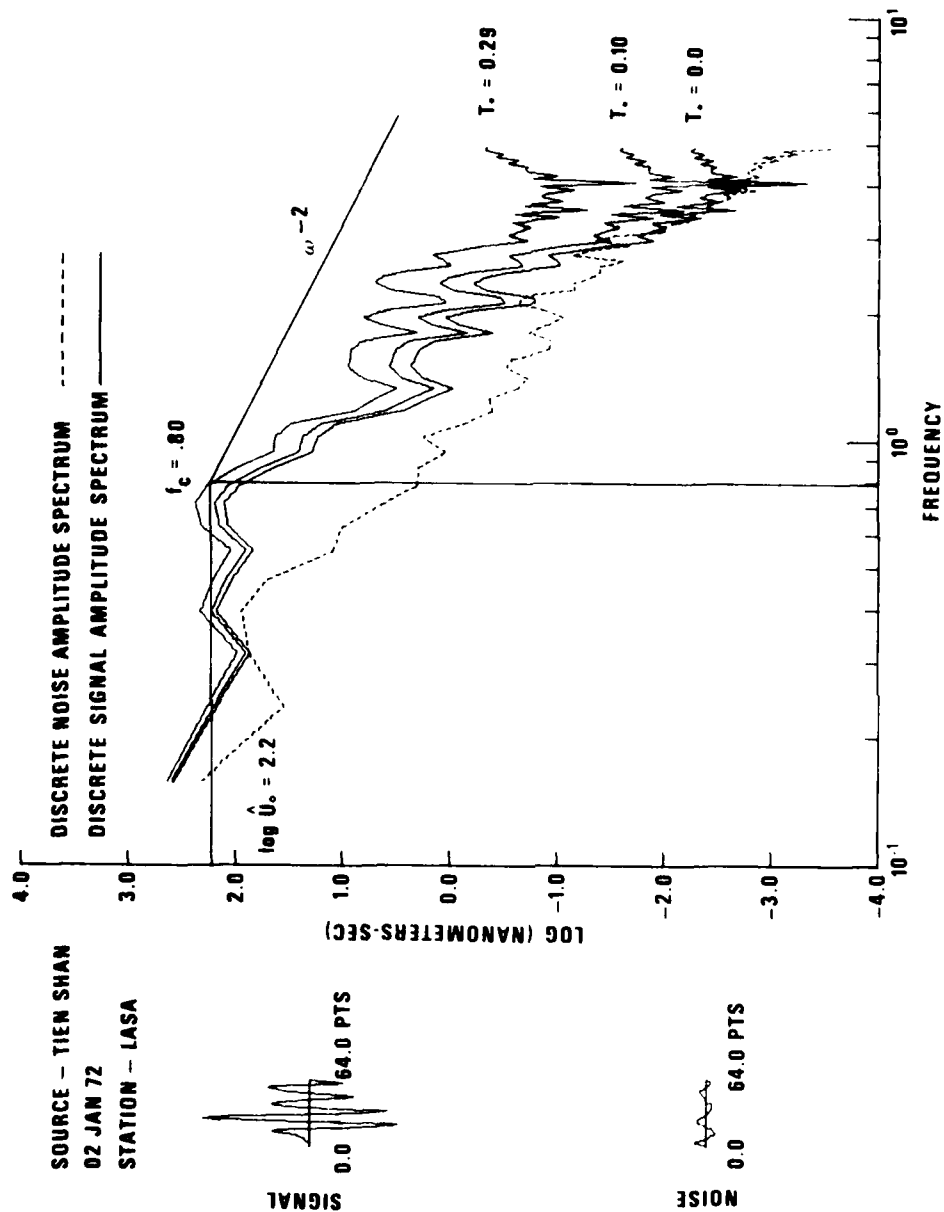


Figure 17 (cont.) LASA A0 and NORSAR C3 subarray spectra of P waves from the 740226 Kamchatka earthquake, and 720102 Tien Shan earthquake, and the 730815 W. Kazakh explosion.

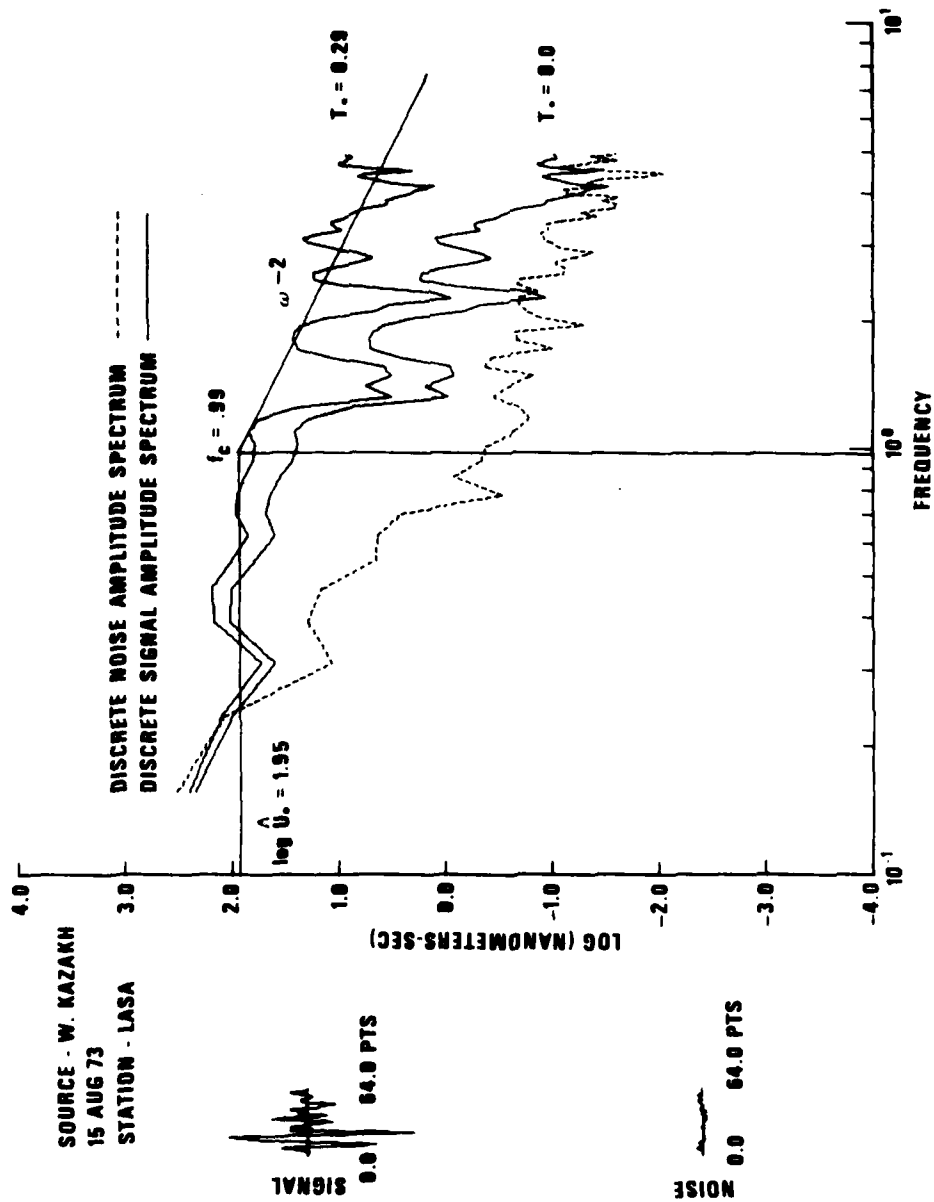


Figure 17 (cont.) LASA A0 and NORSAR C3 subarray spectra of P waves from the 740226 Kamchatka earthquake, and 720102 Tien Shan earthquake, and the 730815 W. Kazakh explosion.

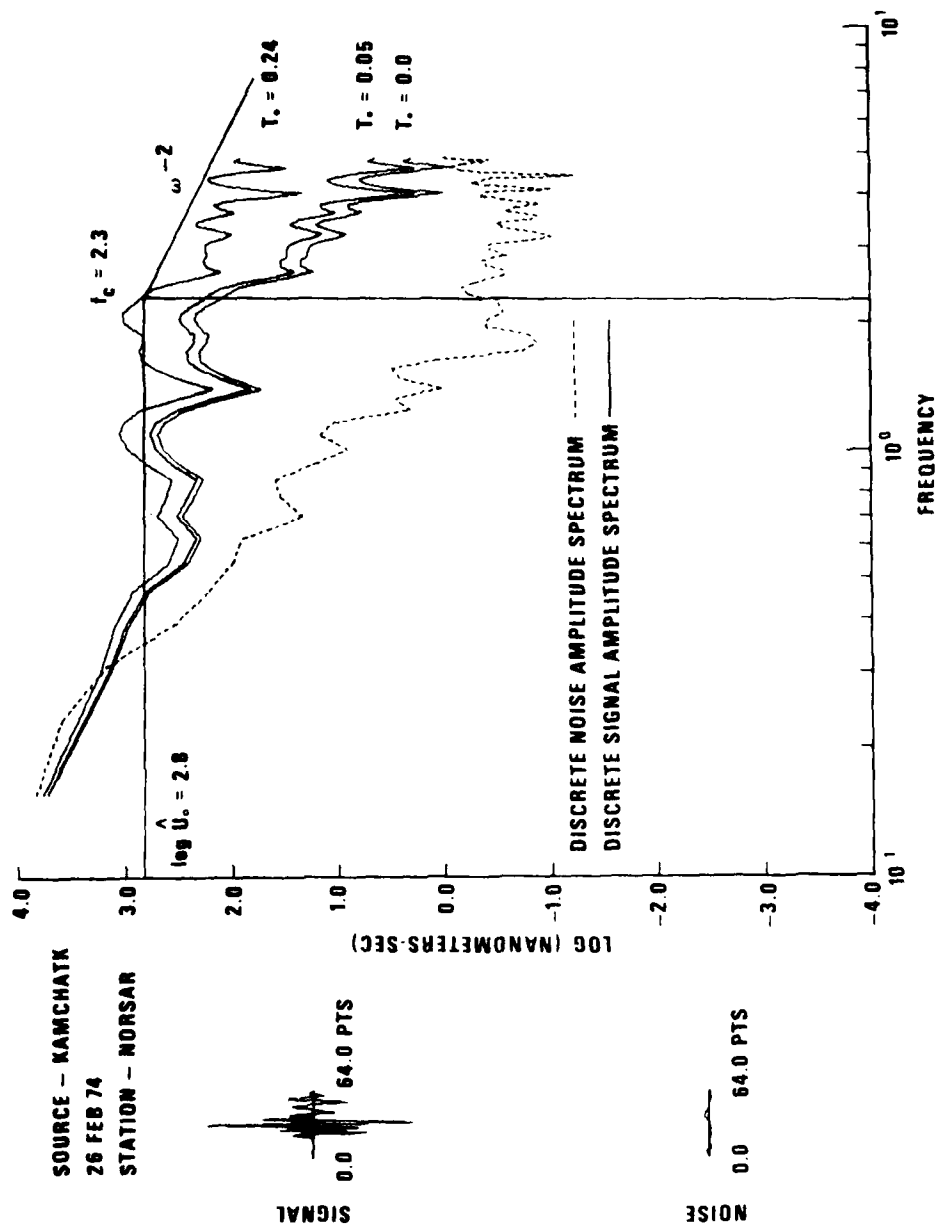


Figure 17 (cont.) LASA A0 and NORSAR C3 subarray spectra of P waves from the 740226 Kamchatka earthquake, and 720102 Tien Shan earthquake, and the 730815 W. Kazakh explosion.

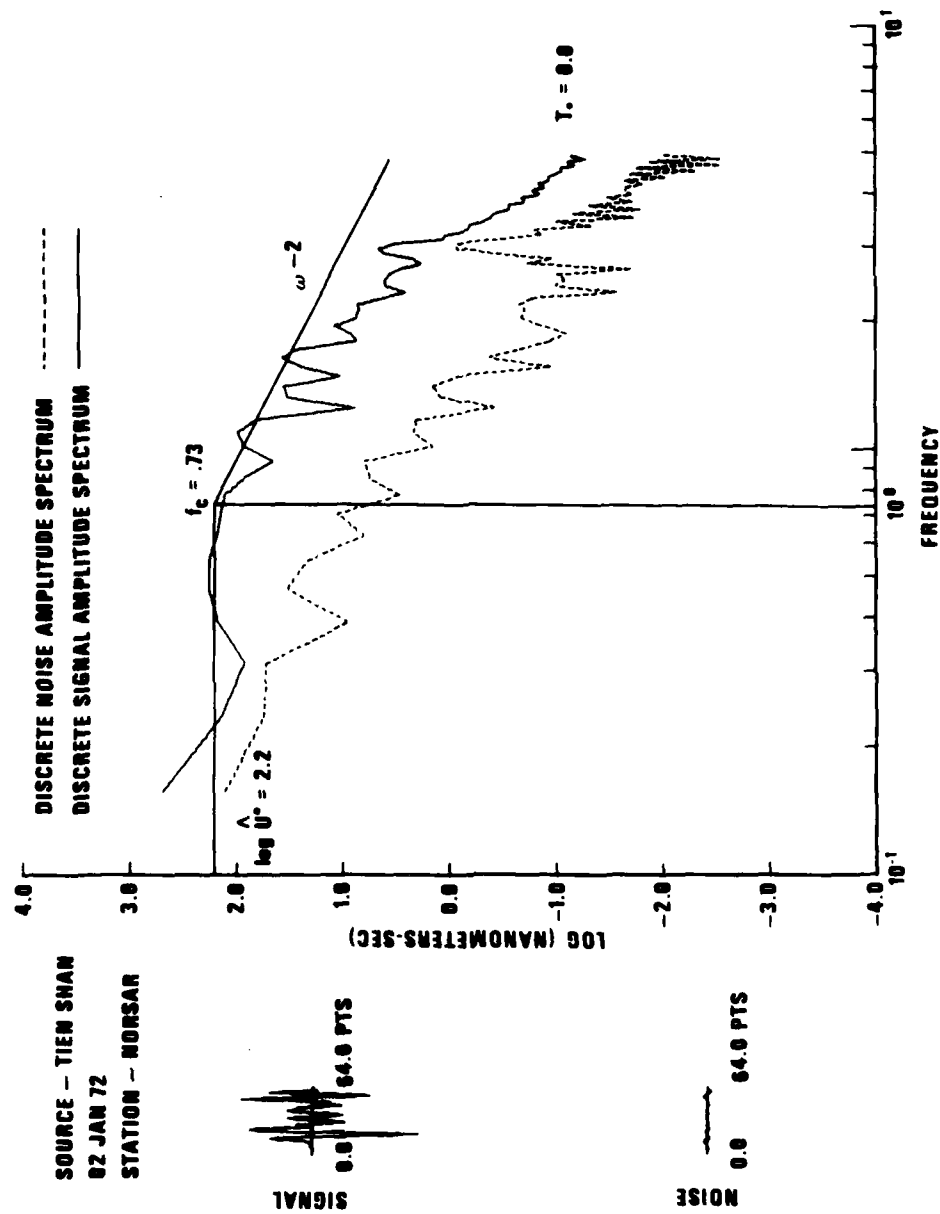


Figure 17 (cont.) LASA A0 and NORSAR C3 subarray spectra of P waves from the 740226 Kamchatka earthquake, and 720102 Tien Shan earthquake, and the 730815 W. Kazakh explosion.

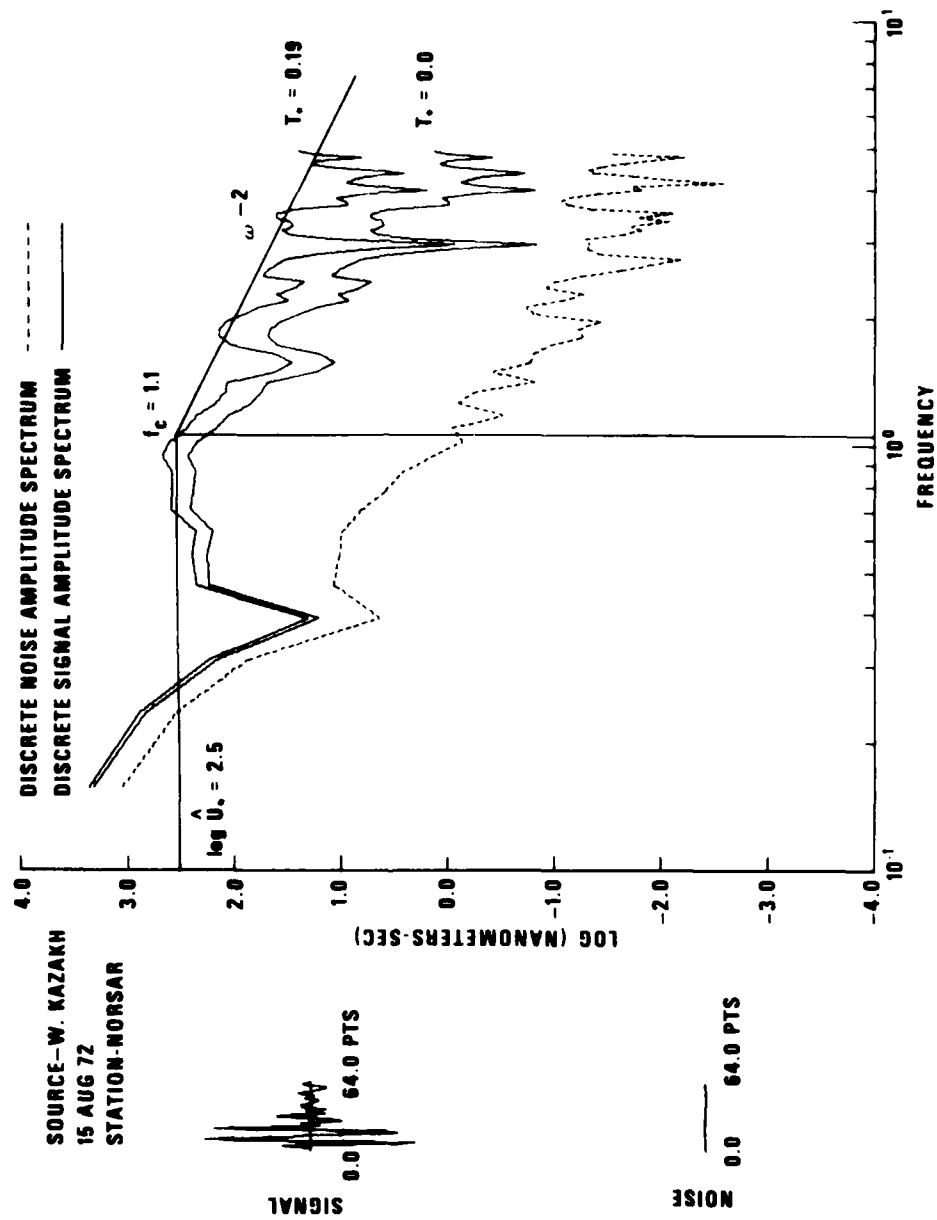


Figure 17 (cont.) LASA A0 and NORSAR C3 subarray spectra of P waves from the 740226 Kamchatka earthquake, and 720102 Tien Shan earthquake, and the 730815 W. Kazakh explosion.

response was removed from the raw spectra to get ground displacement ($t^*=0$), but noise spectra have not been subtracted from the signal spectra. Attenuation was removed by multiplying by the factor $\exp[-\pi f t^*]$ with t^* values (determined in the next section of this report) in order to correct them back to the source. An f^{-2} source model was used for both earthquakes and explosions, and an f^{-3} source model was also used for earthquakes only.

Corner frequencies, long-period spectral levels, and seismic moments have been estimated from the resulting source spectra. Corner frequencies were estimated with the assumptions of complete stress drop and an f^{-2} or f^{-3} asymptotic relation at high frequencies. Both corner frequencies (f_c) and long-period spectral levels (\hat{U}_0) are shown in Figure 17. Occasionally spectra for 25.6-second windows were computed for cases where the signal-to-noise ratio was high. However, for these cases the shapes of the spectra were sufficiently close to those for the 6.4-second windows that little or no additional information was gained.

Seismic moment was calculated from the long-period spectral levels $|U_0|$ using the relation (Hanks and Thatcher, 1972)

$$M_0 = \frac{4\pi\rho\alpha^3 |\hat{U}_0|}{R_{\theta\phi} D}$$

where $R_{\theta\phi}$ was assumed to be unity due to lack of knowledge of the focal mechanism, values of density (ρ) and compressional velocity (α) appropriate to the source region and depth were used, and the divergence factor D was applied (Ben-Menahem et al., 1965). Graphs of moment versus corner frequency are shown in Figures 18 and 19 for all earthquake data at LASA and NORSAR. The events fall between or close to the 100-bar and 1-bar stress drop lines of Hanks and Thatcher (1972), indicating that they are generally of intermediate stress drop. The Kamchatka events, which are generally of higher magnitudes than earthquakes from the other regions, generally possess higher moments and greater stress drops. The Baikal events have generally lower stress drops than the other earthquakes. The M_0 vs. f_c plots can be interpreted in terms

Hanks, T., and W. Thatcher, 1972. A graphical representation of seismic source parameters, J. Geophys. Res., 77, 4393.

LASA DATA

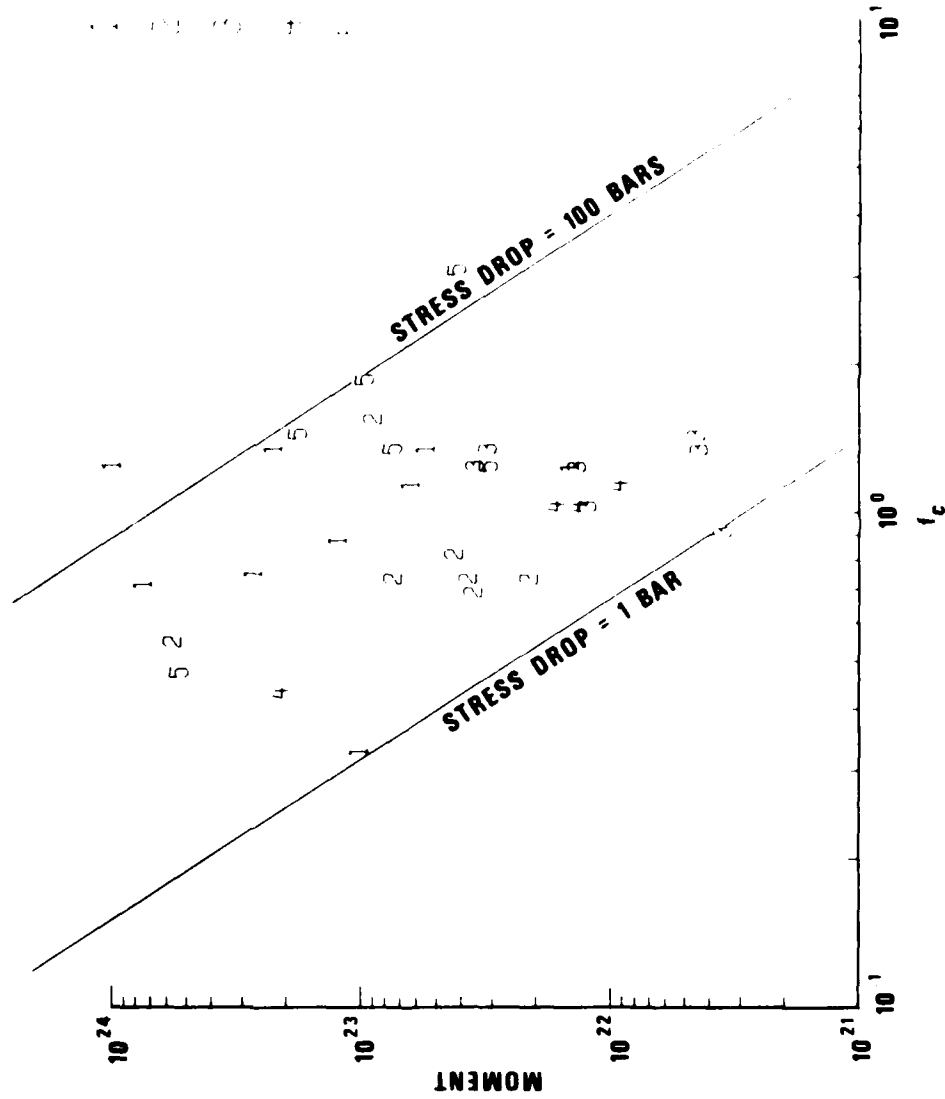


Figure 18 Seismic moment versus corner frequency for earthquakes from all regions from LASA P recordings.

NORSAR DATA

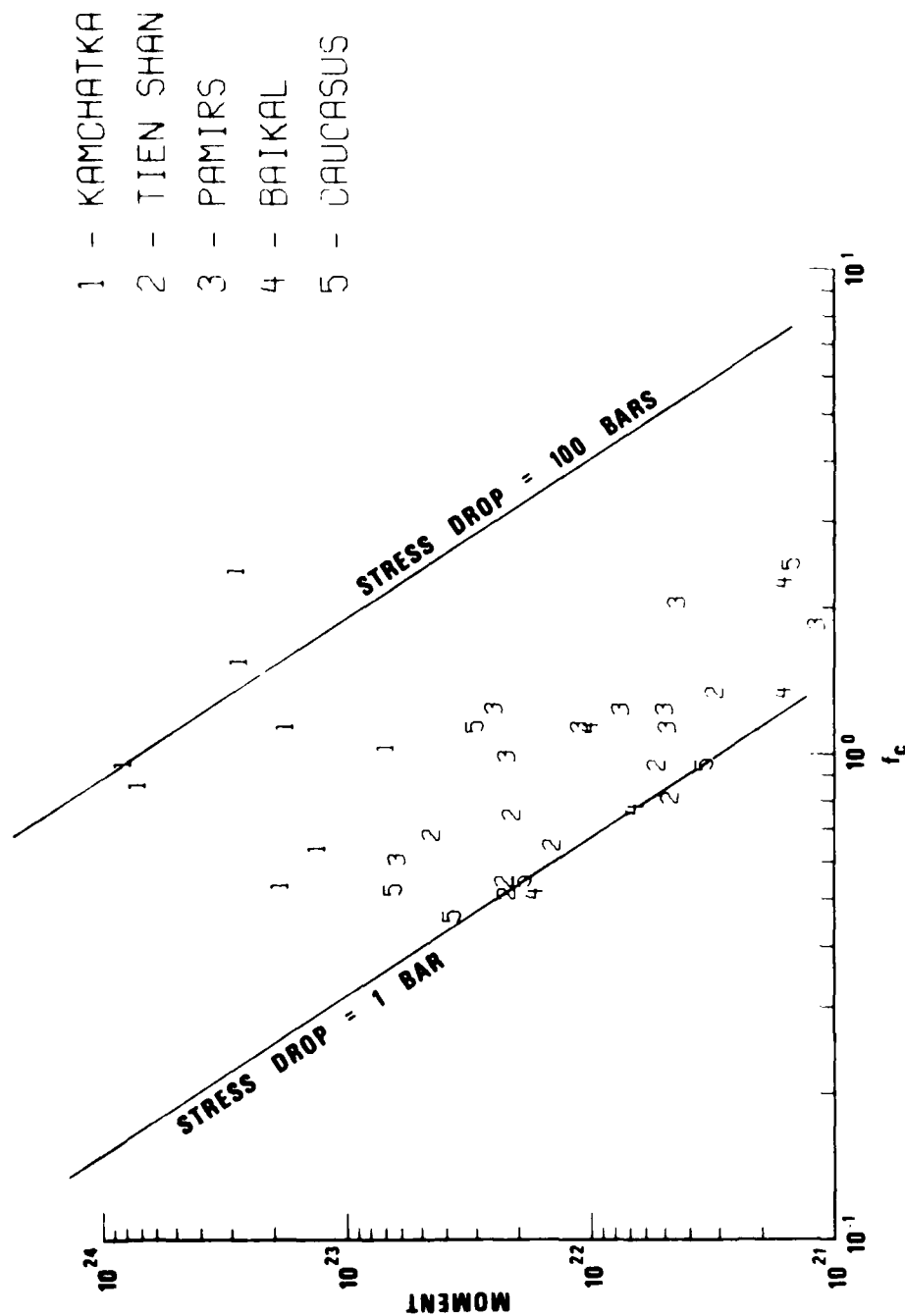


Figure 19 Seismic moment versus corner frequency for earthquakes from all regions from NORSAR P recordings.

of source dimensions rather than stress drop (Thatcher and Hanks, 1972). In either case, the lower the corner frequency at a given M_0 for earthquakes of a region, the easier they are to discriminate from explosions. Any differences between the LASA and NORSAR data sets for any earthquake region can be attributed either to errors in determining the long-period signal levels because few of the estimates were made with certainty or to the assumption that $R_{\theta\phi}$ is unity for both stations.

Attenuation (t^*)

Relative mantle attenuation was measured along paths from each earthquake and explosion region to LASA and NORSAR. The measurement of attenuation is the gross factor t^* , which is travel-time along the ray path divided by the average quality factor, Q .

t^* was determined first by normalizing and then summing the ground displacement ($t^* = 0$) spectra for each path. Figure 20 shows the normalized and summed spectrum for paths from East Kazakh to LASA. If the assumption is made that the explosion source spectrum has an f^{-2} fall off at high frequencies, then

$$A(f) \sim S \cdot f^{-2} \cdot e^{-\pi f t^*}$$

for frequencies above the corner frequency, where $A(f)$ is the observed ground displacement spectrum (corrected for instrument response), S is the source spectrum scale constant, and f is frequency in Hz. Then after taking the natural log of this equation

$$\ln [A(f)] + 2 \cdot \ln(f) = -\pi t^* f + \ln(S)$$

If $\ln [A(f)] + 2 \cdot \ln(f)$ is plotted versus frequency for each path, the slope of the graph is $-\pi t^*$. Figure 21 shows the result of this process for the East Kazakh to LASA path. The slope is calculated in the frequency range 1.0 to 2.5 Hz, where the signal-to-noise ratio was highest, and presumably beyond the corner frequency, so that the high-frequency asymptotic slope of f^{-2} characterizes the source spectrum. Plots such as those in Figure 17 in the five Eurasian reports showed that many of the corner frequencies were above 1 Hz, so that the data may not be well fitted by the above equation; however,

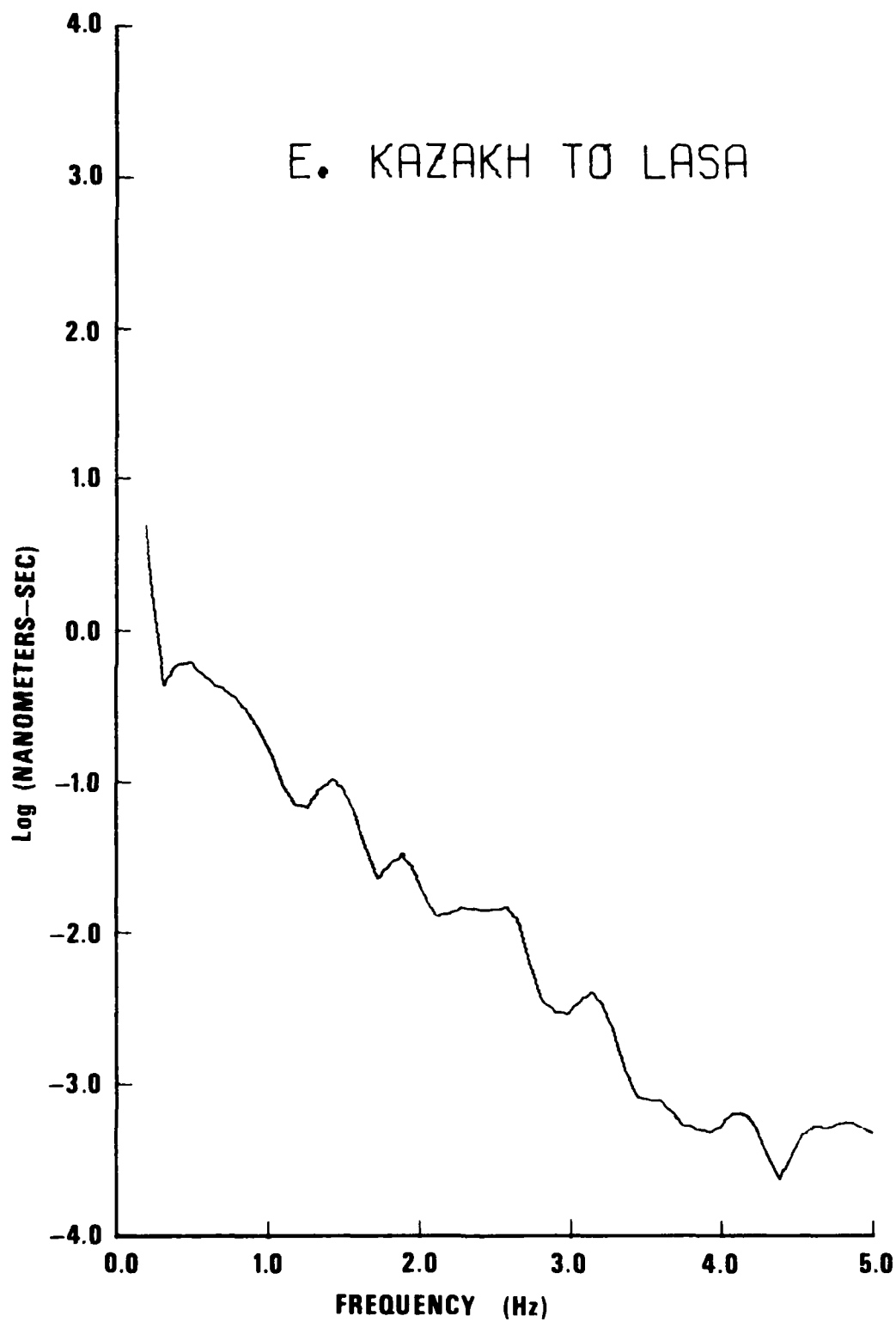


Figure 20 Normalized and summed spectra for the paths from east Kazakh to LASA and to NORSAR.

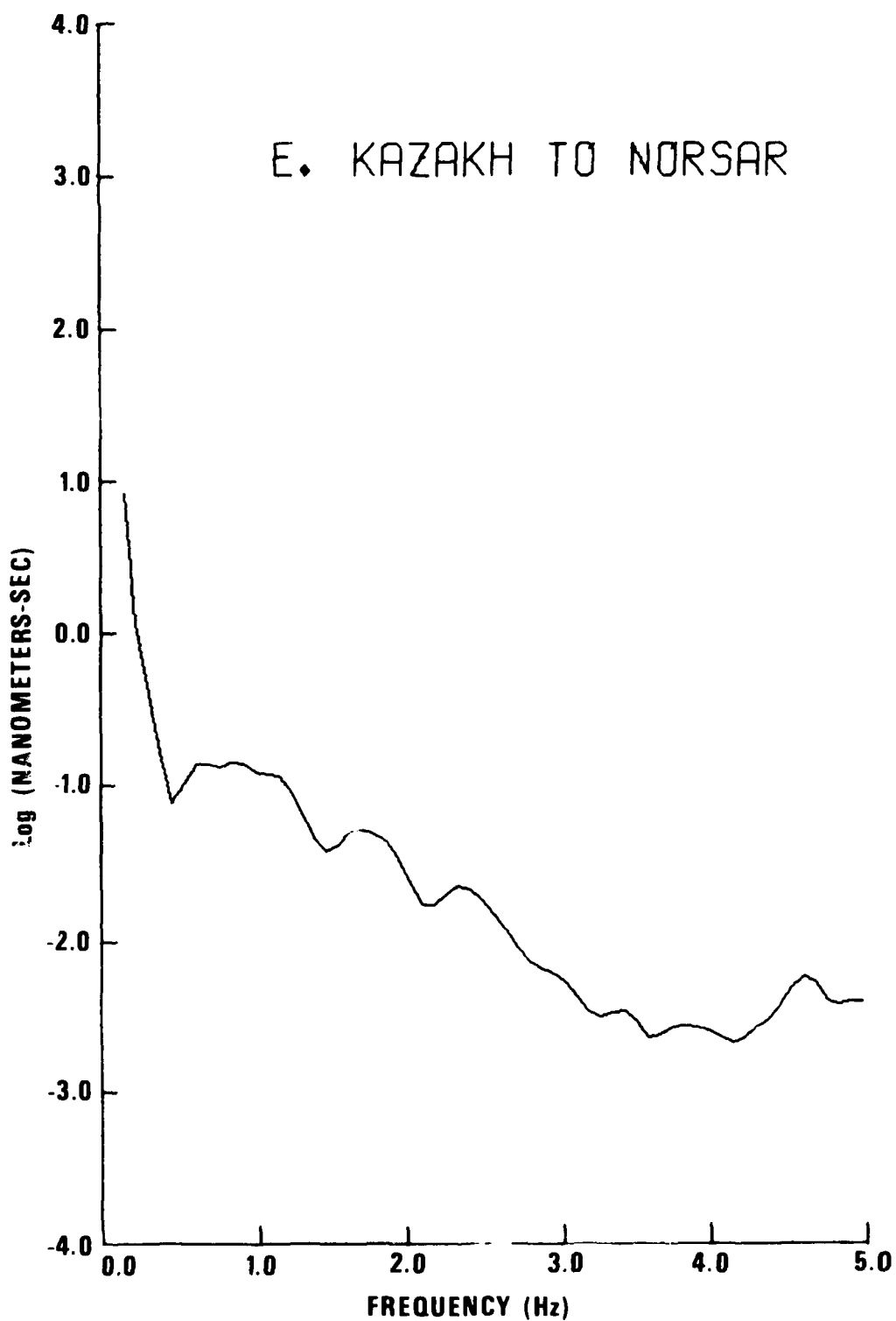


Figure 20 (cont.) Normalized and summed spectra for the paths from east Kazakhstan to LASA and to NORSAR.

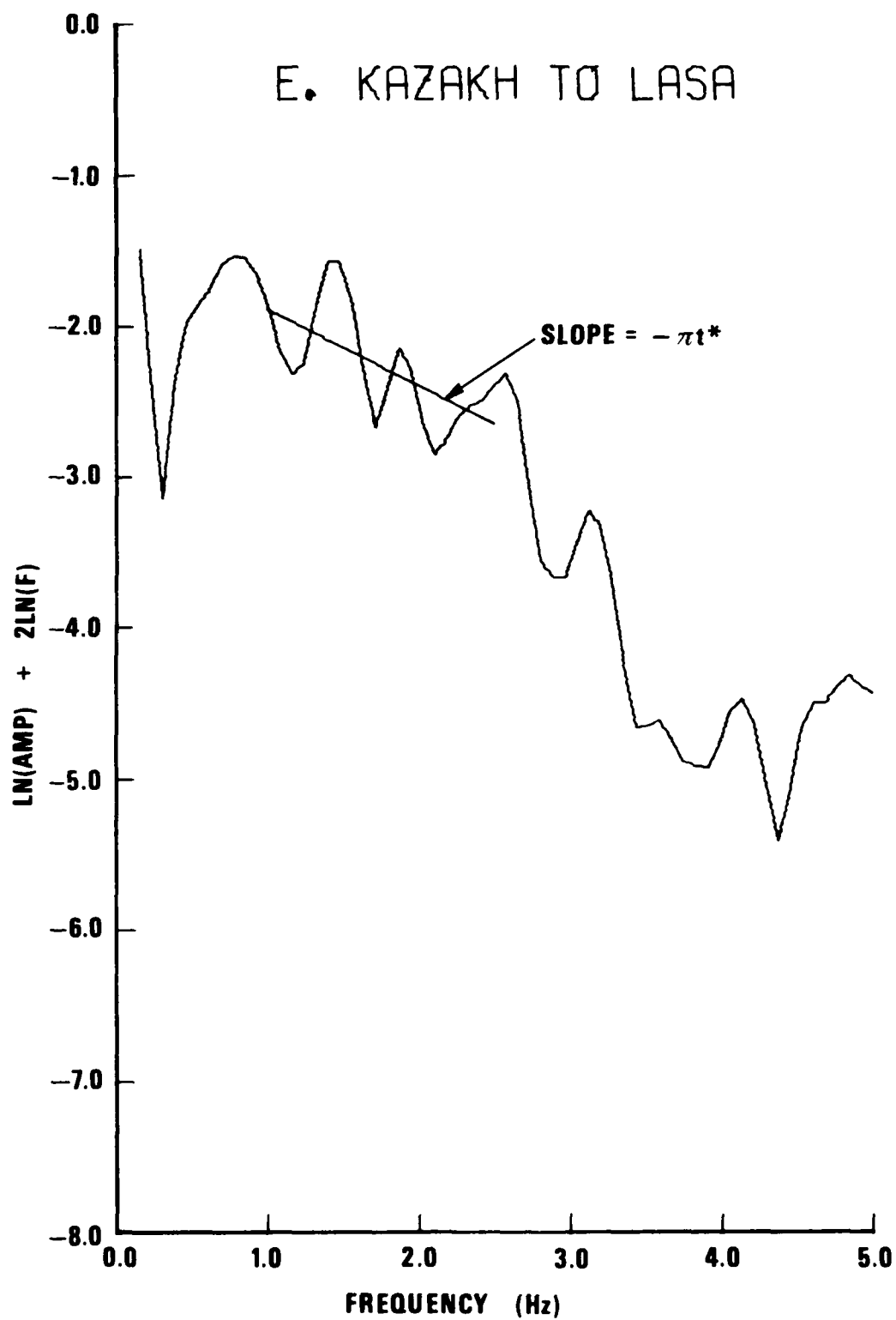


Figure 21 $\ln A(f) + 2 \ln(f)$ frequency for the paths E. Kazakh to LASA and to NORSAR.

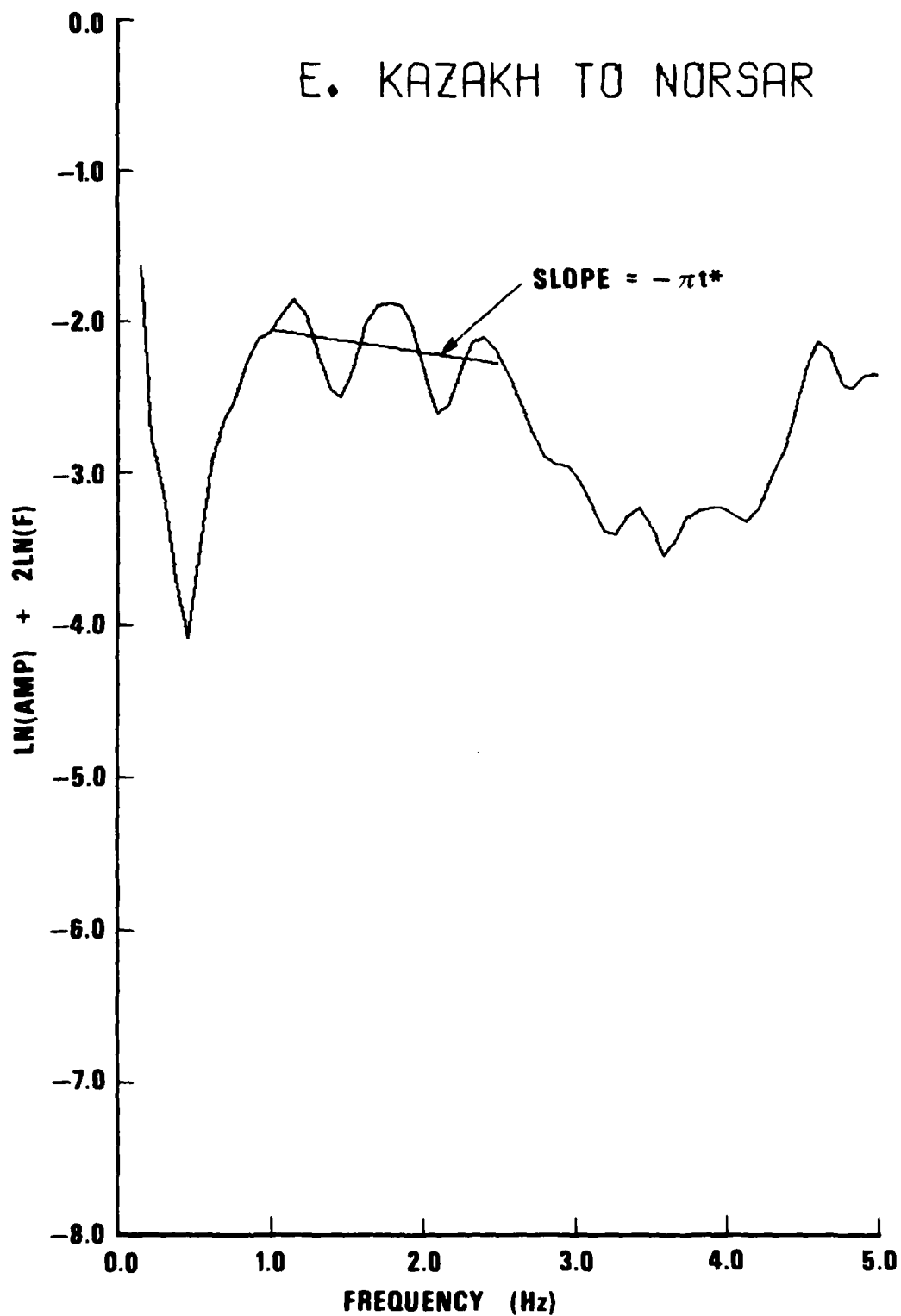


Figure 21 (cont.) $\ln A(f) + 2 \ln(f)$ frequency for the paths E. Kazakh to LASA and to NORSAR.

if a higher frequency range were used, then the average spectra would be seriously contaminated with background noise. The effect of using spectral estimates at frequencies below the corner frequency in the fitting is to bias the estimate of t^* toward a lower value than the actual one, which would explain why some of our t^* values are unrealistically close to zero or even negative. For all events, source spectra with f^{-2} falloff at high frequencies were first assumed in order to estimate t^* . For the earthquakes only, source spectra with f^{-3} falloff at high frequencies were also assumed. The fitting equation for this source spectral model is

$$\ln [A(f)] + 3 \cdot \ln(f) = -\pi t^* f + \ln(S)$$

If the left-hand side of this relation is plotted versus frequency for each path, the slope of the graph is again $-\pi t^*$; but t^* is now based on an assumed f^{-3} source spectrum and will be lower than that obtained from the assumed f^{-2} source spectrum.

The t^* values for f^{-2} and f^{-3} source models for all paths are shown in Table III. Note that for three of the five paths from earthquake regions to NORSAR, assumption of f^{-3} source models resulted in negative t^* values, suggesting that the f^{-3} source model is inappropriate for these earthquake regions or that our fitting interval of 1.0 to 2.5 Hz was improper, as discussed above. Although there is a predominance of theoretical models that imply a f^{-3} source spectrum rather than f^{-2} (Geller, 1976), certain combinations of source-receiver geometry can produce higher-frequency ($\sim f^{-2}$ slope) signals from earthquake models. Note also that in each case the t^* value for the path to LASA is higher, implying more attenuation, than the t^* value for the path to NORSAR, which is largely under shield areas. This result is consistent with the basic visual appearance of signals displayed in Figure 2 through 6. Low t^* values for the paths to NORSAR (t^* from 0. to .34) are in agreement with other t^* results for paths through shield regions (Der and McElfresh, 1977). All paths

Geller, R., 1976. Scaling relations for earthquake source parameters and magnitude, Bull. Seism. Soc. Am., 66, 1501.

Der, Z., and T. McElfresh, 1977. The relationship between anelastic attenuation and regional amplitude anomalies of short-period P-wave in North America, Bull. Seism. Soc. Am., 67, 1303-1317.

Table III
t* Values for all Source Paths to LASA and NORSAR

REGION	PATHS TO LASA			PATHS TO NORSAR		
	No. of Cases	t* for f-2 Source	t* for f-3 Source	No. of Cases	t* for f-2 Sources	t* for f-3 Source
Kamchatka	9	.52+.13	.33+.12	9	.24+.06	.05+.05
Tien Shan	8	.29+.15	.10+.15	9	.00+.05	0.
Pamirs	8	.53+.09	.34+.08	9	.00+.05	0.
Baikal	4	.59+.16	.40+.16	5	.18+.07	0.
Caucasus	6	.63+.08	.44+.08	7	.28+.06	.09+.05
Milrow	1	.23+.10		0		
E. Kazakh	4	.16+.10		4	.05+.08	
W. Kazakh	3	.45+.16		3	.34+.06	
SW. Russia	2	.35+.17		0		
Lop Nor	1	.15+.16		1	0.	
Baikal Explosion	0			1	0.	

Note: For zero values, t* value calculated was negative, which is unrealistic, so t* set equal to zero.

to LASA traverse the anomalous upper mantle of the Western United States; Der and McElfresh (1977) have shown that paths through this region have higher t^* values than paths entirely through shield regions. The paths from Kamchatka and MILROW to both LASA and NORSAR are affected by the dipping lithospheric plate in the source region.

The significant differences in t^* between East and West Kazakh is unexplained. Perhaps corner frequencies are high but variable between the two regions because of differences in shot media, or perhaps different depths result in differing effects of pP. This problem merits further study.

DISCRIMINATION ASPECTS

The first part of this study has been aimed at uncovering seismic source characteristics of the events and propagation path effects on the data set. The second part is aimed at extracting discriminant parameters from the data and examining the utility of these parameters in relation to the characteristics and effects uncovered in the first part. In addition to comparing our entire earthquake signal population to all explosion signals, earthquakes and explosions lying in similar tectonic settings will also be carefully compared.

$$\frac{M_s - m_b}{}$$

In the five Eurasian reports, average M_s and m_b values were independently determined for the earthquakes (Table I) using selected WWSSN and HGLP calculation); and the ALPA, LASA, and NORSAR arrays. Average M_s values were also independently determined for the explosions in Table II. The m_b values for the explosions were taken from the NEIS list because independent calculation of m_b for the explosions fell close to the NEIS values.

The following forms have been used for magnitude computations:

$$m_b = \log \left(\frac{A}{T} \right) + B(\Delta)$$

$$M_s = \log \left(\frac{A}{T} \right) + 1.66 \log \Delta + 0.3$$

where

A = one half the peak-to-peak maximum record amplitude reduced to nm ground displacement;

T = period in seconds (restricted to 17 - 23 sec for M_s calculation);

Δ = epicentral distance in degrees;

B = Gutenberg-Richter correction term for surface-focus P waves.

For the distances at which amplitudes are measured in this report, there are negligible differences between M_s values calculated using the traditional M_s formula above and more accurate formulas with slopes near 1.0 derived by several authors.

Ringdal's (1976) method of magnitude averaging, which includes noise measurements as upper bounds, has been used. With this method, magnitudes at the individual stations are assumed to follow a gaussian distribution. Within this distribution some magnitudes will fall below station thresholds based on the noise level, and Ringdal's method substitutes a noise measurement at those stations that do not detect and then computes the maximum likelihood estimate of magnitude based upon measured signals and noise estimates. The effect of this procedure is to more accurately define the magnitude of events not widely recorded; more specifically, the usual effect is to lower the network magnitude. Because for most events in this study few noise measurements were used, the averages should be very close to results if only measured signal amplitudes were used. As predicted, magnitude averages for events with many readings at the noise level were found to be lower than what would result if only measured signal amplitudes were used.

The $M_s - m_b$ plot is shown in Figure 22. Where only noise measurements were used in the M_s determination, an arrow in the figure represents the maximum " M_s " value. The line $M_s = m_b - 1.5$, that Blandford and Clark (1975) and earlier workers suggested as a suitable Eurasian discrimination line, separated the earthquakes from the explosion population up to $m_b \sim 6$. This line would also separate the suite of Asian events studied by Dahlman et al. (1974). Note that in the Kamchatka, Tien Shan, and Pamir regions events were chosen which, from the NEIS list or from M_s measurements at the long-period arrays, showed low M_s for their m_b . Independent determination of M_s and m_b for those events revealed that they were not anomalously low in M_s for their m_b . In summary, $M_s = m_b - 1.5$ is a discrimination line for our data set except at high magnitude (MILROW) where it should bend upward to account for the fact

Ringdal, F., 1976. Maximum-likelihood estimate of event magnitude, Bull. Seism. Soc. Am., 64, 789.

Dahlman, O., H. Israelson, A. Austegard, and G. Hornstrom, 1974. Definition and identification of seismic events in the USSR, Bull. Seism. Soc. Am., 64, 607.

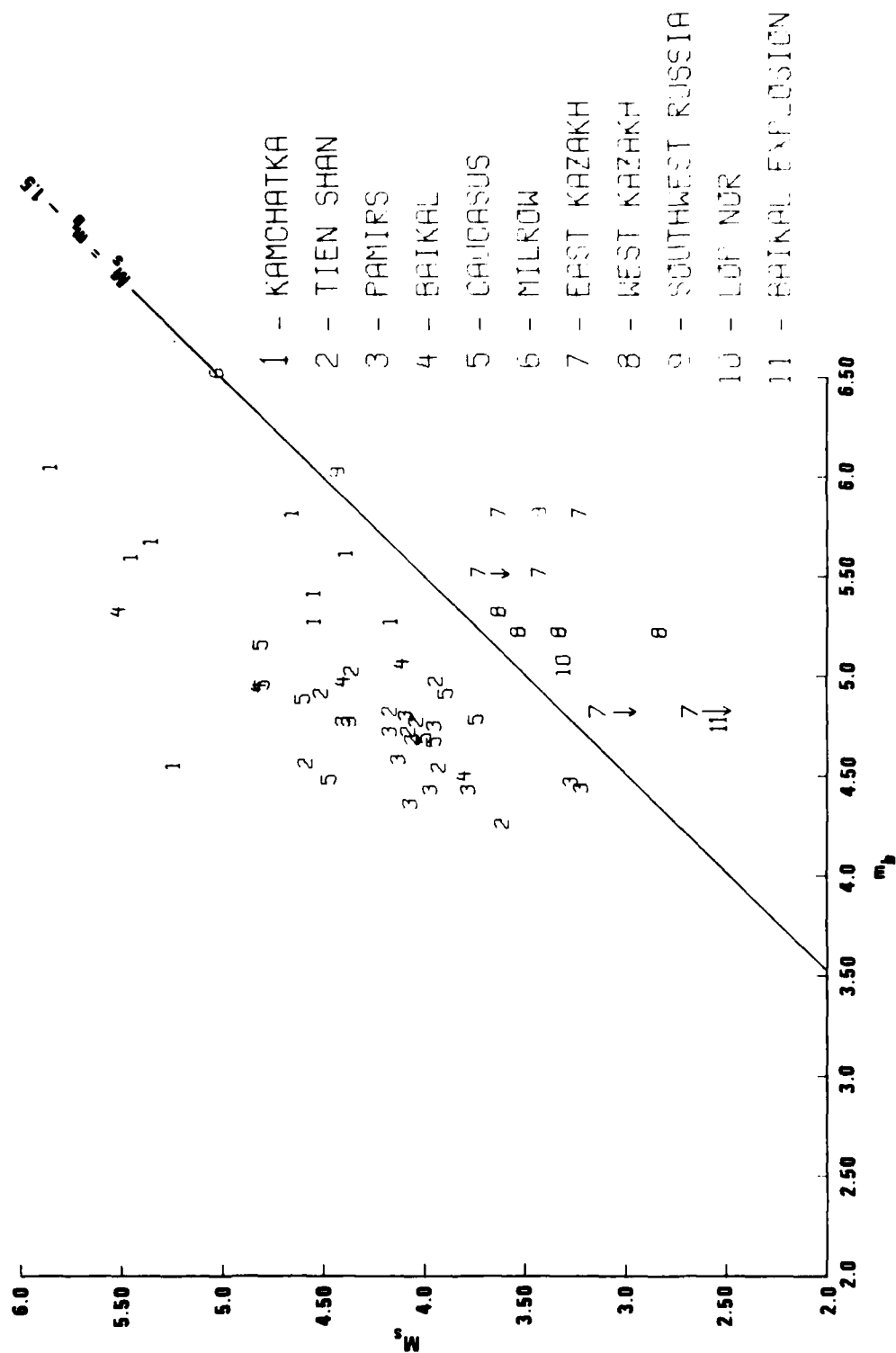


Figure 22 M_s versus m_b for earthquakes and explosions from all regions.

that m_b is measured beyond the corner frequency (von Seggern and Blandford, 1972).

Note, however that the population limits are separated by only 0.5 magnitude units. Then an explosion shot array could move into the earthquake population. In particular a West Kazakh shot array might easily masquerade as a Pamir earthquake.

Corner Frequencies and Long-Period Spectral Levels

Figure 23 is a plot of $|\hat{U}_0|$ versus corner frequency as seen at LASA and NORSAR for all earthquake and explosion data. Few long-period P phases were recorded at the long-period arrays due to the small magnitudes of the events, so values of $|\hat{U}_0|$ were estimated from the spectral data of the short-period vertical component. Hanks and Thatcher (1972) showed that, for a given long-period spectral level, Amchitka Island explosions have a higher corner frequency than Aleutian earthquakes. The physical basis of this discriminant is the smaller source time dimension of the explosion for a given long-period signal level. However, Figure 23 shows no separation between earthquakes and explosions. There is a weak trend toward higher corner frequencies for lower $|\hat{U}_0|$ for the explosions and the earthquakes, but it appears to be steeper than the theoretical relation of f^{-3} derived from the fact that source dimension scales as the cube-root of seismic moment. In Figures 24 and 25 the $|\hat{U}_0|$ values are shown by region for the LASA and NORSAR data respectively; earthquake signals do not separate from explosions in the nearest geographic regions.

One possible reason that the spectral parameters provided poor discrimination was that this study used only short-period P recordings, while Hanks and Thatcher used long-period body-wave recordings. Another possible explanation is that, because of the low magnitudes of events studied here, a clear

von Seggern, D., and R. Blandford, 1972. Source time functions and spectra for underground nuclear explosions, Geophys. J., 31, 83-97.

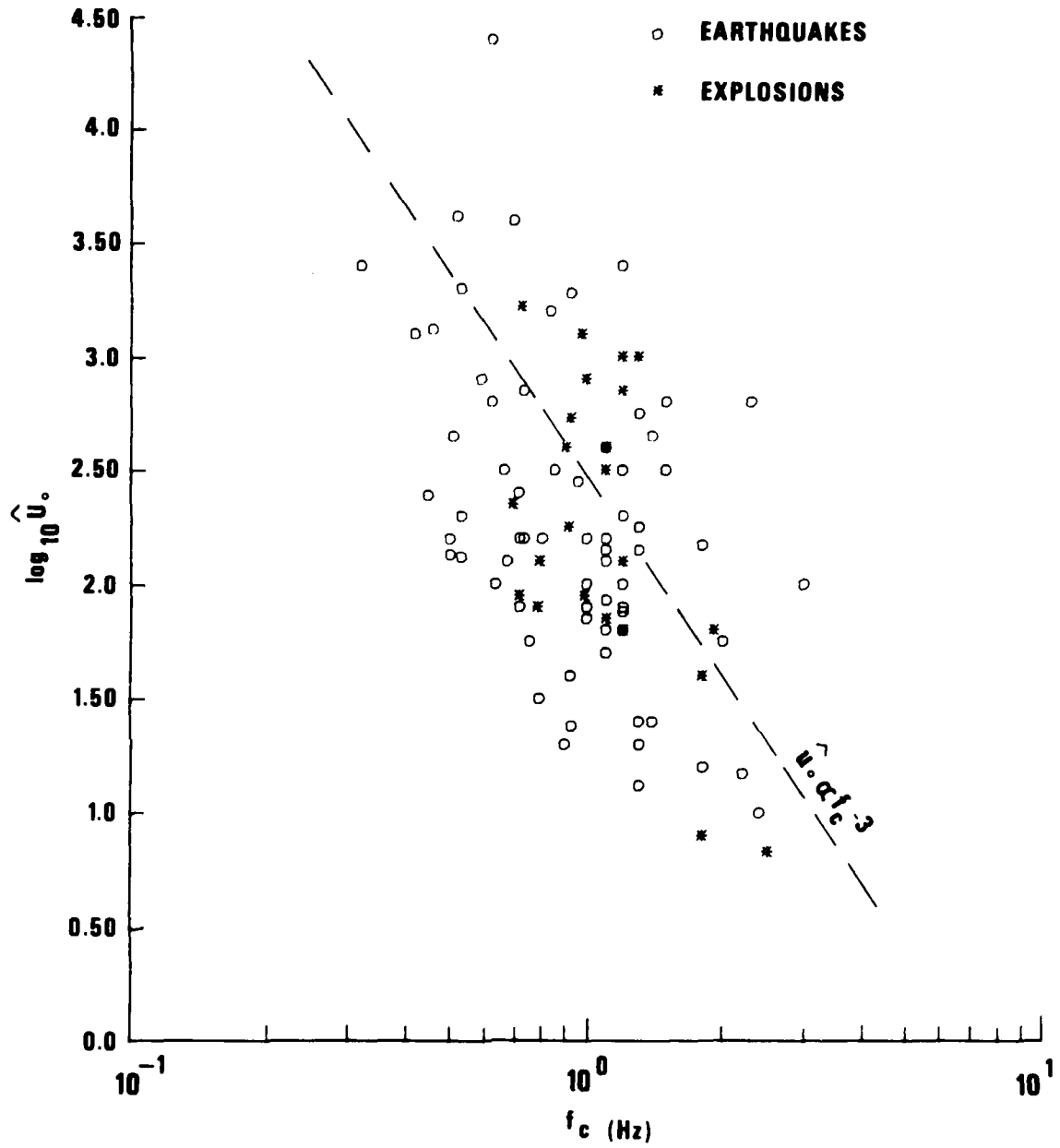


Figure 23 Long-period body-wave spectral level versus corner frequency.

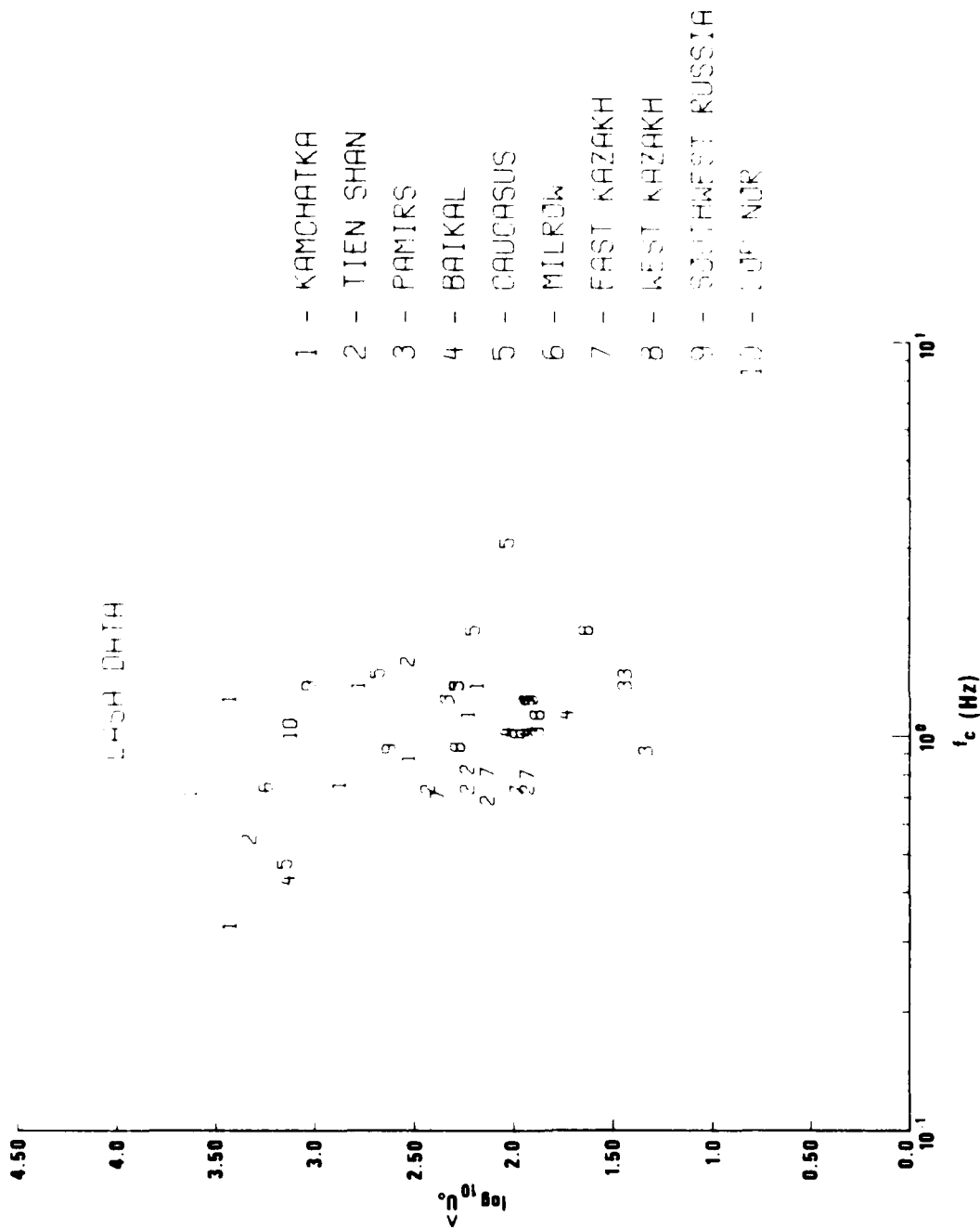


Figure 24 Long-period spectral level versus corner frequency for earthquakes and explosions from all regions from LASH P recordings.

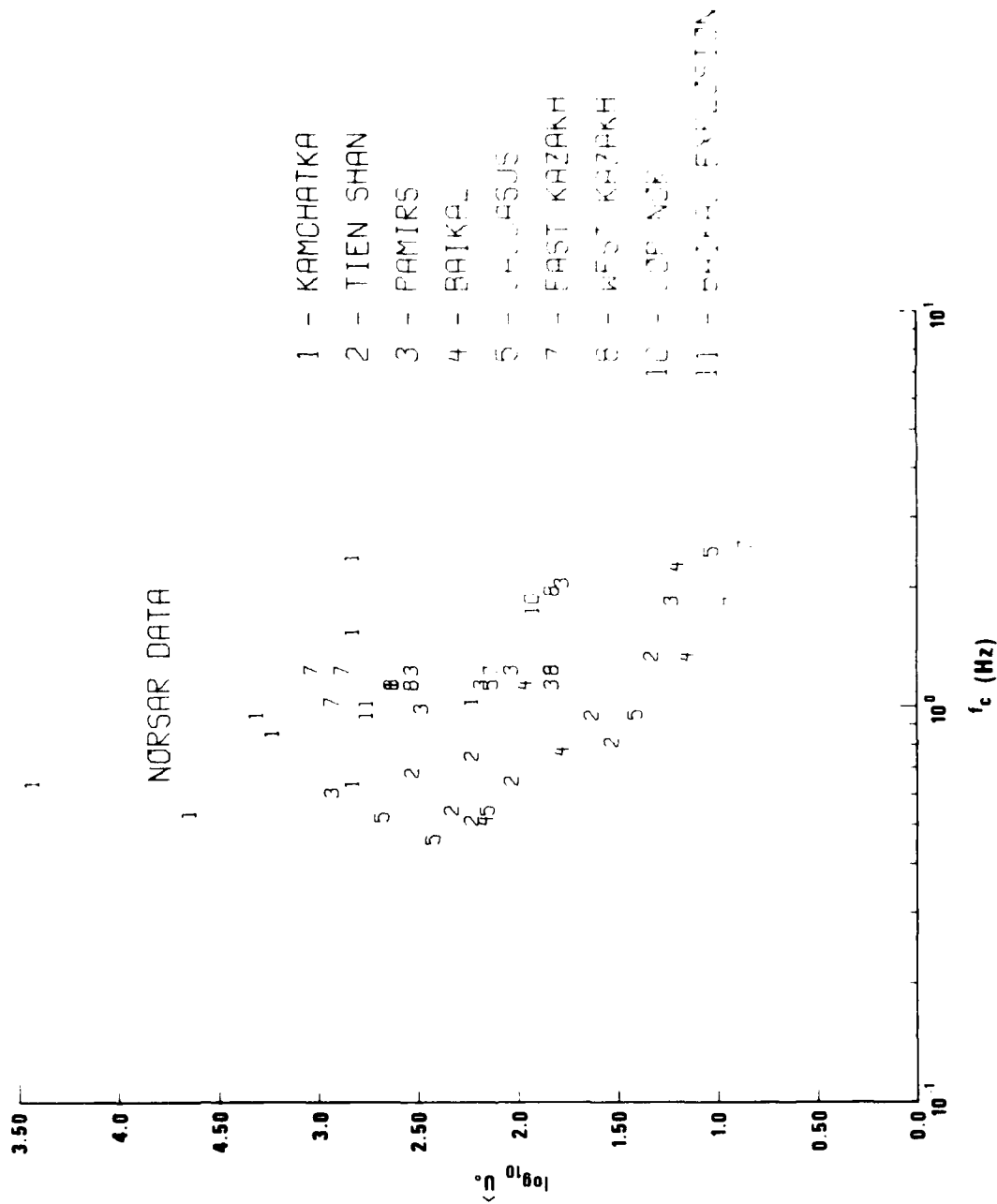


Figure 25 Long-period spectral level versus corner frequency for earthquakes and explosions from all regions from NORSAR P recordings.

estimate of the asymptotic value of $|\hat{U}_0|$ was not possible in most cases. Finally, the lack of discrimination could stem from real characteristics of the sources examined in this study.

Long-Period Body-Wave Excitation

The ratios of long-period P and S displacement to LR displacement was examined as a seismic discriminant for some of the events. For the Pamir, Baikal, and Caucasus earthquakes, too few long-period P or S observations existed to determine the ratios of these quantities to long-period LR ground displacement; all long-period P and S observations from events in these regions were close to the noise level, which is expected for their small magnitudes ($m_b < 5.3$).

The Kamchatka earthquakes were generally of larger magnitudes (up to $m_b = 6.0$), and there were more observations of long-period S and P waves than for the other earthquake regions studied. In von Seggern and Sobel (1976), the ratios SH/LR, SV/LR and P/LR were compared to distributions obtained from LRSM stations for NTS explosions by von Seggern (1972). The median $\log(\text{SH/LR})$ is -0.4 for the Kamchatka earthquakes and the median $\log(\text{SV/LR})$ is roughly -0.6 . Though these values are higher than those of typical NTS explosions recorded at LRSM stations, which lie at roughly -1.2 , the two populations overlap somewhat. The median $\log(\text{P/LR})$ lies at roughly -0.4 , which is higher than typical explosion values which von Seggern found, suggesting that P and SH amplitudes are roughly equal for earthquakes in Kamchatka.

Few SH/LR, SV/LR, and P/LR measurements could be made for the Tien Shan earthquakes. These ratios were generally larger than those of NTS explosions in von Seggern (1972), but ratios for the earthquake and explosion populations again overlapped somewhat.

In general, long-period body-wave excitation is a weak discriminant for the events studied. This is so because of the apparent lack of complete separation and because the long-period body-waves were close to or below the noise level, expected for these small magnitude events, thus making application of the discriminant difficult. A remedy would be to employ Ringdal's

(1976) method of magnitude estimation with some additional technique for cases where no signals are observed.

Short-Period Body-Wave Excitation

The ratio of short-period P displacement to S displacement was also examined as a seismic discriminant. In the Pamir, Baikal, and Caucasus regions there were too few short-period S observations (mostly unreliable with small signal-to-noise) to determine the ratio of S to P ground displacement.

In the Kamchatka region there were more observations of short-period S than for the other earthquake regions studied. In von Seggern and Sobel (1976) the ratios SV/P and SH/P were compared to distributions obtained from LRSM stations for NTS explosions by von Seggern (1972). The spread of S/P ratios for the Kamchatka earthquakes was over two orders of magnitude, reflecting the variations in S/P ratios predicted by radiation patterns for double-couple models of an earthquake. While the NTS explosion population overlapped the Kamchatka sample somewhat, all but one of the nine earthquakes had at least one $\log(S/P)$ which exceeded 0.0, a value not nearly reached by any of the similar explosion log-ratios in von Seggern (1972).

One or more SV/P ground displacement ratios were available for 8 of the 10 Tien Shan events. The median of the Tien Shan data lay at least one order of magnitude above the NTS explosions (Sobel and von Seggern, 1976).

In general, short-period body-wave excitation is a weak discriminant for events studied here for the same reasons that long-period body waves are weak discriminants. Again, lower thresholds or more sophisticated magnitude estimation techniques would render this discriminant more useful.

Recent results for regional distances on the compressional to shear ratio (P_n, P_g)/Lg are encouraging, but no attempt was made to reform these analyses for these events.

Complexities

The "complexity" parameter (Lambert et al., 1969) has been computed as

Lambert, D., D. von Seggern, S. Alexander, and G. Galat, 1969. The LONGSHOT experiment, Vol. III, Comprehensive Analysis, SDL Report No. 234, Tele-dyne Geotech, Alexandria, Virginia 22314.

seen at LASA and NORSAR for all the earthquake and explosion data. Figure 26 shows the complexity values versus m_b . A high value indicated relatively high coda energy (5 to 35 sec after P arrival) relative to the energy in the first 5 seconds of the P wave. Complexity numbers for the earthquakes were often high due to clear pP signals. Complexity numbers for the explosions were low, as would be expected, but overlapped the earthquake population. Low complexity numbers for some of the earthquakes were a result either of noisy records (the calculations include a noise correction) or lack of a clear pP signal. In general, overlapping complexity values for earthquakes and explosions indicated the unreliability of complexity measurements to distinguish event type.

In Figures 27 and 28 complexity values are shown by region for the LASA and NORSAR data, respectively. Complexity values for Kamchatka earthquakes recorded at NORSAR are low because the pP phase for the path to NORSAR originates near a nodal plane of the focal mechanism. The Kamchatka signals recorded at LASA do not separate from the explosion population either. The closest explosion, MILROW, has a relatively high complexity value, possibly due to a plate refraction effect because LASA is within the shadow zone defined by the ray-tracing study of Davies and Julian (1972).

The Tien Shan earthquakes do not separate from the explosion population. In fact, many of the Tien Shan events recorded at LASA have complexities that are among the lowest observed in this study either at LASA or NORSAR. Clear pP signals were not present in most cases. The nearby Lop Nor explosion falls within the complexity range of the Tien Shan earthquakes.

Complexity numbers recorded at LASA for the Pamir earthquakes separate from those recorded at LASA for the nearby East and West Kazakh explosions. This separation partially results from the apparent pP signal on LASA beams for most Pamir events. The complexity numbers recorded at NORSAR for the Pamir earthquakes are generally higher, but they overlap the numbers for the East and West Kazakh explosions recorded at NORSAR. This overlap can be attributed to the fact that NORSAR beams for Pamir events show possible pP signals for only five of the nine cases.

Davies, D., and B. Julian, 1972. A study of short-period P-wave signals from LONG-SHOT, Geophy. J., 29, 185.

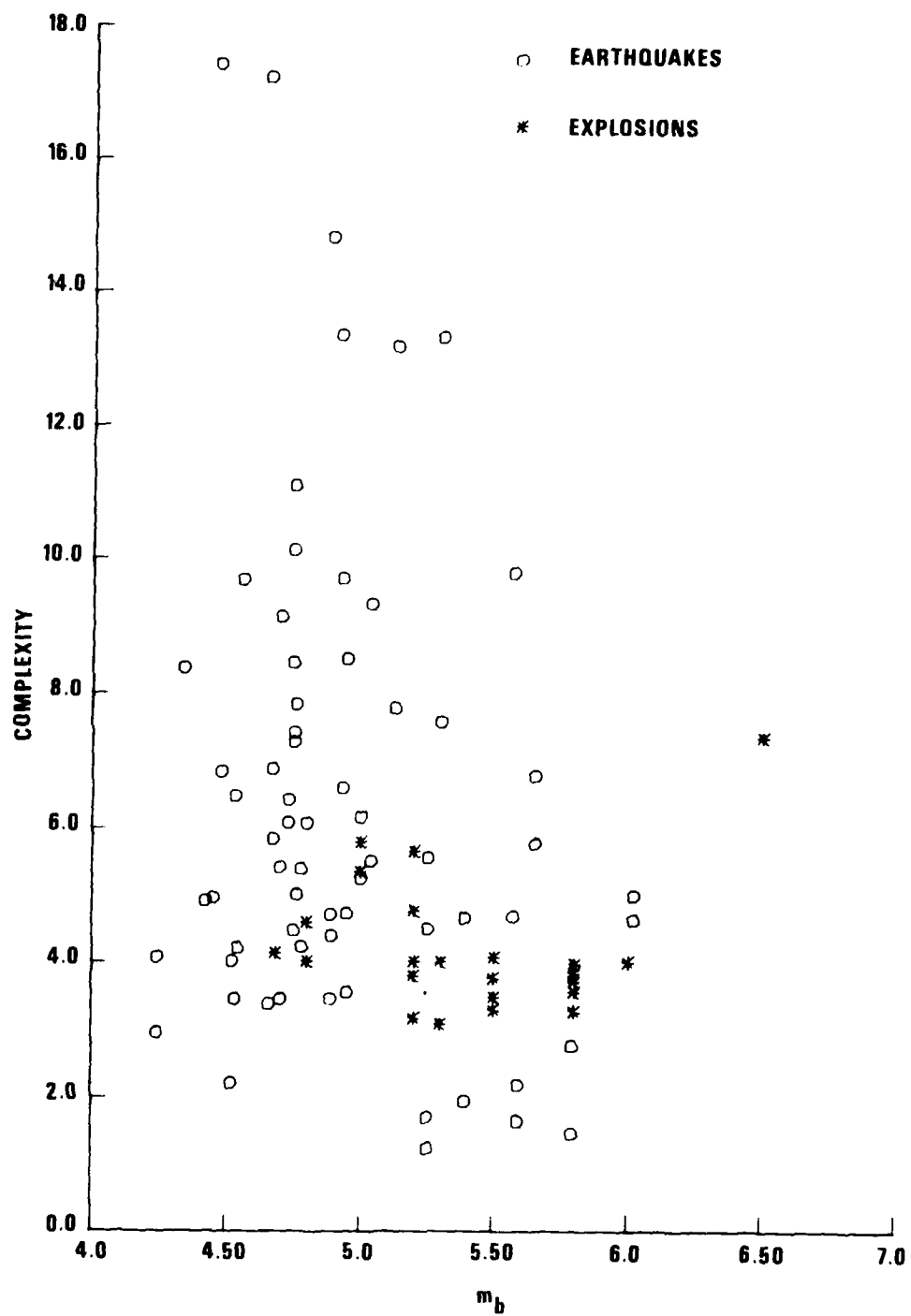


Figure 26 Complexity versus m_b for all events from LASA and NORSAR P recordings.

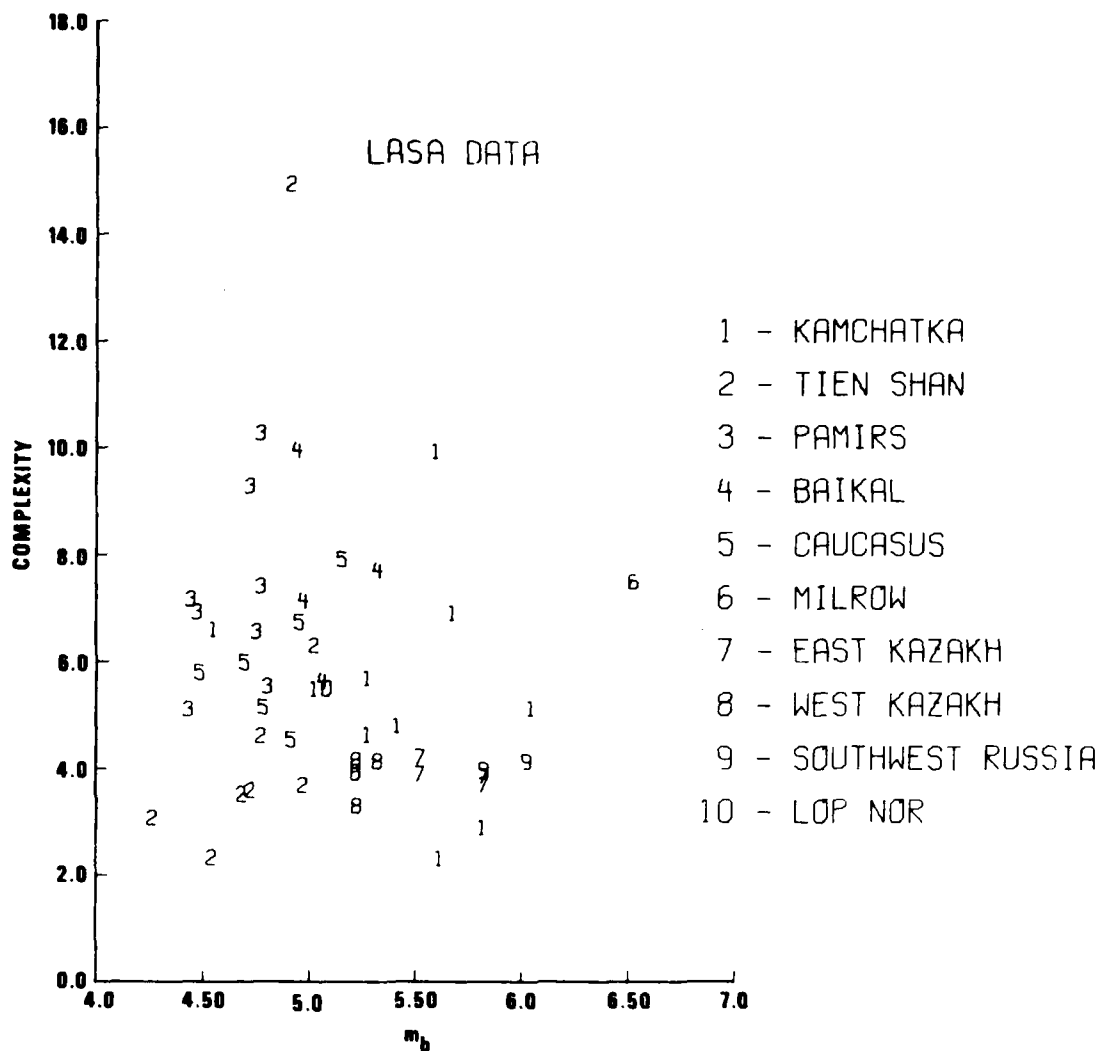


Figure 27 Complexity versus m_b for earthquakes and explosions from all regions from LASA P recordings.

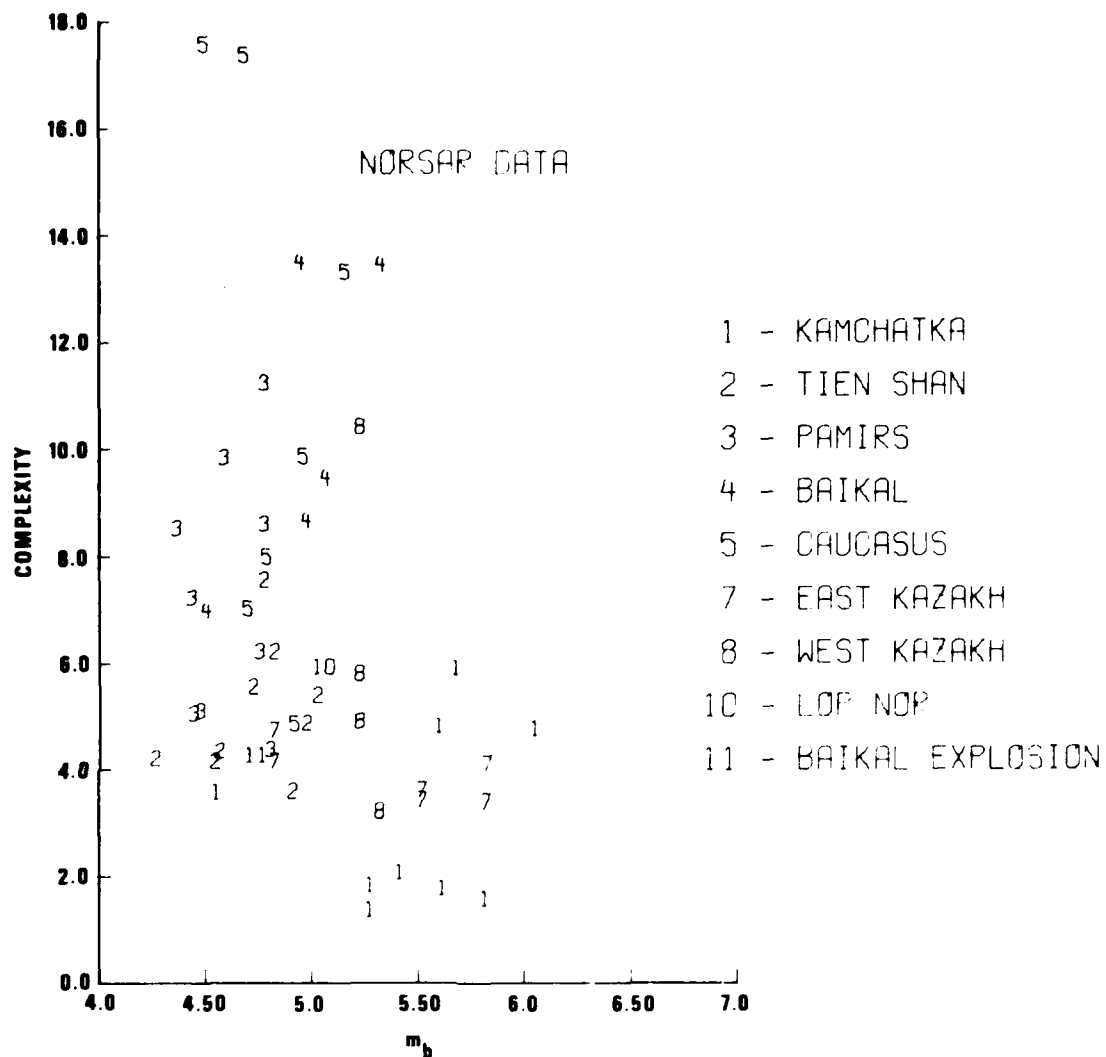


Figure 28 Complexity versus m_b for earthquakes and explosions from NORSAR P recordings.

Complexity numbers recorded at LASA and NORSAR for the Baikal earthquakes separate from the nearby Kazakh explosions and the Baikal explosion, even though only a few pP phases were observed for the Baikal earthquakes on LASA and NORSAR recordings.

Complexity numbers for Caucasus events recorded at LASA separate from the complexity values for W. Kazakh and Southwest USSR explosions. However, complexity values for Caucasus events recorded at NORSAR overlap complexity values for W. Kazakh explosions. Most Caucasus recordings at LASA and NORSAR show apparent pP signals. The lowest complexity value for NORSAR for Caucasus events was for a possible subcrustal event in the Caspian Sea. The low complexity value for this event likely stems from the late arrival of pP and associated crustal reverberation signals beyond the 30-second signal window used. Also, one of the signals recorded at NORSAR for the West Kazakh event group has a high complexity value resulting from a clipped signal. If these two cases are deleted, the complexity values for Caucasus events recorded at NORSAR would separate from the values for Kazakh explosions recorded at NORSAR.

Spectral Ratios

Spectral ratios were calculated at LASA and NORSAR according to the formula (Lacoss, 1969)

$$SR = \frac{\int_{1.55}^{1.95} A(f)df}{\int_{.45}^{.85} A(f)df}$$

where sums of the equivalent terms of the discrete Fourier transform replaced the integrals of the displacement spectrum $A(f)$ over frequency. These ratios are plotted versus m_b in Figure 29 for all the data with no attenuation correction ($t^* = 0$). Spectral ratios did not appear to depend on m_b , M_s , or depth. In general, explosions show larger spectral ratios (and more high frequency energy) than earthquakes, but the two populations do not separate. The spectral ratios were plotted versus m_b for LASA and NORSAR data, respectively, in Figures 30 and 31. In Figures 32 and 33 the LASA and NORSAR data were corrected for attenuation by using t^* values determined for f^{-2} source models for earthquakes and explosions and f^{-3} source models for earthquakes. Bars connect earthquake values where there are two different t^* estimates

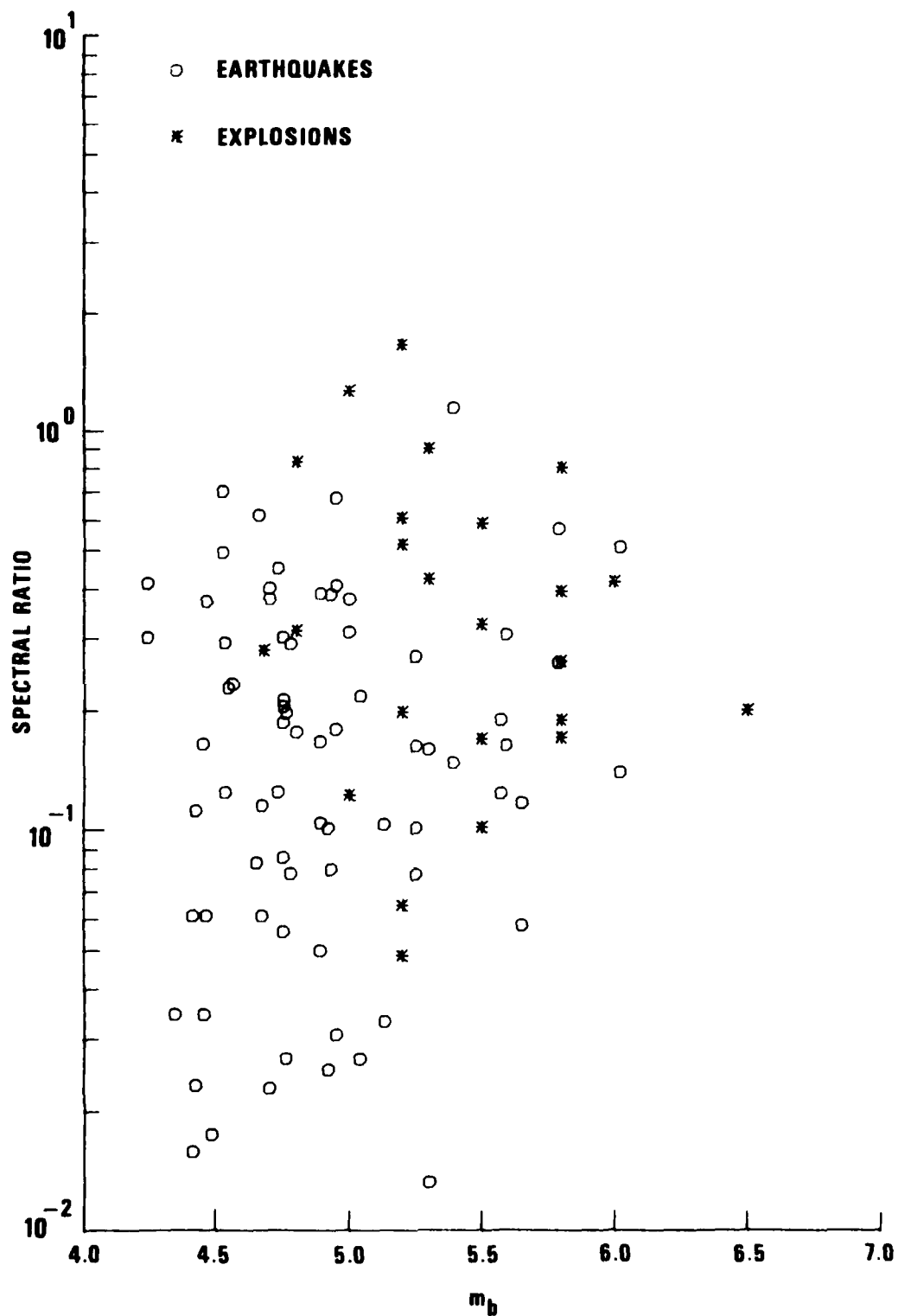


Figure 29 Short-period P spectral ratio versus m_b for all events recorded at LASA and NORSAR for $t^*=0$.

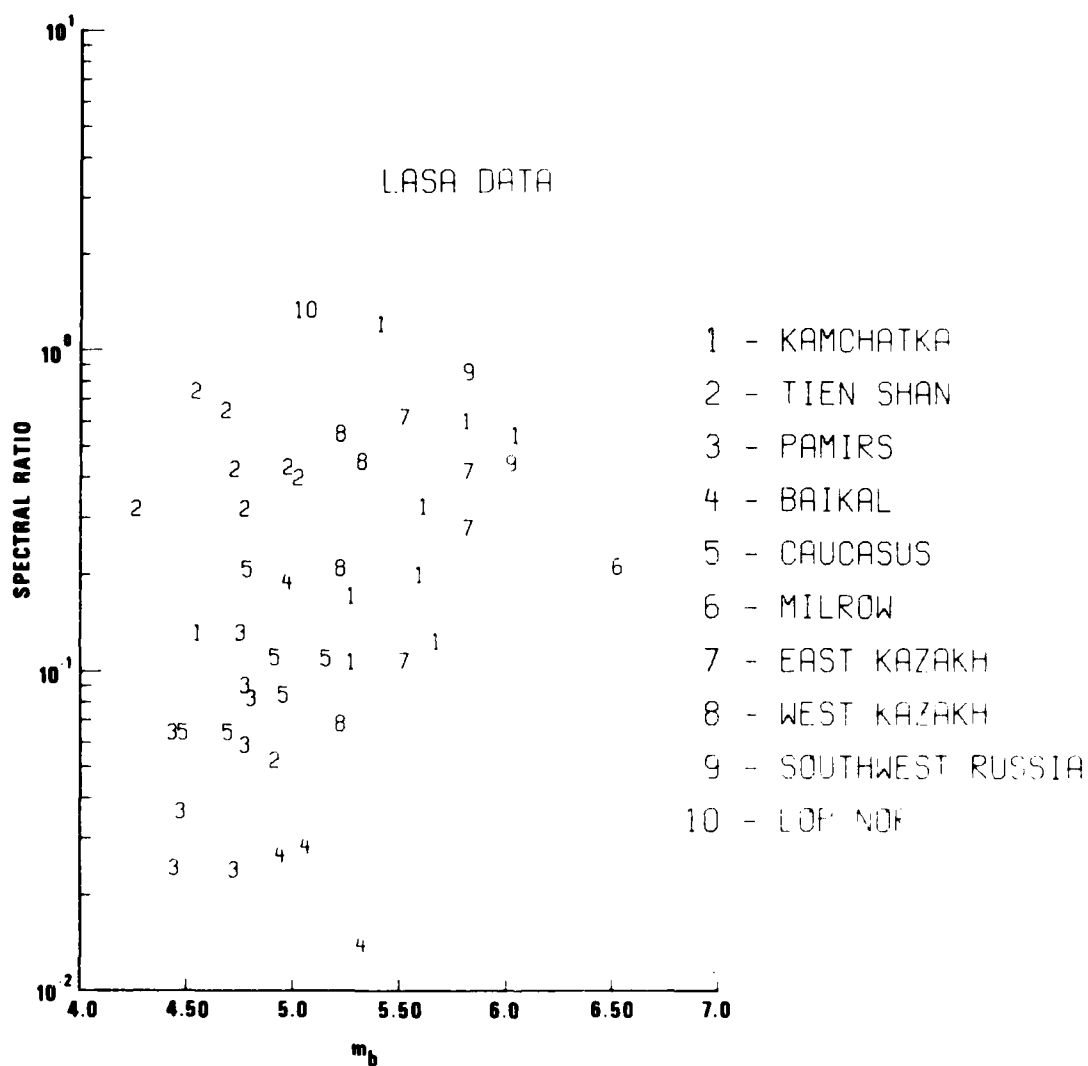


Figure 30 Short-period P spectral ratio versus m_b for earthquakes and explosions from all regions recorded at LASA for $t^*=0$.

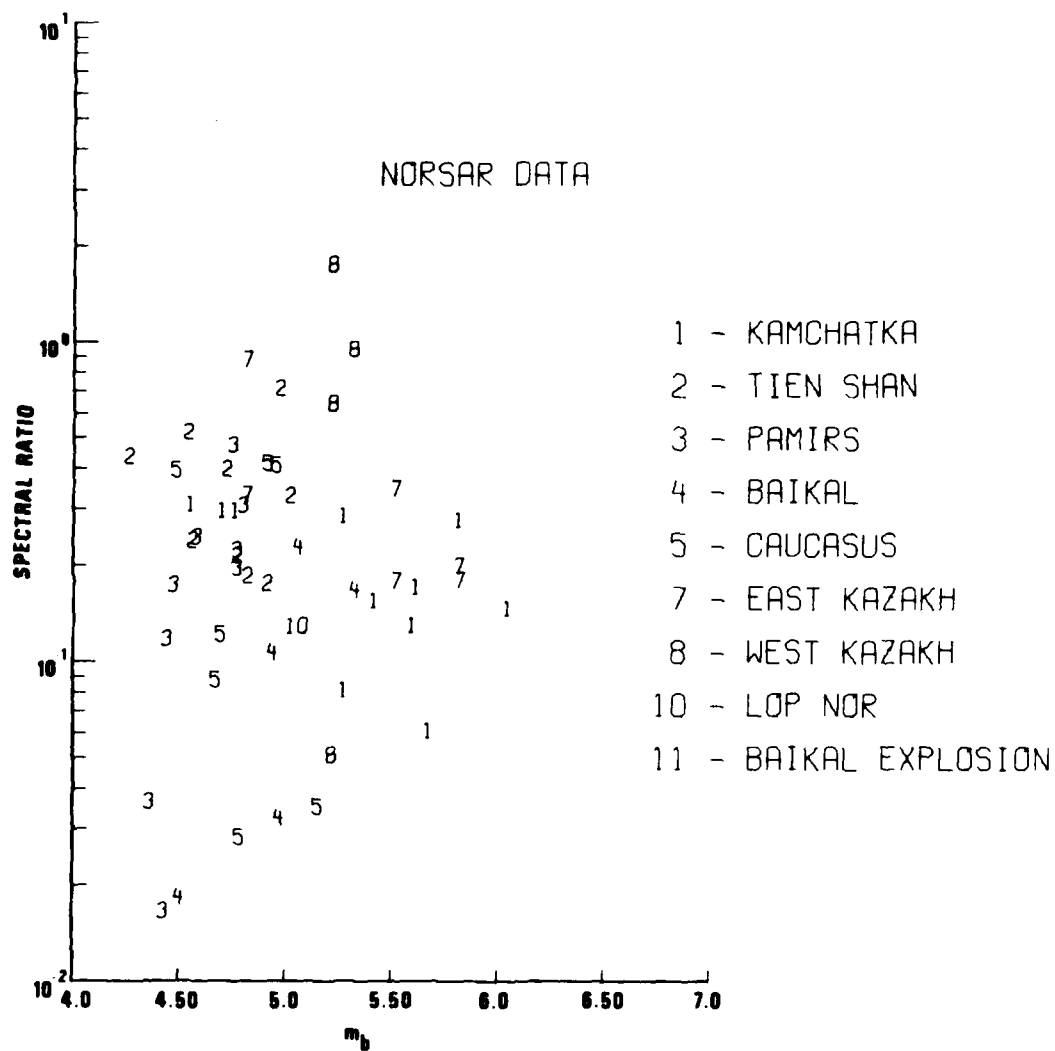


Figure 31 Short-period P spectral ratio versus m_b for earthquakes and explosions from all regions at NORSAR for $t^*=0$.

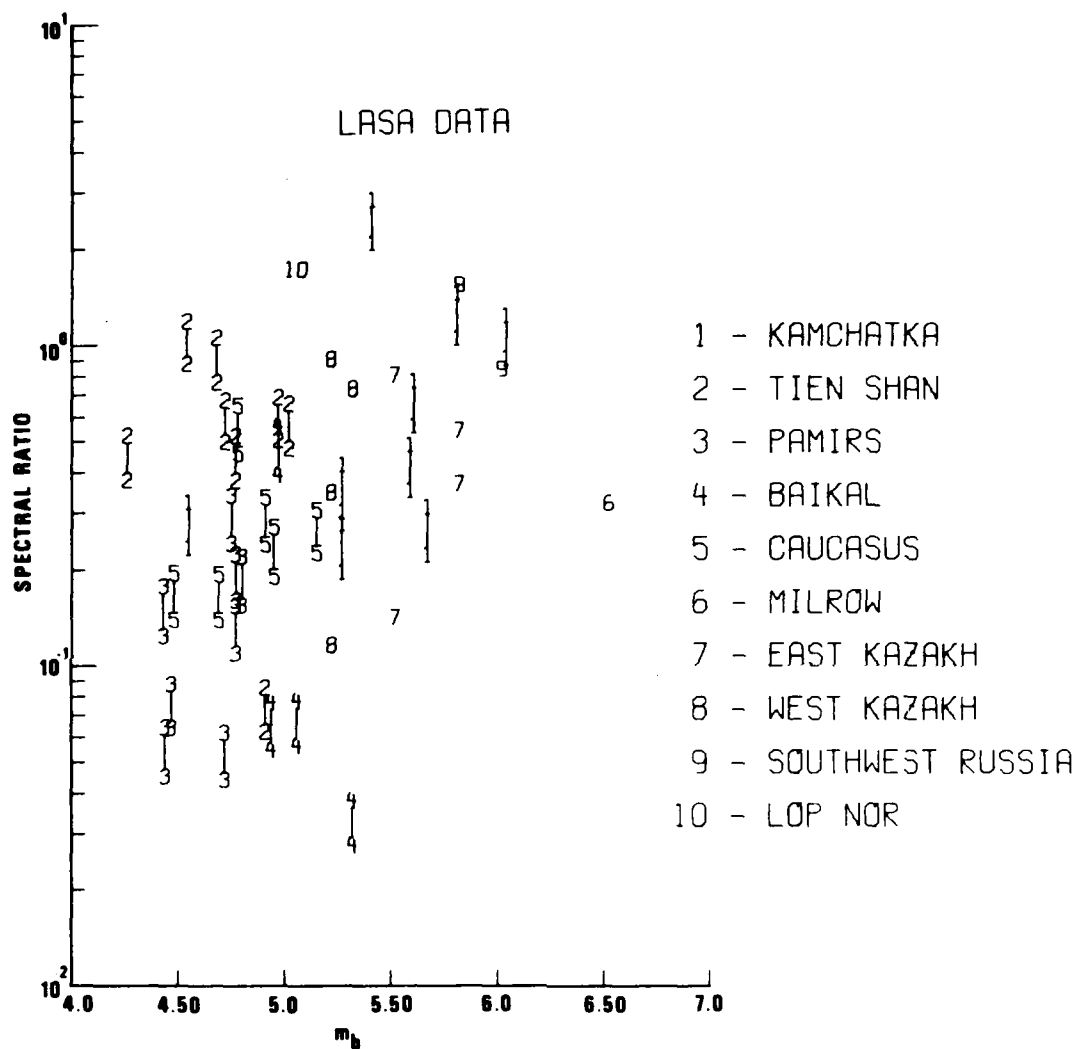


Figure 32 Short-period P spectral ratio versus m_b for earthquakes and explosions from all regions [recorded at LASA]. The t^* values are for f^{-2} source models for earthquakes and explosions and f^{-3} source models for earthquakes.

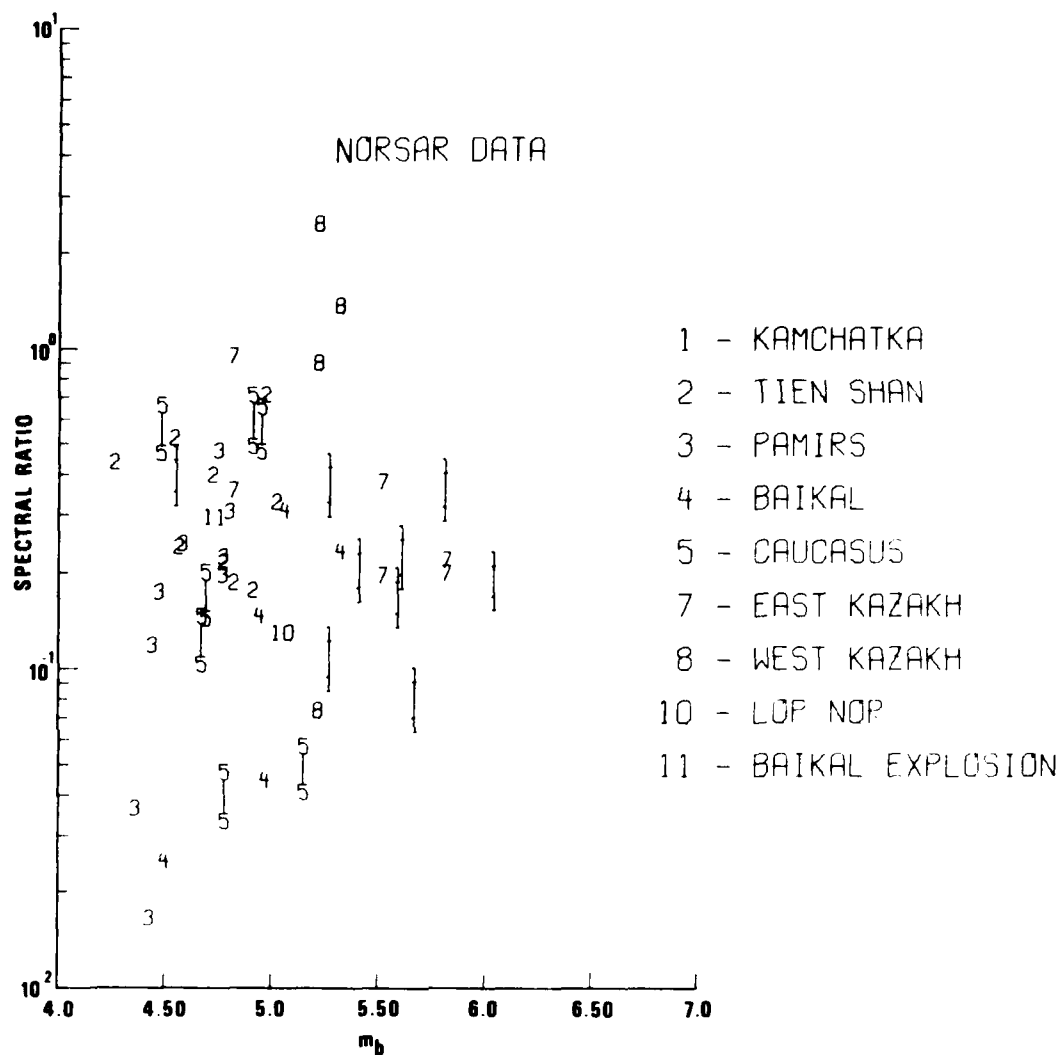


Figure 33 Short-period P spectral ratio versus m_b for earthquakes and explosions from all regions [record at NORSAR]. The t^* values are for f^{-2} source models for earthquakes and explosions and f^{-3} source models for earthquakes.

from the two source models. In general, explosions show larger spectral ratios than earthquakes, but the earthquake data does not separate from explosion data from nearby regions. Lacoss (1969) and von Seggern and Blandford (1977) also reported that spectral ratios overlapped for Eurasian events.

Radiation Patterns

Attempts to identify source mechanisms for the earthquakes were largely unsuccessful in the five Eurasian reports. The efforts were unsuccessful because determination of the fault planes for earthquakes whose magnitudes are below $m_b = 6.0$ is not generally possible with the teleseismic data, and all our earthquakes have m_b less than 6. First motions were determined whenever possible from collected data, which was mostly short-period recordings. Unfortunately, the short-period data were not consistent. Body-waves for all but a few of the presumed earthquakes showed both distinct compressional and dilatational first motions, suggesting that these events were earthquakes. However, the overlapping compressional and dilatational first motions on the first motion diagrams indicated that this was not a reliable discriminant. For body waves from earthquakes with thrust fault mechanisms, such as in Kamchatka, lack of negative first motions at teleseismic distance would not aid discrimination.

In the five Eurasian reports, attempts were also made to find LR radiation patterns for the earthquakes by plotting the antilogs of the M_s values for each event. Only a few observed distributions of amplitudes conformed to any quadrupole radiation pattern. The scatter of amplitudes was, in almost every case, too great to infer the source type as either the double-couple of an earthquake or the uniform dilatation of an explosion. The observed scatter of data points resulted from the small magnitudes of the events studied and the large epicentral distances couple with propagation effects due to varying velocity and Q structures along the source-station paths.

Lacoss, R., 1969. A large-population LASA discrimination experiment, Technical Note 1969-24, Lincoln Laboratory, Lexington, Massachusetts.

Von Seggern, D. H., and R. R. Blandford, 1977. Observed variation in the spectral ratio discriminant from short-period P waves, SDAC Report No. TR-76-12, Teledyne Geotech, Alexandria, Virginia 22314.

Depth of Focus

All earthquakes studied here had apparent pP phases recorded at LASA, NORSAR, or several of the WWSSN stations. pP phases recorded at WWSSN stations agreed with the depths determined at LASA and NORSAR, although for crustal depth events there is little pP moveout at teleseismic distances. Thus, while these events could be tentatively identified as earthquakes on the basis of pP observations, some identifications would be tenuous because explosion recordings occasionally have high coda with apparent pP phases. On the other hand, lack of pP is not a positive indication of an explosion. While no attempts to enhance pP observations were made for these events, such procedures are now under study; and improved depth phase interpretation should be of great value in event identification.

Higher-Mode Observations

Analysis of higher-mode Rayleigh waves was not reported in the five Eurasian reports. Forsyth (1976) showed that higher-mode Rayleigh-wave arrivals are present on a large portion of certain WWSSN seismograms recorded from shallow Asian earthquakes over relatively short continental paths. He also devised a surface-wave magnitude scale based upon higher-mode amplitude which successfully identifies several Asian earthquakes whose fundamental-mode Rayleigh-wave and Love-wave generation was anomalously low. The NORSAR and ALPA long-period vertical beams have been examined for higher modes from the earthquakes of this study, but few cases of clearly recorded higher modes were evident, especially at ALPA, an observation attributable to lower relative amplitude response of long-period array instruments to periods of 5-15 seconds compared to that of the WWSSN instruments and also to some signal loss in beamforming at 3.6 km/sec on the fundamental Rayleigh mode. Thus, routine examination of array recordings for higher modes should be performed with special beamforming and filtering.

In Figure 34 NORSAR signals, 1024 sec long, are plotted from each of the five earthquake regions and from the E. Kazakh and S. W. Russia explosion sites, along with the output of a multiple-filter program for determining

Forsyth, D. W., 1976. Higher-mode Rayleigh waves as an aid to seismic discrimination, Bull. Seism. Soc. Am., 66, 827-842.

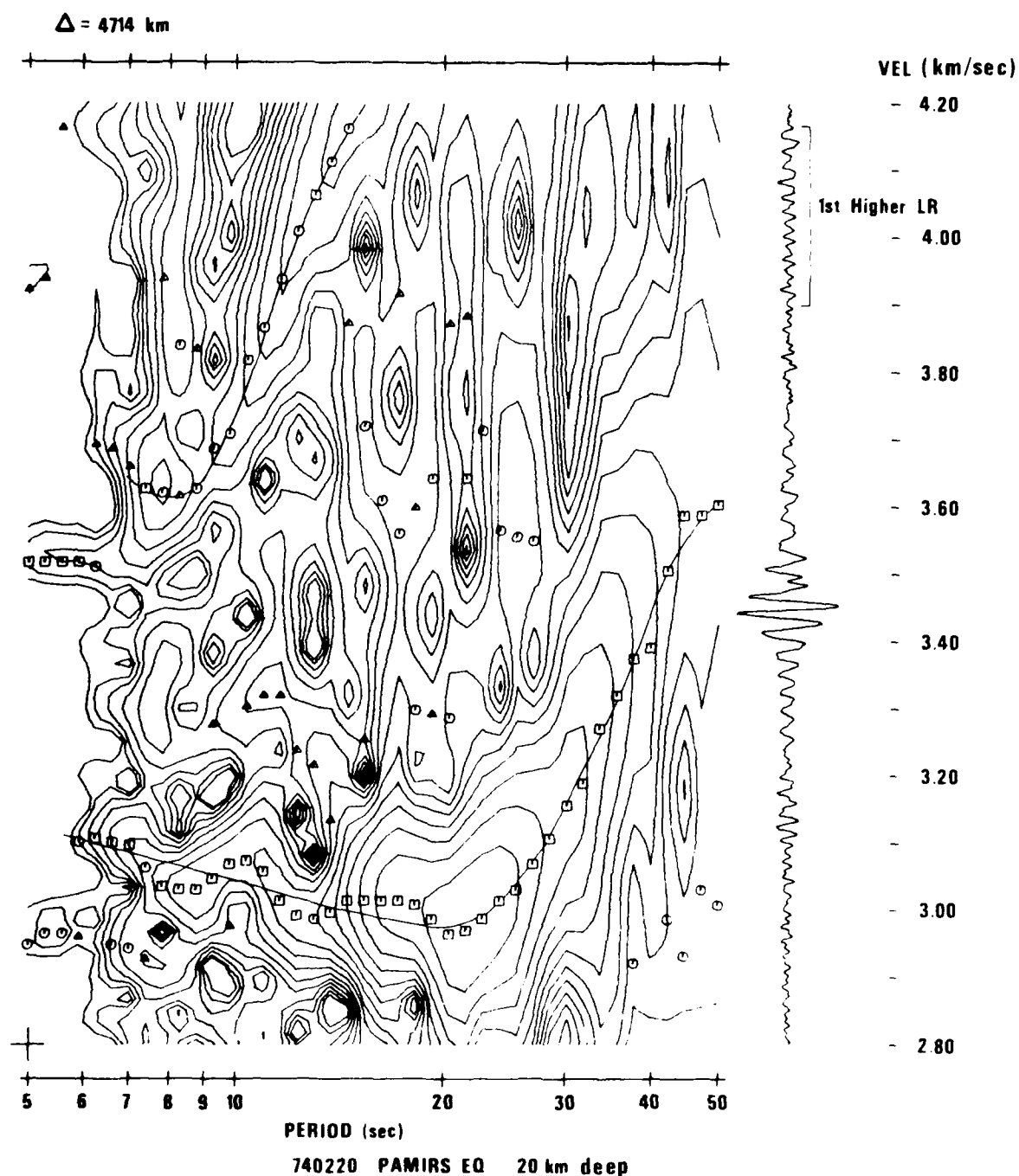


Figure 34 Rayleigh-wave arrivals at NORSAR for five earthquakes and two explosions and velocity versus period plots for determining group-velocity curves.

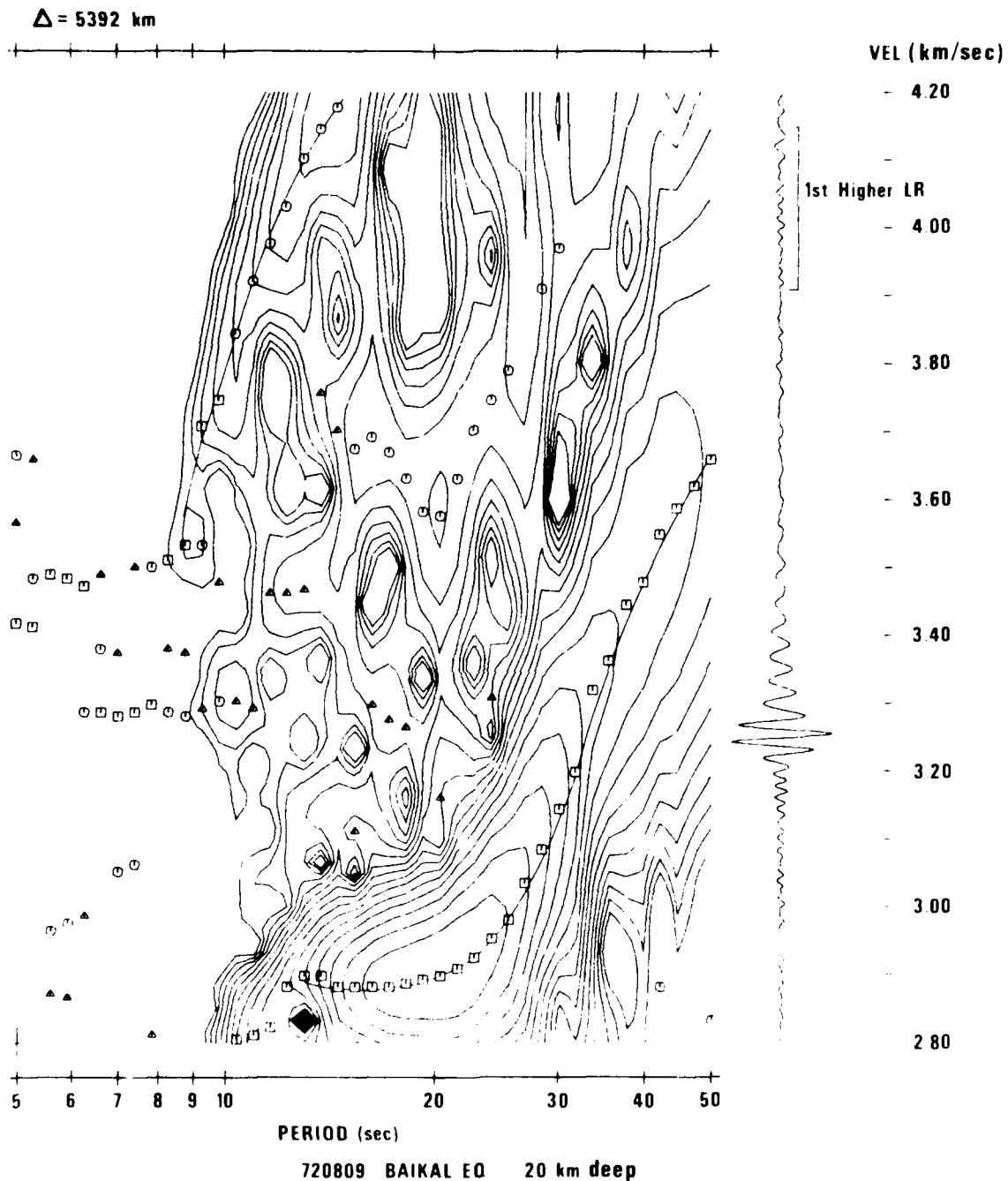


Figure 34 (cont.) Rayleigh-wave arrivals at NORSAR for five earthquakes and two explosions and velocity versus period plots for determining group-velocity curves.

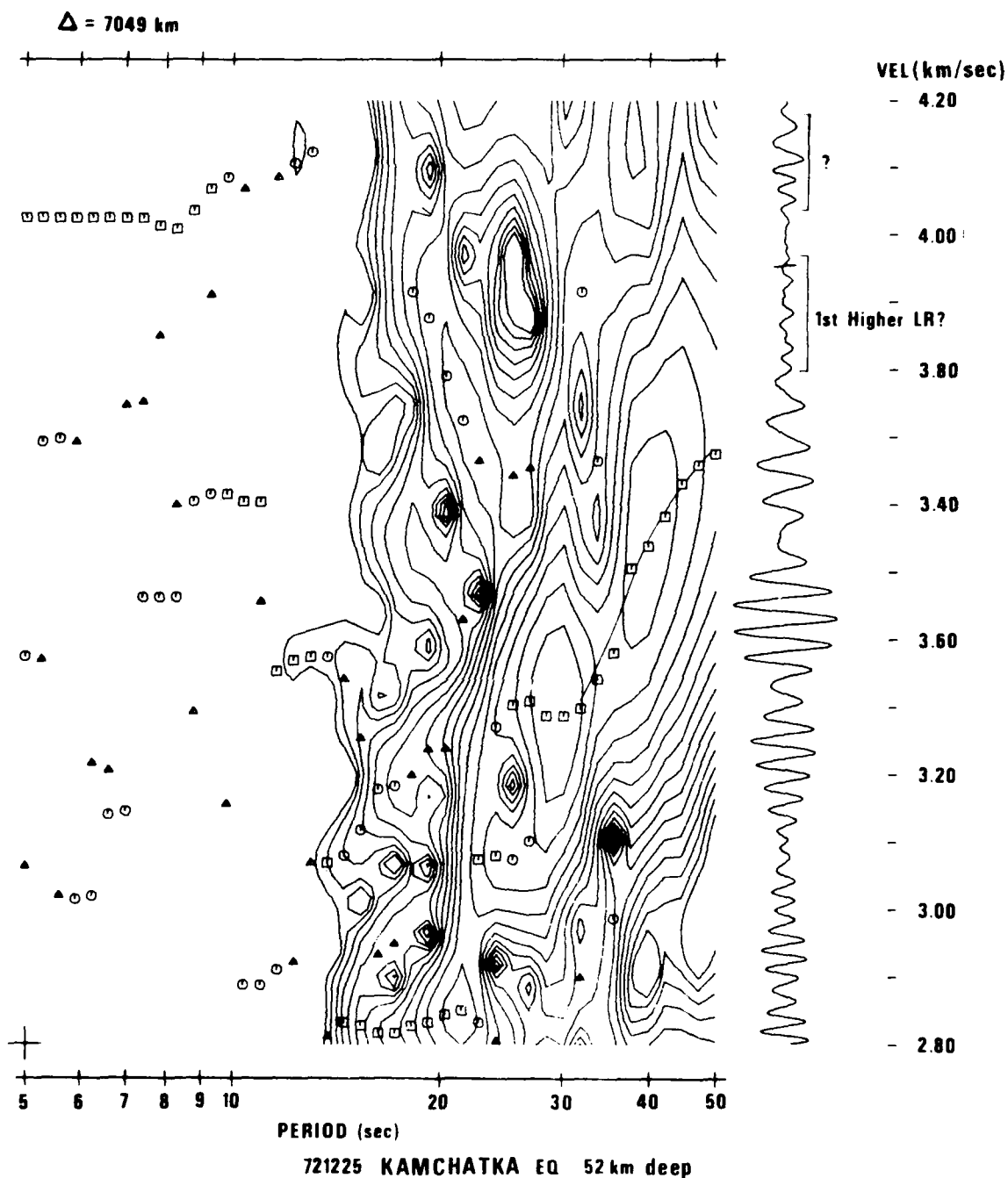


Figure 34 (cont.) Rayleigh-wave arrivals at NORSAR for five earthquakes and two explosions and velocity versus period plots for determining group-velocity curves.

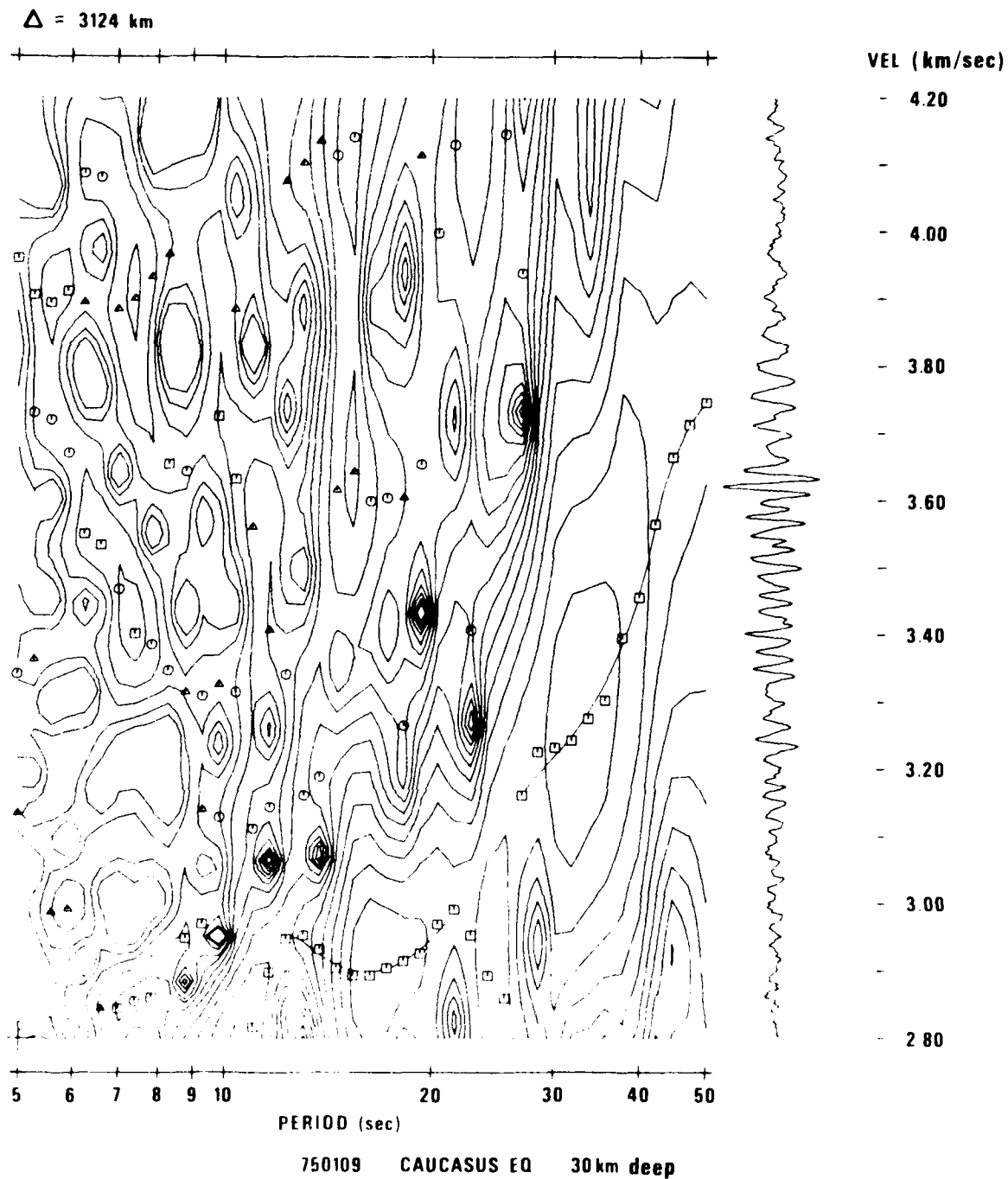
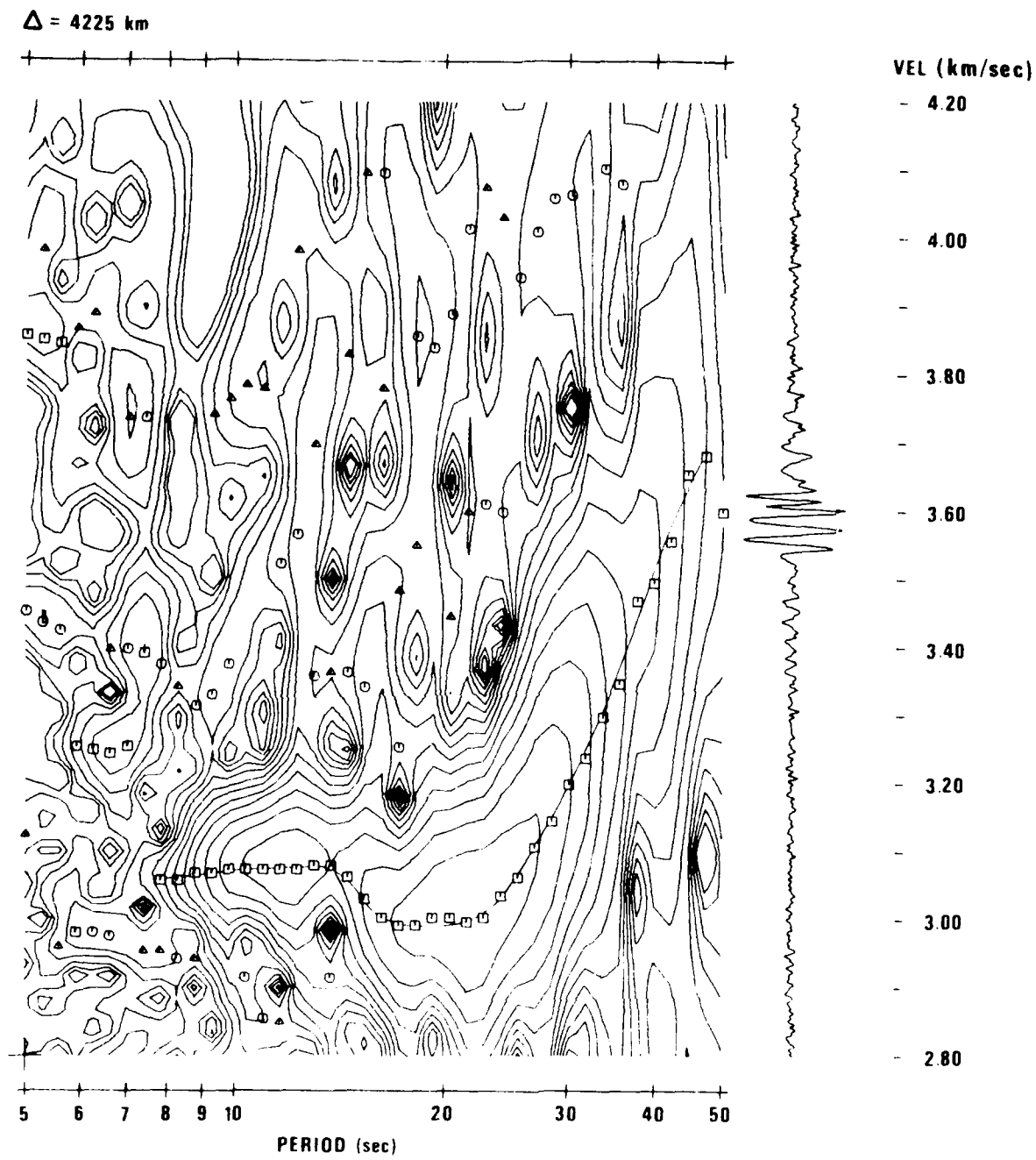


Figure 34 (cont.) Rayleigh-wave arrivals at NORSAR for five earthquakes and two explosions and velocity versus period plots for determining group-velocity curves.



711230 E KAZAKH EX

Figure 34 (cont.) Rayleigh-wave arrivals at NORSAR for five earthquakes and two explosions and velocity versus period plots for determining group-velocity curves.

group-velocity curves. These signals were chosen because of relatively high S/N ratios, but the others from each region are similar, at least in the character of the fundamental mode. The symbols \square , \circ and \triangle are plotted at the first, second, and third highest excursions of the envelope over each of the narrow-band filter outputs, thus allowing easier identification of more than one mode. The velocity scale applies to the contoured plot, not the time series. Higher modes are apparent for the Tien Shan, Pamirs, and Baikal earthquakes, and possible for the Kamchatka and Caucasus earthquakes. Paths to NORSAR from the first three regions are the most uniform, which accounts for better recordings of higher modes. Note that because it arrives much later, the higher mode identified from the Tien Shan earthquake is not identical to the mode from the Baikal or Pamir earthquakes. The higher mode from the two latter regions is the first higher Rayleigh mode that Cramplin (1966) identified for paths from Central Asia to Uppsala. The Kamchatka signal is complex, with a probable multipath phenomenon in the fundamental mode because the path lies near the continental-oceanic boundary in the Arctic. The Caucasus signal is also complex, with the presence of possibly several refracted or scattered wavefronts. On the other hand, fundamental-mode dispersion curves for both explosions are very smooth. Little or no evidence of a higher-mode arrival can be seen for the E. Kazakh explosion. The fairly strong 10-14 second period arrival at 3.9 km/sec for the S. W. Russia explosion is a shear-couple PL wave, and the arrival in the period range of 9-14 seconds and at 3.9 km/sec velocity is possibly the first higher Rayleigh mode. However, the amplitude of this mode relative to the fundamental at the same period is nearly the same on the seismogram. Since this is contrary to theoretical predictions for excitation from a surface-focus source (Forsyth, 1976), the difference might be due to a nearly non-attenuating waveguide for the higher mode, which has its maximum particle motion deeper in the crust.

In summary, although special processing could enhance its presence, higher-mode Rayleigh is not immediately apparent on the majority of seismograms at NORSAR for earthquakes in this study. Also, higher-mode arrivals were found

Cramplin, S., 1966. Higher modes of seismic surface waves: Propagation in Eurasia, Bull. Seism. Soc. Am., 56, 1227-1240.

for an explosion on NORSAR recordings, indicating that the presence of such arrivals is not sufficient to identify an Asian event as an earthquake. Studies of seismograms from earthquakes and nearby explosions, such that paths are nearly common, are required to evaluate fully this possible discriminant.

Correlation with Active Faults

Although the location of an event near a known active fault does not imply that it is necessarily an earthquake, the location might provide significant diagnostic information to be weighed along with quantitative discrimination data. The Kamchatka earthquakes studied here occurred along the coastline within the seismic zone at the top of the lithospheric plate, which is dipping to the northwest under Kamchatka, and are, therefore, unassociated with surface fault traces. Landsat Band 7 satellite photomosaics were made of the Tien Shan, Pamir, Baikal, and Caucasus regions for the Asian regional reports. Most of the events studied in those four regions correlated with presumed active faults inferred from the satellite mosaics.

STEPWISE CLASSIFICATION OF ASIAN SEISMIC EVENTS

In this section all the discrimination parameters are merged through a multi-dimensional approach. The approach used is the stepwise linear discriminant analysis performed by the program BMD02M (Jennrich, 1977). This program was also employed on a data base from Southwestern United States events by von Seggern and Rivers (1977), and a detailed explanation of the theory and use of the program for an applied seismic discrimination experiment can be found there. Briefly, the program takes a given number of variables measured on two or more designated groups, computes the mean of each variable for each group and the variance of each variable (assuming equal variance for all groups), and then proceeds stepwise by entering and deleting variables to form the best weighted linear combination of variables ("linear discriminant function") for each group such that groups are maximally separated. Preset "F-to-enter" and "F-to-remove" levels of the F-statistic are intended to control the final subset of variables used in group classification. However, these values (0.1 and .005 respectively) were purposely set low so that all variables were used. The F-statistic provides some measure of each variable's ability to separate the groups, with higher F values implying more separation than lower ones. Finally, computed a posteriori probabilities for each event are an indication of the degree of confidence in whatever classification was made for it.

Note that results of this experiment are completely valid only for events in this data base. Discriminant functions applied to the data base here are formed on a priori knowledge of the true classification of each event in the same data base, and use of such discriminant functions for new events would be made on the assumption that values of discrimination parameters for the new events possessed a mean-variance structure identical to that of the training set. This assumption would be tenuous because of the small sample of events in the actual data base used here. The purpose of this experiment is firstly, to exploit a multi-dimensional data set of discrimination parameters to determine if improved classification might result compared to simply using $M_s - m_b$, for

Jennrich, R. I., 1977. Stepwise regression, in Statistical Methods for Digital Computers, K. Enslien et al., eds., John Wiley & Sons, New York, NY.

instance, secondly, to quantitatively focus on the discrimination capability of each parameter measured for the Asian events; and thirdly, to identify those events in the data base which are hardest to classify overall.

The six parameters used in the stepwise discrimination are:

- 1) m_b - conventional body-wave magnitude average for an event;
- 2) M_s - surface-wave magnitude for an event, computed by Ringdal's method if possible;
- 3) f_c - corner frequency estimated from the attenuation-corrected spectra;
- 4) C_p - complexity of the P wave as determined over the first 35 sec of signal;
- 5) SR - spectral ratio from a spectrum corrected for attenuation to an f^{-2} source;
- 6) \hat{U}_0 - long-period spectral level estimated from the attenuation-corrected spectra.

Note that f_c , SR, and \hat{U}_0 are all derived quantities, not primary measurements, due to attenuation corrections made to the spectra. The t^* values used are listed in Table III. Again, note that these attenuation corrections are not precise and that they may have led to erroneous source spectral estimates. Yet the original Asian reports show that f_c and \hat{U}_0 are relatively unaffected by the attenuation correction. For the earthquake SR, correction to an f^{-2} or f^{-3} source does not make a great difference in the positions of these values relative to explosion values (see Figures 29 to 33), and they should be adequate for the analysis. Note that for the last four of the six parameters, only LASA and NORSAR values were computed. These values will be used separately and as an average quantity in classification experiments.

Classification of Events According to Regions

While the main effort is aimed toward discrimination between natural and artificial events, the classification of the earthquakes according to source region on the basis of parameters measured for the purpose of earthquake-explosion discrimination presents an interesting analysis. Results of this analysis will indicate the degree of regional effects on some, but

not all, parameters. Because of their limited number, such analysis was not attempted for explosions.

For earthquakes in the five regions, the LASA and NORSAR values for parameters 3 through 6 were first averaged in this experiment while values for parameters 1 and 2 (m_b and M_s) are from Table I; results are listed in Table IV at the right. Only nine of the forty earthquakes were classified outside of their true group on the basis of a posteriori probabilities. The high F-statistic for m_b is artificial, attributable to the fact that events selected for each region spanned somewhat different magnitude ranges. Thus, any differences in spectral parameters f_c and \hat{U}_0 are connected to the magnitude range and therefore may not represent region-dependent source differences. However, C_p should be relatively independent of magnitude and therefore represents a real source effect. Spectral ratio is seen to have the least classification potential, and this is not unexpected when consideration is given to the wide range of this value as measured at LASA and NORSAR (Figures 32 and 33).

The experiment was repeated using LASA and NORSAR estimates separately for parameters 3 through 6, and the results are shown in Table IV. The proportion of misclassifications dropped somewhat compared to results with averaged parameters, suggesting that station effects are an important aid in earthquake classification.

The fact that the earthquakes separated fairly well into regions on the basis of the six measured discrimination parameters was a significant result pointing to the need for using regionalized discriminant functions. The significance is exaggerated in our experiment because of the lack of a planned sampling procedure for the earthquakes; for example, all the Kamchatka earthquakes have larger m_b than the Pamir ones.

Discrimination of Earthquakes and Explosions on a Regional Basis

Past studies (e.g., Liebermann and Pomeroy, 1969, or Weichert and Basham,

Liebermann, R. C., and P. W. Pomeroy, 1969. Relative excitation of surface waves by earthquakes and underground explosions, J. Geophys. Res., 74, 1575-1590.

Weichert, D. H., and P. W. Basham, 1973. Deterrence and false alarms in seismic discrimination, Bull. Seism. Soc. Am. 63, 1119-1132.

Table IV

Results for Classification of
Earthquakes Into Five Regions

Classification Table	True Region*	Result				
		LASA				
	1	5	0	0	4	0
	2	0	6	1	0	0
	3	0	0	7	0	0
	4	0	0	0	4	0
	5	0	0	1	1	4
		NORSAR				
	1	9	0	0	0	0
	2	0	7	0	1	0
	3	0	0	8	0	1
	4	0	0	1	4	0
	5	0	1	0	1	4
		COMBINED				
	1	8	1	0	0	0
	2	0	8	0	1	0
	3	0	0	6	1	3
	4	0	0	1	4	0
	5	0	0	2	0	5

F-Statistics	LASA	NORSAR	COMBINED
m_b	10.4	11.8	13.2
M_s	2.3	2.6	1.9
C_p	4.4	10.1	6.5
\hat{f}_c	3.9	4.4	3.6
U_o	1.9	3.8	3.5
SR	0.8	1.4	1.0

- * 1 - Kamchatka
 2 - Tien Shan
 3 - Pamirs
 4 - Baikal
 5 - Caucasus

1973) as well as this analysis, suggested that discrimination on a regional basis will be more successful than when all events are treated together. Through this approach there is no need to determine regional correction factors, which are often significant but difficult to accurately evaluate. Following this reasoning, earthquakes in the five regions will be grouped with explosions in the data base which are in closest proximity to the region. Unfortunately, the degree of proximity in most of the five cases is inadequate to confidently claim that regional effects are truly common to the explosions and earthquakes. This is especially true since the explosions, with one or two exceptions, are in aseismic areas. The pairings were as follows (numbers in parentheses identify regions):

- 1) Kamchatka/Milrow (1/6)
- 2) Tien Shan/Lop Nor, E. Kazakh (2/10,7)
- 3) Pamirs/E. Kazakh, W. Kazakh (3/7,8)
- 4) Baikal/Baikal explosion (4/11)
- 5) Caucasus/W. Kazakh, S.W. Russia (5/8,9)

The program was executed three times for each of these pairings: first using LASA data only for parameters 3 through 6, then NORSAR data only for them, and finally using the LASA/NORSAR average value (the LASA or NORSAR value alone was used if both did not have a value). Values of parameters 1 and 2 (m_b and M_s) are from Tables I and II. Pertinent results are listed in Tables V through IX which contain two-way classification tables and F-statistics for the six parameters. Misclassifications would be identified by a posteriori probabilities <0.5 of belonging to the correct source category, but in fact none of the events considered were misclassified, with a probability of .975 being the lowest found for any of the events.

Discrimination of Earthquakes and Explosions Without Regionalization

Although regionalized discrimination is preferred, there is some interest in the discrimination of all events in the data base together. These results are listed in Table X. Using LASA or NORSAR alone gave perfect separation of the groups, although several events had a posteriori probabilities of being in the correct group which were much lower than in regionalized experiments, as low as .74. Using LASA-NORSAR averages for these four parameters also resulted in no misclassifications. However, the a posteriori probability of the 741021 Kamchatka earthquake was a low .54. The Kamchatka earthquake has low M_s and

very low complexity for an earthquake, but our examination (von Seggern and Sobel, 1976) of more types of data affirms that this event is not an explosion. While near misclassification of this event using the combined array data suggests that averaging discrimination parameters over stations may not be worthwhile, the use of merely two stations as opposed to either alone is not sufficient to state this with confidence. Furthermore, von Seggern and Rivers (1977) have shown elsewhere that discriminant functions based on a six-station network average are superior to those based on single-station values in separating earthquakes and explosions in the Southwestern United States.

Table XI presents the results of classification with short-period data only, which comprises five of the six variables used above. The numerous misclassifications indicate the importance of long-period data (M_s in this case) in discriminating Asian events. Note that spectral ratio is heavily weighted for NORSAR, as Figure 33 would suggest, which may be a reflection of the good high-frequency recording of that array.

Value of Different Discrimination Parameters for Asian Events

The set of parameters used thus far in these stepwise discrimination functions did not include what are thought to be among the best discriminants: depth of focus, Love-wave magnitude, and shear-wave magnitude. Depth of focus could not be quantitatively handled in the program, and the viewpoint was taken that depth was unknown and, therefore, inconsequential to discrimination. No Love-wave or shear-wave magnitudes were entered because of the paucity of data gathered on these phases in the original five Asian regional reports. So, considering the six parameters available in all cases, Table IV through XI suggest that routinely measured m_b and M_s parameters are essential data. Beyond those two, the classification power of the remaining parameters is marginal, especially in the experiment treating all events together (Table XI). Complexity weighs heavily in a few cases, but it is not consistent between LASA and NORSAR. The spectral parameters f_c , U_o , and SR also exhibit this inconsistency. For all parameters but spectral ratio, there is no clearly better performance at one array than at the other. By using the spectral ratio, classification power at NORSAR seems definitely to be enhanced.

Table V

Results for Classification of
Events from Kamchatka/Amchitka

	LASA	NORSAR	COMBINED												
Classification Table	<table><tr><td>9</td><td>0</td></tr><tr><td>0</td><td>1</td></tr></table>	9	0	0	1	<table><tr><td></td><td></td></tr><tr><td></td><td></td></tr></table>					<table><tr><td>9</td><td>0</td></tr><tr><td>0</td><td>1</td></tr></table>	9	0	0	1
9	0														
0	1														
9	0														
0	1														

		<u>LASA</u>	<u>COMBINED</u>
F-Statistics	m_b	5.5	5.5
	M_s	0.8	0.2
	C_p	0.1	6.2
	f_c	*	*
	\hat{U}_c	4.0	2.5
	SR	2.7	*

* indicates variables not entered, so $F < .01$

Note: no NORSAR data on Milrow explosion

Table VI

Results for Classification of Events
From Tien Shan/Lop Nor, E. Kazakh

	LASA	NORSAR	COMBINED												
Classification															
Table	<table><tr><td>7</td><td>0</td></tr><tr><td>0</td><td>5</td></tr></table>	7	0	0	5	<table><tr><td>8</td><td>0</td></tr><tr><td>0</td><td>7</td></tr></table>	8	0	0	7	<table><tr><td>9</td><td>0</td></tr><tr><td>0</td><td>7</td></tr></table>	9	0	0	7
7	0														
0	5														
8	0														
0	7														
9	0														
0	7														

		<u>LASA</u>	<u>NORSAR</u>	<u>COMBINED</u>
F-Statistics	m_b	24.3	22.4	25.0
	M_s	16.8	18.8	21.2
	C_p	0.3	3.7	0.5
	f_c	0.1	2.1	0.6
	\hat{U}_o	0.1	7.3	0.7
	SR	2.0	3.6	0.4

Table VII

Results for Classification of Events
From Pamirs/E. Kazakh, W. Kazakh

	LASA	NORSAR	COMBINED
Classification Table	7 0	9 0	10 0
	0 8	0 10	0 10

		<u>LASA</u>	<u>NORSAR</u>	<u>COMBINED</u>
F-Statistics	m_b	49.1	31.9	34.1
	M_s	10.4	20.7	23.6
	C_p	0.4	0.1	0.1
	f_c	5.3	0.1	0.1
	\hat{U}_o	1.0	3.9	5.4
	SR	3.0	5.4	6.3

Table VIII

Results for Classification of Events
From Baikal/Siberia

Classification Table	LASA	NORSAR	COMBINED												
	<table><tr><td></td><td></td></tr><tr><td></td><td></td></tr></table>					<table><tr><td>5</td><td>0</td></tr><tr><td>0</td><td>1</td></tr></table>	5	0	0	1	<table><tr><td>5</td><td>0</td></tr><tr><td>0</td><td>1</td></tr></table>	5	0	0	1
5	0														
0	1														
5	0														
0	1														

		<u>NORSAR</u>	<u>COMBINED</u>
F-Statistics	m_b	8.8	1.5
	M_s	7.4	7.4
	C_p	*	*
	f_c	*	*
	\hat{U}_o	12.0	26.6
	SR	1.3	7.8

* indicates variables not entered, so $F < .01$

Note: no LASA data on presumed Siberian explosion

Table IX

Results for Classification of Events
From Caucasus/W. Kazakh, S.W. Russia

Classification Table	LASA	NORSAR	COMBINED												
	<table><tr><td>6</td><td>0</td></tr><tr><td>0</td><td>6</td></tr></table>	6	0	0	6	<table><tr><td>6</td><td>0</td></tr><tr><td>0</td><td>4</td></tr></table>	6	0	0	4	<table><tr><td>7</td><td>0</td></tr><tr><td>0</td><td>6</td></tr></table>	7	0	0	6
6	0														
0	6														
6	0														
0	4														
7	0														
0	6														

		<u>LASA</u>	<u>NORSAR</u>	<u>COMBINED</u>
F-Statistics	m_b	10.0	12.1	17.0
	M_s	0.3	8.6	13.7
	C_p	16.8	2.7	*
	f_c	3.1	1.3	0.2
	\hat{U}_o	2.6	2.3	1.4
	SR	0.4	3.9	1.2

* indicates variable not entered, so $F < .01$

Table X

Results for Classification of Events
From all Asian Regions

	LASA	NORSAR	COMBINED												
Classification Table	<table><tr><td>33</td><td>0</td></tr><tr><td>0</td><td>12</td></tr></table>	33	0	0	12	<table><tr><td>37</td><td>0</td></tr><tr><td>0</td><td>12</td></tr></table>	37	0	0	12	<table><tr><td>40</td><td>0</td></tr><tr><td>0</td><td>15</td></tr></table>	40	0	0	15
	33	0													
0	12														
37	0														
0	12														
40	0														
0	15														

		<u>LASA</u>	<u>NORSAR</u>	<u>COMBINED</u>
F-Statistics	m_b	18.0	44.4	84.9
	M_s	63.6	32.8	21.6
	C_p	1.6	2.1	1.5
	f_c	0.6	*	0.1
	\hat{U}_o	*	0.3	0.4
	SR	0.2	5.3	1.3

* indicates variable not entered, so $F < .01$

Table XI

Results for Classification of Events
From all Asian Regions Using All
Short-Period Data

	LASA	NORSAR	COMBINED
Classification Table	28 5	32 5	35 5
	1 11	4 8	2 13

		<u>LASA</u>	<u>NORSAR</u>	<u>COMBINED</u>
F-Statistics	m_b	18.0	5.5	15.0
	M_g	*	*	*
	C_p	5.2	0.4	0.6
	f_c	0.1	6.6	0.1
	\hat{U}_o	8.7	1.3	11.6
	SR	0.2	7.5	4.6

* M_g not used

SUMMARY

Earthquakes from Kamchatka, the Tien Shan, the Pamirs, the Baikal rift zone, and the Caucasus and explosions from the Aleutians, E. Kazakh, W. Kazakh, Southwest Russia, Lop Nor, and Baikal were examined in the seismic discrimination context. One of the major points of the investigation was to see whether or not seismic signals from those broad regions exhibited any uniform character, thereby indicating uniform source-path factors for a given region. However, observations of short-period P waveforms recorded both at LASA and NORSAR revealed few similarities in waveforms from any region to either array. Observations of long-period Rayleigh waves recorded at NORSAR showed only some similarity among waveforms from any region to NORSAR, except for the explosion signals.

Determining individual fault-plane solutions on the basis of first motion was impossible for most of the earthquakes because of the small magnitudes of most events. The authors also were unable to determine a radiation pattern from the LR amplitudes, probably a result of varying propagation effects. Corner frequencies, long-period spectral levels, and seismic moments were estimated from the short-period LASA and NORSAR spectra. The seismic moments indicate that the earthquakes are of intermediate stress drop (tens of bars). The authors measured t^* , a measure of mantle attenuation, along the paths from each earthquake and explosion region to LASA and NORSAR. In general, t^* values for the paths to LASA were higher (implying more attenuation) than the t^* values for the paths to NORSAR, which are largely through shield areas.

The following discriminants were most successful in separating earthquakes from explosions in the data set:

- Surface-wave versus body-wave magnitude provided complete separation of explosions and earthquakes; the event magnitudes were based on Ringdal's (1976) maximum-likelihood method in most cases. One could accept $M_s = m_b - 1.5$ as a discrimination line for the data set. In the Kamchatka, Tien Shan, and Pamir regions, events were chosen which, from the NEIS list or from measurements at NORSAR, were of low M_s for their m_b . Independent determination in this study of M_s and m_b for those events revealed that they were not anomalously low in M_s for their m_b .

Although the events studied here separated on the $M_s - m_b$ plot into earthquakes and explosions, note that there are other areas in Asia, notably near 30°N , 95°E , where earthquakes do not clearly separate from explosions on an $M_s - m_b$ plot. Also, shot arrays could be used to raise the M_s of an explosion by about $0.3 M_s$ units or more without affecting m_b , placing it close to the earthquake population studied here.

- All earthquakes in this study had apparent pP signals recorded at LASA, NORSAR, or several of the WSSN stations. Although little moveout can be detected at teleseismic distances for shallow earthquakes, determination of this phase is probably the second best available discriminant. pP was not identified for the explosions but does not function as a positive discriminant.

Among the unreliable discriminants in this data set are: corner frequencies, long-period spectral levels, long-period and short-period body-wave excitation, complexities, spectral ratios, radiation patterns, correlation with active faults, and observations of higher modes. Still, each worked well for particular station-region pairs and deserves consideration for regional discrimination. It is suggested that regionalized discriminants will have enhanced value if the size of the regions is substantially smaller than those of the five studied here.

Discrimination parameters m_b , M_s , corner frequency (f_c), complexity (C_p), spectral ratio (SR), and long-period spectral level (\hat{U}_0) were merged in a stepwise linear discrimination analysis program. When parameters were averaged for each earthquake source region, the earthquakes separated fairly well into regions on the basis of the six discrimination parameters, suggesting the need for regionalized discriminant functions. When events in each of the five earthquake regions and the explosions in closest proximity to each region were treated separately, the earthquakes separated from the explosions. For the entire data set, using all six parameters with LASA and NORSAR average values for f_c , C_p , SR and \hat{U}_0 , all the earthquakes separated well from the explosions except the 741021 Kamchatka earthquake, which has low M_s and low complexity, and the Baikal explosion, which has very little data and no LASA record. Using LASA or NORSAR data alone gave perfect separation of the groups. Of course, if M_s were enhanced by a shot array we would expect that the stepwise linear discriminant program would still misclassify the event. Using only the short-period

discriminants in the analysis (that is, not using M_s) resulted in numerous misclassifications, emphasizing the importance of long-period data in discrimination of Asian events. The discrimination would be even poorer if complexity were enhanced in a shot array. Considering the six discriminants analyzed here, the parameters m_b and M_s are essential data, but the classification power of the remaining four is marginal.

The low magnitudes of the events in this study (m_b from 4.2 and M_s from 3.2) made clear discrimination difficult with the available data and probably represent nearly the lowest threshold of multi-discriminant analysis for the stations studied here. The installation of high-quality SRO stations in Asia will permit the examination of lower-magnitude events with multi-station digital data.

REFERENCES

- Ben-Menahem, A., S. Smith, and T. Teng, 1965. A procedure for source studies from spectrums of long-period seismic body waves, Bull. Seism. Soc. Am., 55, 203.
- Blandford, R., and D. Clark, 1975. Variability of seismic waveforms recorded at LASA from small subregions of Kamchatka, SDAC TR-75-12, Teledyne Geotech, Alexandria, Va. 22314. ADA 028 968
- Bungum, H., and D. Tjostheim, 1976. Discrimination between Eurasian earthquakes and underground explosions using the $m_b:M_s$ method and short-period autoregressive parameters, Geophy. J., 45, 371.
- Crampin, S., 1966. Higher modes of seismic surface waves: Propagation in Eurasia, Bull. Seism. Soc. Am., 56, 1227-1240.
- Dahlman, O., H. Israelson, A. Austegard, and G. Hornstorm, 1974. Definition and identification of seismic events in the USSR, Bull. Seism. Soc. Am., 64, 607-636.
- Davies, D., and B. Julian, 1972. A study of short-period P-wave signals from LONGSHOT, Geophy. J., 29, 185.
- Der, Z., and T. McElfresh, 1977. The relationship between anelastic attenuation and regional amplitude anomalies of short-period P-waves in North America, Bull. Seism. Soc. Am., 67, 1303-1317.
- Forsyth, D. W., 1976. Higher-mode Rayleigh waves as an aid to seismic discrimination, Bull. Seism. Soc. Am., 66, 827-842.
- Geller, R., 1976. Scaling relations for earthquake source parameters and magnitude, Bull. Seism. Soc. Am., 66, 1501.
- Hanks, T., and W. Thatcher, 1972. A graphical representation of seismic source parameters, J. Geophy. Res., 77, 4393.
- Jennrich, R. I., 1977. Stepwise regression, in Statistical Methods for Digital Computers, K. Enslien et al., eds., John Wiley & Sons, New York, NY.
- Lacoss, R., 1969. A large-population LASA discrimination experiment, Technical Note 1969-24, Lincoln Laboratory, Lexington, Massachusetts.
- Lambert, D., D. von Seggern, S. Alexander, and G. Galat, 1969. The LONG SHOT experiment, Vol. II, Comprehensive Analysis, SDL Report No. 234, Teledyne Geotech, Alexandria, Va. 22314. ADA 698 319
- Liebermann, R. C., and P. W. Pomeroy, 1969. Relative excitation of surface waves by earthquakes and underground explosions, J. Geophys. Res., 74, 1575-1590.

REFERENCES (Continued)

- Medvedev, S. V. (ed.), 1968. Seismic Zoning in the USSR, Keter Publ. House, Jerusalem, Israel (English translation).
- Molnar, P., and P. Tapponnier, 1975. Cenozoic tectonics of Asia: effects of a continental collision, Science, **189**, 419.
- Ringdal, F., 1976. Maximum-likelihood estimate of event magnitude, Bull. Seism. Soc. Am., **66**, 789.
- Sobel, P. A., and D. H. von Seggern, 1976. Study of selected events in the Tien Shan Region in a seismic discrimination context, SDAC Report No. TR-76-9, Teledyne Geotech, Alexandria, Va. 22314. ADA 038 293
- Sobel, P. A., D. H. von Seggern, E. I. Sweetser, and D. W. Rivers, 1977a. Study of selected events in the Pamirs in a seismic discrimination context, SDAC Report No. TR-77-3, Teledyne Geotech, Alexandria, Va. 22314.
- Sobel, P. A., D. H. von Seggern, E. I. Sweetser, and D. W. Rivers, 1977b. Study of selected events in the Baikal rift zone in a seismic discrimination context, SDAC Report No. TR-77-5, Teledyne Geotech, Alexandria, Va. 22314.
- Sobel, P. A., D. H. von Seggern, E. I. Sweetser, and D. W. Rivers, 1977c. Study of selected events in the Caucasus in a seismic discrimination context, SDAC Report No. TR-77-6, Teledyne Geotech, Alexandria, Va. 22314.
- Stauder, W., and L. Mualchin, 1976. Fault motion in the large earthquakes of the Kurile-Kamchatka Arc and of the Kurile-Hokkaido corner, J. Geophys. Res., **81**, 297.
- Von Seggern, D. H., 1972. Seismic shear waves as a discriminant between earthquakes and underground nuclear explosions, SDL Report No. 295, Teledyne Geotech, Alexandria, Va. 22314.
- Von Seggern, D. H., and R. Blandford, 1972. Source time functions and spectra for underground nuclear explosions, Geophys. J., **31**, 83-97.
- Von Seggern, D. H., and W. D. Rivers, 1977. Seismic discrimination of earthquakes and explosions with application to the Southwestern United States, SDAC Report No. TR-77-10, Teledyne Geotech, Alexandria, Va. 22314.
- Von Seggern, D. H., and P. Sobel, 1975. Experiments in refining M_s estimates for seismic events, SDAC Report No. TR-75-17, Teledyne Geotech, Alexandria, Va. 22314. ADA 032 074
- Von Seggern, D. H., and P. A. Sobel, 1976. Study of selected Kamchatka earthquakes in a seismic discrimination context, SDAC Report No. TR-76-10, Teledyne Geotech, Alexandria, Va. 22314.

REFERENCE (Continued)

Von Seggern, D. H., and R. R. Blandford, 1977. Observed variation in the spectral ratio discriminant from short-period P waves, SDAC Report No. TR-76-12, Teledyne Geotech, Alexandria, Va. 22314.

Weichert, D. H., and P. W. Basham, 1973. Deterrence and false alarms in seismic discrimination, Bull. Seism. Soc. Am., 63, 1119-1132.